

Charles University in Prague  
Faculty of Science  
Department of Physical and Macromolecular Chemistry

# Diploma thesis



## Modelling of Ligand-Binding Site Structure of the Human MT2 Melatonin Receptor

Karel BERKA

Supervisor : RNDr. Tomáš Obšil PhD.

Prague 2006

# Acknowledgements

I am deeply grateful to my supervisor RNDr. Tomáš Obšil PhD. for his detailed and constructive comments and advices, and for his important support throughout this work.


I wish to express my warm and sincere thanks to Ing. Jan Teisinger CSc., and RNDr. Petr Mazna PhD. for their support during experimental stage of my diploma thesis.

During this work I have collaborated with many colleagues for whom I have great regard, and I wish to extend my warmest thanks to all those who have helped me with my work in the Department of Physical and Macromoleculal Chemistry at the Charles University in Prague and Institute of Physiology at the Academy of Sciences of the Czech Republic, especially RNDr. Veronika Obšilová, PhD., RNDr. Jan Šilhán, Mgr. et Mgr. Evžen Bouřa and Bc. Eliška Nedbálková.

I owe my thanks to my parents for their support during my study. Without their encouragement and understanding it would have been impossible for me to finish this work. My special gratitude is due to my brothers for their loving support.

I confirm that this Diploma Thesis is based on the work, which I have done by myself under the supervision of RNDr. Tomáš Obšil, PhD. at Department of Physical and Macromoleculal Chemistry, Charles University in Prague. I have properly quoted all the references used in this work.

In Prague, ..... 2006

Karel Berka 

# List of abbreviations

The standard single and three letter codes for amino acid residue types are used throughout;

3D	3-dimensional
4P-ADOT	4-Phenyl-2-acetamidotetraline
4P-PDOT	4-Phenyl-2-propionamidotetraline
AD	Alzheimer's disease
AS CR	Academy of Sciences of the Czech Republic
BLAST	Basic local alignment search tool
BLOSUM	Blocks substitution matrix
BSA	Bovine serum albumin
C $\alpha$	Alpha carbon (carbon atom which is in main chain of protein)
cAMP	Cyclic adenosine monophosphate
cDNA	complementary deoxyribonucleic acid
cGMP	Cyclic guanosine monophosphate
DMEM	Dulbecco's modified Eagle medium
DNA	Deoxyribonucleotide acid
ECL	Extracellular loop
EDTA	Ethylenediaminetetraacetic acid
ER	Endoplasmatic reticulum
FFT	Fast Fourier transformation
G protein	Guanidine triphosphate exchanging protein
GEP	Gap extension penalty
GES hydrophobicity	Goldman, Engelman and Steitz hydrophobicity scale
GOP	Gap opening penalty
GPCR	G-protein coupled receptor
GPCRDB	Cross-reference database about GPCRs
H	Helix
hMT1	Human melatonin receptor Type 1
hMT2	Human melatonin receptor Type 2
HEK293	Human embryonic kidney cell line 293
HSP	High scoring pair
LJ potential	Lennard-Jones potential
LINCS	Linear constraint solver for molecular simulations.
MD	Molecular dynamics
ML1	High affinity melatonin receptors
ML2	Low affinity melatonin receptors
mRNA	Messenger ribonucleic acid
MT1	Melatonin receptor Type 1
MT2	Melatonin receptor Type 2
MT3	Melatonin receptor Type 3
NCBI	National Center for Biotechnology Information
NMR	Nuclear magnetic resonance
NPT ensemble	Isothermal-isobaric ensemble
OPLS-AA/L	Optimised potential for liquid systems of aminoacids from LMP2/cc-pVTZ(-f) calculations
PAM	Percentage of Acceptable point Mutations per 10 <sup>8</sup> years

PBS	Phosphate-buffered saline solution
PCR	Polymerase Chain Reaction
PDB	Protein DataBank file format to store atomic coordinates
<i>Pfu</i> Polymerase	<i>Pyrococcus furiosus</i> Polymerase
PME	Particle Mesh Ewald sum method
POPE	1-palmitoyl-2-oleoyl-sn-glycero-3-phosphoethanolamine
PSI-BLAST	Position-specific iterated BLAST
QR2	NRH:quinone oxidoreductase 2
RMSD	Root mean square deviation
RT-PCR	Real-time polymerase chain reaction
SCN	Supraschiasmatic nucleus
SS bridge	Disulphide bridge
<i>Taq</i> Polymerase	<i>Thermus Aquaticus</i> Polymerase
TM	Transmembrane
WT	Wild-type

# Content

Acknowledgements .....	2
List of abbreviations.....	3
Content.....	5
Table of figures .....	7
Abstract.....	8
1 Introduction .....	9
1.1 Biochemical background.....	9
1.1.1 Melatonin, the hormone of darkness .....	9
1.1.2 G protein-coupled receptors (GPCRs) .....	11
1.1.3 Structure of bovine rhodopsin in the dark state .....	12
1.1.4 Melatonin receptors.....	16
1.2 General approach of homology modelling.....	17
1.3 Programs and algorithms.....	19
1.3.1 Template search .....	19
1.3.2 Prediction of transmembrane segments.....	19
1.3.3 Sequence Alignment .....	21
1.3.4 Homology modelling.....	22
1.3.5 Ligand docking .....	24
1.3.6 Molecular dynamics .....	25
1.3.7 Experimental binding assays .....	28
2 Goals of diploma thesis.....	29
3 Materials & Methods .....	30
3.1 Theoretical part.....	30
3.1.1 Sequence.....	30
3.1.2 Template search .....	30
3.1.3 Trans membrane region prediction .....	30
3.1.4 Homology modelling.....	30
3.1.5 Automated ligand docking.....	31
3.1.6 Molecular dynamics .....	31
3.2 Experimental methods.....	33
3.2.1 Materials .....	33
3.2.2 Site directed mutagenesis of Gly121 .....	33
3.2.3 Transfection .....	34
3.2.4 Binding assays .....	35
3.2.5 Immunocytochemistry.....	35
4 Results.....	36
4.1 Result from theoretical part.....	36
4.1.1 Template search .....	36
4.1.2 Trans membrane predictions.....	36
4.1.3 Consensus TM prediction.....	38
4.1.4 Alignments.....	39
4.1.5 Homology model building.....	40
4.1.6 Docking of 2-iodomelatonin into the receptor.....	44
4.1.7 Molecular dynamics .....	49
4.1.8 Analysis of the MD results .....	53
4.2 Experimental results.....	56

4.2.1	Plasmid preparation.....	56
4.2.2	Binding assay.....	56
5	Discussion.....	58
5.1	Summary of mutational data.....	58
5.1.1	Potential role of His208.....	60
5.1.2	Is disulphide bridge between Cys113 and Cys190 present?.....	60
5.1.3	Tunnel presence.....	61
5.2	Final model.....	62
6	Conclusion.....	63
7	References.....	64
8	Appendixes.....	70
8.1	Human MT2 melatonin receptor sequence.....	70
8.2	Maps of plasmids.....	70
8.2.1	pcDNA3.....	70
8.2.2	pFLAG-CMV-2.....	71
8.3	Alignments.....	72
8.3.1	Alignment I.....	72
8.3.2	Alignment II.....	72
8.3.3	Alignment III.....	73
8.4	Gromacs run scripts.....	74
8.4.1	Energy minimization.....	74
8.4.2	Pre-run with positional restraints.....	74
8.4.3	Full production run.....	75
8.4.4	Steepest descent minimization of average structure.....	76
8.4.5	Conjugated gradient minimization.....	77
8.5	Site-directed mutagenesis data.....	78
8.6	Author's publications.....	79

# Table of figures

<b>Figure 1.1</b> - Melatonin (N-acetyl-5-methoxy tryptamine) structure .....	9
<b>Figure 1.2</b> - Physiology of melatonin secretion .....	10
<b>Figure 1.3</b> - Amino acid sequence of bovine rhodopsin encoded as 1U19 [25]. .....	13
<b>Figure 1.4</b> – Overall structure of bovine rhodopsin encoded as 1U19 [25].....	14
<b>Figure 1.5</b> – Ramachandran plot of bovine rhodopsin (PDB ID 1U19, chain A) [25].	15
<b>Figure 1.6</b> - From structure to function .....	18
<b>Figure 4.1</b> – GES hydrophobicity profile of hMT2 sequence.....	36
<b>Figure 4.2</b> – TMPred prediction results. ....	37
<b>Figure 4.3</b> – TopPred prediction results. ....	37
<b>Figure 4.4</b> – TMHMM prediction results. ....	38
<b>Figure 4.5</b> – Consensus TM prediction. ....	38
<b>Figure 4.6</b> – Comparison of models obtained using the Alignment I. ....	41
<b>Figure 4.7</b> – Position of cysteines in models based on Alignment I. ....	41
<b>Figure 4.8</b> - Comparison of models obtained using the Alignment II.....	42
<b>Figure 4.9</b> - Position of cysteines in models based on Alignment II.....	42
<b>Figure 4.10</b> - Comparison of models obtained using the Alignment III.....	43
<b>Figure 4.11</b> - Position of cysteines in models based on Alignment III. ....	43
<b>Figure 4.12</b> – RMS histogram for docking results of 2-iodomelatonin into Model I. ..	44
<b>Figure 4.13</b> – Prediction of 2-iodomelatonin binding into the pocket of Model I. ....	45
<b>Figure 4.14</b> – RMS histogram for docking results of 2-iodomelatonin into Model II. ..	46
<b>Figure 4.15</b> – Prediction of 2-iodomelatonin binding into the pocket of Model II.....	47
<b>Figure 4.16</b> – RMS histogram for docking results of 2-iodomelatonin into Model III. ....	47
<b>Figure 4.17</b> – Prediction of 2-iodomelatonin binding into the pocket of Model III. ....	48
<b>Figure 4.18</b> – Snapshot of the end of lipid bilayer re-equilibration. ....	50
<b>Figure 4.19</b> – Snapshot of the simulation system with Complex I. ....	50
<b>Figure 4.20</b> – Complex I after the energy minimization seen from above .....	51
<b>Figure 4.21</b> – Complex I after pre-run MD simulation seen from above.....	51
<b>Figure 4.22</b> – Energy and RMSD profiles of system with Complex I. ....	52
<b>Figure 4.23</b> – Snapshot taken from the end of MD production run with Complex II... ..	52
<b>Figure 4.24</b> – Ligand-binding site of Complex I before MD simulation .....	53
<b>Figure 4.25</b> – Ligand-binding site of Complex I after MD simulation .....	53
<b>Figure 4.26</b> – Ligand-binding site of Complex II before MD simulation .....	54
<b>Figure 4.27</b> – Ligand-binding site of Complex II after MD simulation.....	54
<b>Figure 4.28</b> – Ligand-binding site of Complex III before MD simulation.....	55
<b>Figure 4.29</b> – Ligand-binding site of Complex III after MD simulation.....	55
<b>Figure 4.30</b> – Sequencing of the DNA of hMT2 melatonin receptor.....	56
<b>Figure 4.31</b> – Saturation binding assay for G121A mutant receptor .....	57
<b>Figure 4.32</b> – Saturation binding assay for Wild-type receptor.....	57
<b>Figure 5.1</b> – Possible tunnel positions proposed for Complexes I and III.....	61
<b>Figure 5.2</b> – Final model of the human MT2 melatonin receptor.....	62
<b>Figure 6.1</b> – Ligand-binding site of the human MT2 melatonin receptor .....	63
<b>Figure 8.1</b> - The complete sequence of MT2 melatonin receptor (NP_005950) [33]... ..	70
<b>Figure 8.2</b> – map of the vector pcDNA3 (Invitrogene, USA) .....	70
<b>Figure 8.3</b> - map of the vector pFLAG-CMV-2 (Sigma Aldrich, USA) .....	71
<b>Figure 8.4</b> - Alignment I .....	72
<b>Figure 8.5</b> - Alignment II.....	73
<b>Figure 8.6</b> - Alignment III.....	73

# Abstract

Melatonin (N-Acetyl-5-methoxytryptamine) is the main hormone synthesized by the vertebrate pineal gland. In mammals, the melatonin is known to play an important role in the regulation of physiological and neuroendocrine functions, such as synchronization of seasonal reproductive rhythms, and entrainment of circadian cycles.

MT2 receptor is a G-protein coupled receptor (GPCR) and its activation modulates a wide range of intracellular messengers, e.g. cAMP, cGMP, or  $\text{Ca}^{2+}$ . All GPCRs are thought to share the basic structural organization characterized by bundle of seven putative transmembrane domains that form a ligand-binding site. Despite growing collection of experimental data, in most cases the actual arrangement of transmembrane domains and their conformational changes induced by the ligand-binding are not completely understood. Recently published high-resolution crystal structure of bovine rhodopsin (Palczewski *et al.* (2000) [1]) enabled homology modelling of other GPCR structures, such as human melatonin MT2 receptor.

Main goals of this diploma thesis are: (1) to create a homology model of human melatonin MT2 receptor; (2) to select residues possibly involved in the ligand binding for site-directed mutagenesis; (3) to perform flexible docking of melatonin molecule into the predicted ligand-binding site; (4) to compare obtained results with experimental data based on site-directed mutagenesis.



# 1 Introduction

## 1.1 Biochemical background

### 1.1.1 Melatonin, the hormone of darkness

Melatonin is a neural hormone (firstly isolated in 1958 [2]) which has a significant role in the biologic regulation of circadian rhythms, sleep, mood, and perhaps reproduction, tumour growth, aging [3], and memory [4]. (Figure 1.1)

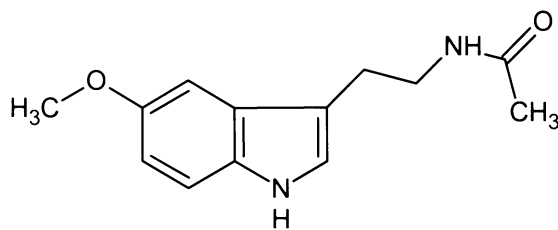


**Figure 1.1** - Melatonin (N-acetyl-5-methoxy tryptamine) structure

#### 1.1.1.1 Circadian cycles

Hormone melatonin, or N-acetyl-5-methoxytryptamine, is produced from serotonin by pineal gland in humans. Signal for melatonin production is transmitted by the hormone norepinephrine through the suprachiasmatic nucleus (SCN) of the hypothalamus. The synthesis and release of the melatonin are inhibited by light and stimulated by darkness. Light has two effects on melatonin: day-night light cycles modify the rhythm of its secretion and brief pulses of intense light abruptly suppress its production. Alternations affect mainly the timing for suprachiasmatic nucleus.

Hormone is secreted by passive diffusion into the bloodstream. In humans, melatonin secretion increases soon after the sunset, peaks in the middle of the night and gradually falls during second half of the night. Melatonin is rapidly metabolized, mainly in the liver by hydroxylation and, after conjugation with sulphuric or glucuronic acid is excreted in the urine.

The indigestion of melatonin affects the speed of falling asleep as well as the quality of sleep. Melatonin has also a hypnotic effect [5].

### 1.1.1.2 Immunity

Melatonin may augment the immune response such as the inhibition of tumour growth and counteraction of stress-induced immunodepression [6].

Melatonin itself can act as a radical scavenger, however antioxidant effects of melatonin occur only at very high concentration [6-9].

### 1.1.1.3 Aging and Alzheimer disease treatment

Secretion of melatonin differs with age. Small children younger than 3 months have very small non-circadian secretion; highest nocturnal peak is at the age of about two years, after which secretion declines gradually [3]. This decline can be taken into account with a significant reduction of sleep continuity and quality with aging [10].

Patients with Alzheimer's disease (AD) have even more reduced secretion of the melatonin, while melatonin supplementation helps to slow the progress of AD [11, 12]. These facts are also in agreement with melatonin-induced nerve regeneration in rats [13]. On the other hand, chronic melatonin therapy fails to alter main AD feature - beta-amyloid burden from previous brain damage. This diminishes the possibility of melatonin treatment during an established AD [14].

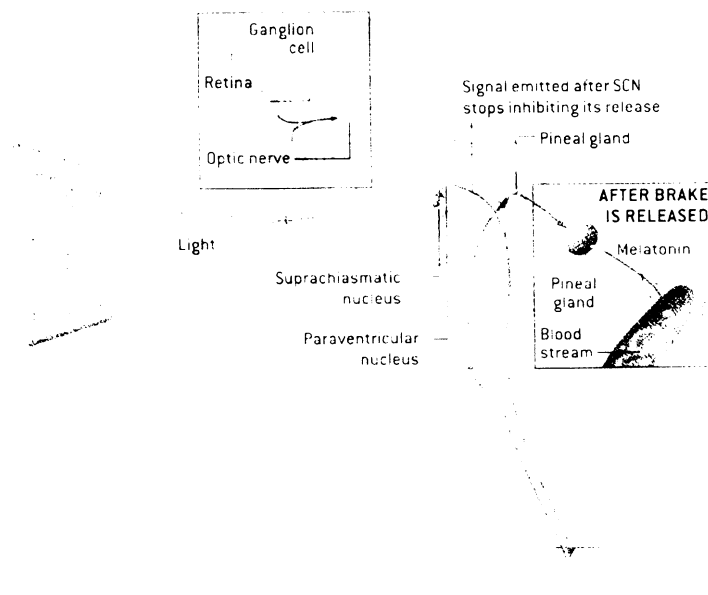


**Figure 1.2** - Physiology of melatonin secretion

Melatonin is produced in the pineal gland. The production and secretion of melatonin are mediated by postganglionic retinal nerve fibres that pass to SCN then to the superior cervical ganglion, and finally to the pineal gland. Release of the melatonin is inhibited by light.

## 1.1.2 G protein-coupled receptors (GPCRs)

G protein-coupled receptors (GPCRs) constitute the largest family of signal transduction membrane proteins, which mediate responses of a variety of bioactive molecules. As a result, GPCRs play a crucial role in many essential physiological processes as diverse as neurotransmission, cellular metabolism, secretion, cell growth, immune defences, and differentiation [15].

Not surprisingly, GPCRs are the most privileged targets for the drugs currently used in clinics. This reflects not only the broadness of potential application but also the fact, that GPCRs are by far the easiest targets for small organics molecules. In fact, they are naturally built to recognise a single structure among the widest variety of extracellular chemicals. And last but not least reason is that they are exposed and reachable on the cell surface.

Although varying in molecular sizes, all GPCR contain seven hydrophobic helices that span the lipid bilayer and dictate the typical architecture of the receptor:

Seven transmembrane (TM) domains formed by helices are bundled to form a polar internal tunnel and to expose N-terminus and three extracellular loops to the exterior. C-terminus with three intracellular loops is exposed to the cytosol of the cell interior.

GPCRs have been clustered in a number of classes/families by sequence analysis. System of GPCRs taken from GPCR database [16]:

- class A consist of rhodopsin like receptors;
- class B is secretin like class;
- class C is metabotropic glutamate or pheromone class;
- class D is the fungal pheromone;
- class E stands for the cAMP receptors;
- class F is the frizzled/smoothened family.

All GPCRs share the common molecular strategy of signal transduction. There are two different types of ligands – (1) agonist promotes allosteric interactions between the receptor and one or more members of the family of G proteins, while (2) antagonist binding does not activate G proteins. These are specialized GTPases that broadcast the signal to a host of intracellular enzymes or ion channels.

GPCR oligomerization seems to have functional advantages either during GPCRs maturation in endoplasmatic reticulum (ER) and probably also for modulation of receptor function [17-20].

Main problem of studies of GPCRs is still in the lack of good structural data. So far, the only GPCR whose structure has been resolved with atomic detail is rhodopsin in the dark state [1].

### **1.1.2.1 Class A GPCRs – Rhodopsin like**

Greatest numbers of GPCRs stands in this family like muscarinic acetylcholine, cannabinoid, dopamine, histamine, olfactory, prostanoid, and also melatonin receptors. This caused that this family is by far the most studied GPCR family. The overall homology among all family A receptors is low and restricted to a small number of highly conserved key residues distributed in all seven helices.

The most conserved residues in each helix are at position 50 according to the arbitrary numbering scheme by Ballesteros and Weinstein [21]. (Figure 1.3)

### **1.1.3 Structure of bovine rhodopsin in the dark state**

Close structural relationship between visual and hormonal signalling system was very surprising fact at the beginning of GPCRs studies. Rhodopsin is involved in molecular transformation of light energy into a neuronal signal transmitted to the secondary neurons of the retina and ultimately to the brain.

Rhodopsin became the founder of family A GPCRs and the best source of high-resolution structural information. Bovine rhodopsin is the first and the only GPCR with known 3D structure (PDB access code 1F88 with resolution 2.80 Å [1], 1HZX with 2.80 Å [22], 1L9H with 2.60 Å [23], 1GZM with 2.65 Å [24], 1U19 with 2.20 Å [25]).

Bovine rhodopsin contains 348 amino acids and folds into seven TM helices varying in length from 19 to 34 residues, and one cytoplasmic helix, H8. The seven TM domains contain a mix of canonical  $\alpha$ - and 3.10-helices, and they possess a large number of kinks, twists, and bends (Figure 1.4). These conformational anomalies are present at all structures solved to date [26].

N-term

MNGTEGPNFYVPFSNKTGVVRSPPFEAPQYYLAEP 34

H1

WQFSMLAAYMFLLIMLGFPINFLTLTYTVQ 64

H1

HKKLRT 70

H2

PLNYILLNLAVADLFMYFGGFTTTLTYSLH 100

E1

GYFVF 106

H3

GPTGCNLEGGFATLGGEIALWSLVVLAIERVYVVC 140

H2

KPMSNFRFG 149

H4

ENHAIMGVAF<sup>11</sup>TWVMALACAAPPLVG 174

E2

WSRYIPEGMQCS**C**GIDYYTPHE**ETNN** 200

H5

ESFVIYMPV<sup>11</sup>VHFIIP<sup>11</sup>LIVIFFCYGQL 226

H3

VFTVKEAAAQQQESA 241

H6

TTQKAEKEVTRMVIIMYIAFLICWLPYAGVAFYIFTH 278

E3

QGSDFGP 285

H7

H8

IFMTIPAFFAKTSAVYNPVIYIMMN**KQFRNCMYTTL** 321

C-term

CCGKNPLGDDDEASTTVSKTETSQVAPA 348

**Figure 1.3** - Amino acid sequence of bovine rhodopsin encoded as 1U19 [25]. Colour highlights indicate the secondary structure computed on the structure. In detail, violet means canonical  $\alpha$ -helices, and yellow stands for strand, whereas cyan, orange, and pink indicate, respectively, type 3-, 4-, and 5-turns. The most conserved amino acids in each helix are in red colour. These amino acids are at position 50 according to the arbitrary numbering scheme by Ballesteros and Weinstein [21]. Bold characters indicate the conserved members of the E/DRY, FxxCWxP, and NPxxY motifs in H3, H6, and H7, respectively. Boxed characters indicate the cytoplasmic H8. Figure taken from Fanelli and De Benedetti [26]

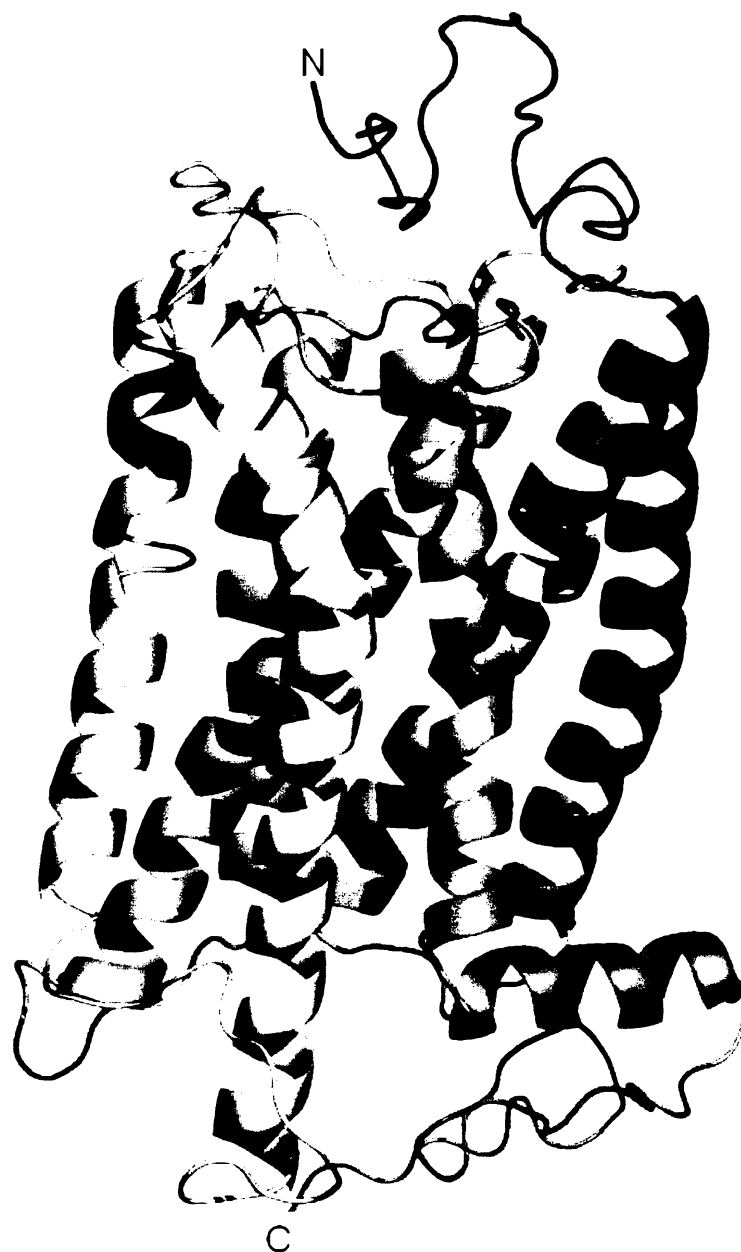


**Figure 1.4** – Overall structure of bovine rhodopsin encoded as 1U19 [25].

Bovine rhodopsin contains 7 TM helices. H1 (dark blue) is tilted from the membrane normal, and it contains a bend. H2 (light blue) is tilted from the membrane normal about the same as H1. H3 (grey green) is the longest (48 Å), the most tilted and the most buried helix. The cytosolic extension of H3 is particularly important, because it contains the highly conserved E/DRY motif. H4 (green, behind yellow H6) is the shortest helix; it is almost perpendicular to the membrane and deviates from an ideal helix at its extracellular end. H5 (green) is tilted from the membrane normal. H6 (yellow) is the second longest helix. Its cytosolic half is almost orthogonal to the membrane plane, whereas its extracellular half is bent. H7 (orange) shows a considerable distortion and elongation in the region around the retinal attachment. In addition to these TM helices, another short helix in the cytoplasmic surface, termed H8, is located at the cytosolic end of H7 and it is almost orthogonal to the membrane normal.

Drawings were done by the software PYMOL 0.95 (<http://pymol.sourceforge.net/>)

Due to the transmembrane position of protein, Ramachandran plot [27] of the rhodopsin contains many anomalies (Figure 1.5). It can be said that structural anomalies should be found on many GPCRs.

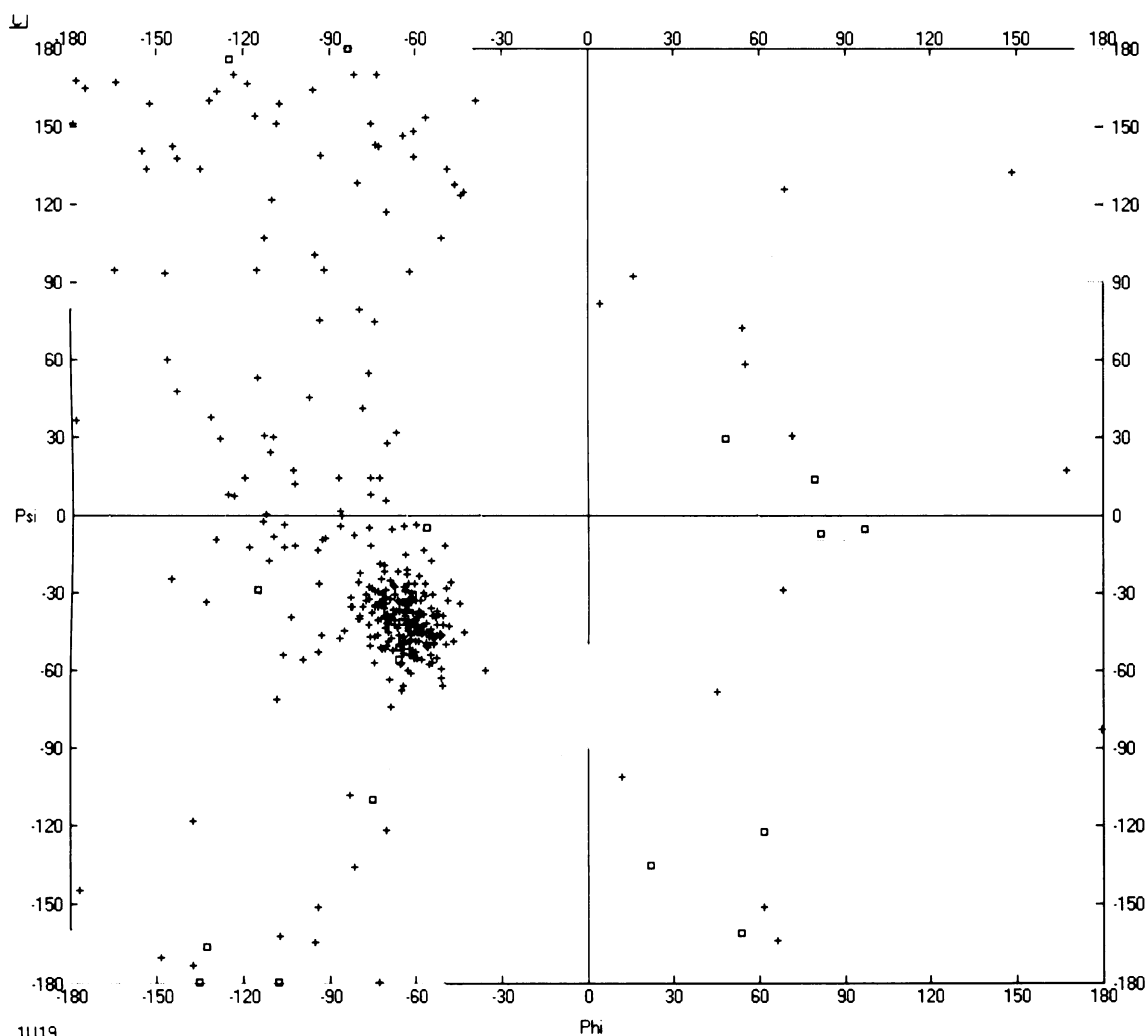


**Figure 1.5** – Ramachandran plot of bovine rhodopsin (PDB ID 1U19, chain A) [25]. Amino acids are visualised as crosses while glycines are visualised as squares. 16 amino acids are in the disallowed region. Anomalous residues S176 and H195 can be found in extracellular loops, whether anomalous residues K141, T229, A235, N238, S240, A241, C323, K325, L328, D331, A333, S338, E341 and P347 have its positions in intracellular domain. Ramachandran plot [27] was generated by DeepView/Swiss-PDBViewer 3.7.

## 1.1.4 Melatonin receptors

Two different affinity groups of melatonin receptor sites have been reported: ML1 (high affinity) sites and ML2 (low affinity) sites. [28, 29]

ML1 melatonin receptors, which belong to the GPCR receptor family, in result act as an inhibitor of adenylase cyclase activity in target cells. Activation of human recombinant melatonin receptors of ML1 subtype inhibits cAMP and cGMP formation. Two types of ML1 receptors were found using PCR analysis in human. These types are called Mel1a (MT1) and Mel1b (MT2). Another subtype (Mel1c) has been found in *Xenopus* fish [30].

On contrary, activation of ML2 (MT3) melatonin receptors is coupled to the stimulation of phosphoinositide hydrolysis.

### 1.1.4.1 MT1 receptor

This type of receptor is expressed in the hypophysial pars tuberalis and the suprachiasmatic nucleus.

Work carried out with recombinant hMT<sub>1</sub> receptors led to the identification of various analogues as inverse agonists (e.g., luzindole, 4P-PDOT) for the MT<sub>1</sub> receptor [31]. (Inverse agonist blocks hMT<sub>2</sub> receptors strengthening hMT<sub>1</sub> signalling).

In certain native tissues (e.g. sheep pars tuberalis, rat cerebral and caudal arteries) melatonin responses are presumably mediated through the activation of MT1 receptors.

MT1 melatonin receptors modulate neuronal firing, arterial vasoconstriction, cell proliferation in cancer cells, and reproductive and metabolic functions [30, 32].

### 1.1.4.2 MT2 receptor

Mel1b melatonin receptor is expressed mainly in retina [33] and, to the lesser extent, in the brain.

The availability of selective MT<sub>2</sub> receptor antagonists (4P-PDOT, 4P-ADOT, luzindole) has led to the identification of functional MT2 melatonin receptors in retina (inhibition of dopamine release) [34], in the circadian timing system (phase shifting of circadian rhythms) [35], induce vasodilatation and inhibition of leukocyte rolling in arterial beds, and enhance immune responses [32].

The mRNA transcripts for MT2 receptors have been localized in the hippocampus using both *in situ* hybridization [9] and RT-PCR analysis [33].



Inhibitory effect of melatonin on long-term potentiation was lost only in mice without MT2 receptors as well as with MT2 selective antagonists [4], while long-term potentiation is considered as a cellular basis of learning and memory.

Luzindole has an anti-depressive effect, which is mediated by MT2 melatonin receptor [36].

#### **1.1.4.3 MT3 melatonin receptors**

The MT3 receptors show different pharmacological profile than MT1 and MT2 melatonin receptors and interacts also with lower nanomolar affinity [37].

Two ligands for MT3 receptors (selective antagonist prazosin, agonist 5-MCA-NAT) do not bind to MT1 or MT2 receptors within hamster brain membranes [38].

At a functional level, MT3 receptors appear to signal through an increase in phosphoinositide turnover. However, MT3 receptor has been recently identified as an enzyme NRH: quinone oxidoreductase 2 (QR2). The relationship between the multiple physiological functions of melatonin and this enzyme remains unclear. Because of the relationship of QR2 with the redox status of cells, these studies could bring the first tools for a molecular rationale of the antioxidant effects of melatonin [39].

## **1.2 General approach of homology modelling**

Approach based on understanding of relationships between the structure and function is widely used in modern drug design (Figure 1.6). However such approach needs structural information, which in many cases is not available.

Comparative or homology modelling is a technique that enables protein structure prediction on the basis of sequence similarity between the target (model) and the template (known 3D structure). Successful model building requires relatively high sequence homology between the template and target sequences.

The starting point is the identification of all known protein structures that share some sequence homology with the target sequence. The second step is the selection of most appropriate structures as modelling templates. Search in the template library with BLASTP2 searching algorithm can be used for this purpose [40].

Next step in the process of model building is the sequence alignment. This task can be performed using various programs like Clustal W [41]. Gaps are thoroughly used to overcome sequence variations between the target and templates. Several factors affect

the final result of structure modelling e.g. the quality of sequence alignment or the modelling algorithm used for model building [42].

Next step is the model building itself. Almost any modelling method described in review by Wallner and Elofsson [42] can be used for this task, for example SwissMODEL server in connection with DeepView/SwissPDBViewer [43] or Modeller package [44].

When the structure of protein-ligand complex is needed, docking procedure can be used to predict the position and interactions of the ligand within the ligand binding site, for example using the Autodock package [45].

Any structural model should be thoroughly evaluated using experimental data gained from structure-function studies (e.g. site-directed mutagenesis).

The structure of protein-ligand complex can be refined using the molecular dynamics (MD) simulation. MD simulations can help to find more realistic structure or predict conformational changes etc. [46]. Several software packages are available for MD calculations like GROMACS [47], AMBER [48], CHARMM [49] or NAMD [50].

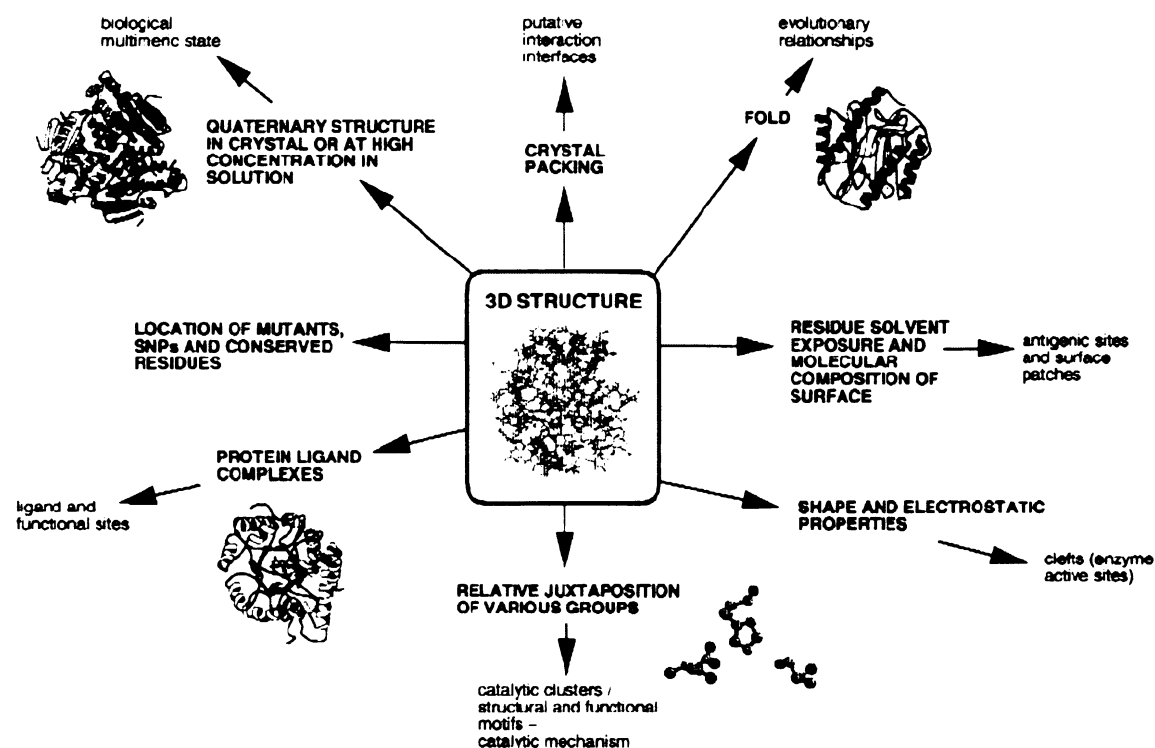


**Figure 1.6** - From structure to function

A summary of information that can be derived from three-dimensional structure, relating to biological function.

Figure taken from Thornton *et al.* [51]

## 1.3 Programs and algorithms

### 1.3.1 Template search

The starting point of protein structure modelling is to identify protein structures closely related to the target sequence. Identification can be performed using different search algorithms e.g. BLAST or PSI-BLAST over structural database.

#### 1.3.1.1 BLAST

The BLAST algorithm is a heuristic search method that seeks „words“ of length  $W$  (default = 3 in blastp) that score at least  $T$  (threshold) when aligned with the query and scored with a substitution matrix. Words in the database that score  $T$  or greater are extended in both directions in an attempt to find a locally optimal ungapped alignment or HSP (high scoring pair) with a score of at least  $S$  (raw score) or an  $E$  (expectance) value lower than the specified threshold. HSPs that meet these criteria will be reported by Blast, provided they do not exceed the cut-off value specified for number of descriptions and/or alignments to report.

Blastp2 is a BLAST version for searching for protein-protein similarities and can be found at NCBI blastp server on <http://www.ncbi.nlm.nih.gov/blast/> (last used 8.3.2006). Blastp template search is done on PDB database.

PDB database [52] contains published experimentally-determined 3D structures of proteins. These structures can be used as templates for homology modelling.

### 1.3.2 Prediction of transmembrane segments

Prediction which parts of the protein structure are located inside the membrane is very useful information for the quality of homology modelling of membrane spanning proteins like human MT2 receptor. Different approaches can be used for this task.

First group of methods investigates local properties of amino acid sequences like hydrophobicity to decide which sub-sequences are most likely to span the membrane, usually in a sliding window approach. We can mention programs DAS [53], SOSUI [54] and TMPred [55] from this group.

PHDhtm [56] should also be in the first group, because of local approach. Main difference is that PHDhtm uses neuronal network instead of sliding window.

Global methods are programs HMMTOP [57] and TMHMM [58, 59], which both implement Hidden Markov Models to determine the statistically most probable topology for the whole protein. The basic principle is to define a set of states, each corresponding to a region or specific site in the proteins being modelled. Each state has an associated probability distribution over the 20 amino acids characterising the variability of amino acids in the region it models. The amino acid probabilities and the transition probabilities are learned by standard inference techniques that compute the maximum posterior probabilities given a prior and the observed frequencies.

Combined approach is represented by programs MEMSAT [60], TMAP [61] and TopPred [62]. Results from local methods are evaluated by global heuristics over the distribution of amino acids, i.e. the positive-inside rule postulates different distribution of positively charged residues in extracellular and intracellular loop regions

From these various groups, programs TMPred, TMHMM and TopPred have been selected for prediction of the membrane topology of hMT2 receptor.

### **1.3.2.1 TMPred**

TMpred algorithm is based on the statistical analysis of TMbase [55], a database of naturally occurring transmembrane proteins. The prediction is made using a combination of several weight-matrices for scoring.

The current release of TMbase (TMbase25) is based on SwissProt release 25. Important data fields include, for example, the putative transmembrane sequence, the sequence of the flanking regions, taxonomic information, the presumed orientation of the segment, calculated values for hydrophobicity and hydrophobic moment, and grouping into families by either functional or sequence relatedness of the proteins.

TMpred is available at [http://www.ch.embnet.org/software/TMPRED\\_form.html](http://www.ch.embnet.org/software/TMPRED_form.html) (last used 8.3.2006).

### **1.3.2.2 TMHMM**

Program TMHMM [58] uses hidden Markov model for transmembrane prediction [59] with an architecture that corresponds closely to the biological system. The model is cyclic with 7 types of states for helix core, helix caps on either side, loop on the cytoplasmic side, two loops for the non-cytoplasmic side, and a globular domain state in the middle of each loop. The two loop paths on the non-cytoplasmic side are used to model short and long loops separately, which corresponds biologically to the two

known different membrane insertions mechanisms.

Another two states were added into version 2.0 for possible globular proteins. Models are estimated both by maximum likelihood and a discriminative method.

TMHMM is available online at <http://www.cbs.dtu.dk/services/TMHMM-2.0/> (last used 8.3.2006).

### **1.3.2.3 TopPred**

TopPred [62] combine two approaches: hydrophobicity scale and positive-inside rule [63]. Program can use three different hydrophobicity scales: Kyte and Doolittle [64], Gunnar and von Heijne [63], and Goldman, Engelman and Steitz [65]. TM segments are then founded on hydrophobicity scale by specified cut-offs.

TopPred is available at <http://bioweb.pasteur.fr/seqanal/interfaces/toppred.html> (last used 8.3.2006).

## **1.3.3 Sequence Alignment**

Comparison or alignment of sequences can be done globally across their entire length or locally in some regions. Global alignment uses gaps for insertions and deletions and is appropriate for sequences that are known to share similarity over their whole length, while local alignment can show ungapped conserved domains.

All alignment algorithms rely on scoring matrix based on observed probability of changes between two amino acids at the same place in protein sequence. Two main scoring matrices for amino acid substitution are PAM (Percentage of Acceptable point Mutations per  $10^8$  years) [66] and BLOSUM (BLOcks SUBstitution Matrix) [67].

There are also two subtracting parameters for governing gaps in global alignment: gap opening penalty (GOP) and gap extension penalty (GEP).

Usual output of the programs is alignment with the highest score.

### **1.3.3.1 Clustal W**

Clustal W is a general purpose multiple sequence alignment program for DNA or proteins. It calculates the best match for the selected sequences with using any probability matrices for amino acid substitution.

Clustal W is available online at <http://www.ebi.ac.uk/clustalw/> (last used 8.3.2006).

### 1.3.3.2 Probability matrices for amino acid substitutions

PAM matrices are based on global alignments of closely related proteins. The PAM 1 is the matrix calculated from comparisons of sequences with no more than 1% divergence. Scores are derived from a mutation probability matrix where each element gives the probability of the amino acid X mutating to the amino acid Y after a particular evolutionary time, for example after 1 PAM, or 1% divergence.

BLOSUM matrices are based on local multiple alignments of more distantly related sequences. For instance, BLOSUM 62, the default matrix in BLAST, is a matrix calculated from comparisons of sequences with no less than 62% identity.

Comparisons of closely related sequences should use BLOSUM matrices with higher numbers and PAM matrices with lower numbers. Conversely, BLOSUM matrices with low numbers and PAM matrices with high numbers are preferable for comparisons of distantly related proteins.

## 1.3.4 Homology modelling

Homology or comparative modelling is a method that enables protein structure modelling on the basis of sequence similarity between the target (model) and the template (known 3D structure). Successful model building requires relatively high sequence homology between the template and target sequences.

### 1.3.4.1 SwissMODEL with Deep View/Swiss PDB Viewer

Model-building using SwissMODEL [43] is composed from several steps:

Firstly program checks sequence identity of target with the model. Then program creates ProMod II run [68], which makes a superposition of template structure or structures to prepare a framework for new sequence. This framework has gaps for new loops. ProMod II builds these lacking loops from internal loop database to complete model backbone. When all alpha carbon atoms are connected, side chains are selected from a library of allowed rotamers sorted by their frequency in template structures. Model is then verified by an analysis of 3D content [69] and Conolly surface areas in comparison with template. Lastly, structure is refined by energy minimization with Gromos96 force field.

User can input just its sequence to produce model with templates from SwissMODEL Blast. Other possibility is providing SwissMODEL with pre-processed alignment. This step can be done also inside program DeepView/SwissPDBViewer

interactively. DeepView program can prepare SwissMODEL jobs including rough first superposition of model backbone on template structure backbone with specified alignment, which can be edited on the fly.

DeepView program is an application for visualization and analysis of protein structures such as measuring of distances and angles, superimposing similar structures, Ramachandran plot, and many more.

SwissMODEL server service and DeepView/SwissPDBViewer program package are available at address <http://swissmodel.expasy.org/> (last used 8.3.2006).

#### **1.3.4.2 Modeller**

Program Modeller implements comparative protein structure modelling by satisfaction of inputted spatial restraints. The output is a 3D structure that satisfies these restraints as well as possible. Restraints can in principle be derived from a number of different sources. These include related protein structures (comparative modelling), NMR experiments (NMR refinement), rules of secondary structure packing (combinatorial modelling), cross-linking experiments, fluorescence spectroscopy, image reconstruction in electron microscopy, site-directed mutagenesis, intuition, residue-residue and atom-atom potentials of mean force, *etc.* The restraints can operate on distances, angles, dihedral angles, pairs of dihedral angles and some other spatial features defined by atoms or pseudo atoms. Modeller automatically derives the restraints only from the known related structures and their alignment with the target sequence.

A 3D model is obtained by optimisation of a molecular probability density function. The molecular probability density function for comparative modelling is optimised with the variable target function procedure in Cartesian space that employs methods of conjugate gradients and molecular dynamics with simulated annealing.

Modeller has many other possibilities including *de novo* modelling of loops in protein structures, optimisation of various models of protein structure with respect to a flexibly defined objective function, multiple alignments of protein sequences and/or structures, clustering, searching in sequence databases, comparison of protein structures, *etc.*

Modeller is available at <http://salilab.org/modeller/> (last used 8.3.2006).

## 1.3.5 Ligand docking

Ligand docking predicts the structure of protein-ligand complex. Structure of the complex is predicted by search in protein potential energy surface. Programs use variety of algorithms for this purpose; *i.e.* simulated annealing, Monte Carlo search or genetic Lamarckian search algorithm.

### 1.3.5.1 AUTODOCK

AutoDock [45] is a suite of automated docking tools. It can predict binding of ligands to a receptor of known or predicted 3D structure. AutoDock package implements a rapid energy evaluation by precalculating atomic affinity grids. Search procedures (simulated annealing or genetic algorithms with local search) then seek in grids for global minimum.

Program suite contains three programs whose inputs and outputs cooperate with graphical front-end AutoDockTools. Docking analysis starts with program AutoTors prepares ligand and selects rotatable bonds of the ligands. Program AutoGrid then calculates atom affinity grids in specified space of the receptor and lastly program AutoDock performs the docking search of the ligand. Each of these steps can be governed from AutoDockTools interface. AutoDockTools package also contains a viewer that enables with visual analysis of docking complexes sorted by docking energy.

Program can be downloaded at <http://www.scripps.edu/mb/olson/doc/autodock/> (last used 12.3.2006).

### 1.3.5.2 PRODRG server service

The Dundee PRODRG2 server converts coordinates for small molecules in PDB format or by drawing molecules online to the following topology formats: AutoDock, GROMOS, GROMACS, WHAT IF, REFMAC5, CNS, O, SHELX, HEX and MOL2. In addition, coordinates for hydrogen atoms are generated. PRODRG2.5 with more options is now available in beta stage.

PRODRG server can be found <http://davapc1.bioch.dundee.ac.uk/programs/prodrgr/> (last used 12.3.2006).



## 1.3.6 Molecular dynamics

The structure of protein-ligand complex can be refined using molecular dynamics (MD) simulation. Processes such as melting, adsorption, segregation, formation of molecular complexes, and protein denaturation can be analyzed, and phenomena such as protein or complex stability, conformational changes in time, enzyme reactivity and membrane permeability can be investigated by MD. Such studies may lead not only to improved understanding of protein function, but also to practical results such as engineered proteins or materials with properties optimized for particular applications [46, 70]

### 1.3.6.1 Basics of molecular dynamics

Molecular dynamics simulations calculate future positions and velocities of particles, based on their current positions, velocities and molecular structure using basic Newton's equations of motion.

The force on a particle  $i$ ,  $\mathbf{F}_i$  is equal to the negative gradient of the potential energy,  $U$ , which is stored in database structure called force field:

$$\mathbf{F}_i = -\nabla_i U(\mathbf{r}_1, \dots, \mathbf{r}_N) = -\frac{\partial U(\mathbf{r}_1, \dots, \mathbf{r}_N)}{\partial \mathbf{r}_i}, \quad (1.1)$$

where  $N$  is the number of particles or atoms in system and  $\mathbf{r}_i$  is vector of a position of particle  $i$ .

This force accelerates particle with acceleration  $\mathbf{a}_i(t)$  at a given time:

$$\mathbf{F}_i = m_i \mathbf{a}_i(t) = m_i \frac{d^2 \mathbf{r}_i(t)}{dt^2}, \quad (1.2)$$

where  $m_i$  is mass of the particle. Equations (1.1) and (1.2) given together yields:

$$-\frac{\partial U(\mathbf{r}_1, \dots, \mathbf{r}_N)}{\partial \mathbf{r}_i(t)} = m_i \frac{d^2 \mathbf{r}_i(t)}{dt^2}, \quad (1.3)$$

which is the equation of motion for the molecular system of  $N$  particles.

The potential functions  $U$  can be subdivided into three parts:

1. *Non-bonded*: Lennard-Jones (LJ) or Buckingham, and Coulomb or modified Coulomb interactions. The nonbonded interactions are computed on the basis of a neighbour list (a list of non-bonded atoms within a certain radius), in which exclusions are already removed.

2. *Bonded*: covalent bond stretching, angle-bending, improper dihedrals, and proper dihedrals. These are computed on the basis of fixed lists of atom groups.
3. *Special*: position restraints and distance restraints, based on fixed lists based on topology of the system.

Due to the complicated nature of potential energy function, which is given by all of above interactions, there is no analytical solution to the equation (1.3). Solution is numerical integration within small steps (usually in the femtosecond-scale).

Initial positions and velocities of particles are needed for start of the molecular dynamics simulation. The coordinates of initial position are provided from model structure after energy minimization to reduce the potential energy of the system. Initial distribution of velocities is determined from a random Gaussian distribution conforming to the required temperature and corrected to diminish an overall momentum motion. Temperature  $T$  is easily calculated from kinetic energy and equipartition theorem:

$$T = \frac{\sum_{i=1}^N m_i \mathbf{v}_i^2}{3N k_B}, \quad (1.4)$$

while  $\mathbf{v}_i$  is velocity of particle  $i$  and  $k_B$  is the Boltzmann constant.

Evolving of the system is then directed by time integration algorithm like Leap-frog, which uses old positions  $\mathbf{r}_i(t)$  and velocities  $\mathbf{v}_i(t + \frac{1}{2}\delta t)$  to compute new positions  $\mathbf{r}_i(t + \delta t)$  after the small time step  $\delta t$ :

$$\mathbf{r}_i(t + \delta t) = \mathbf{r}_i(t) + \mathbf{v}_i(t + \frac{1}{2}\delta t)\delta t, \quad (1.5)$$

Velocities are also updated with the same time step frequency, but “leap” over position updates with  $\frac{1}{2}\delta t$ :

$$\mathbf{v}_i(t + \frac{1}{2}\delta t) = \mathbf{v}_i(t - \frac{1}{2}\delta t) + \mathbf{a}_i(t)\delta t, \quad (1.6)$$

while  $\mathbf{a}_i(t)$  is computed from potential  $U$  at time  $t$  with equation (1.3).

This global MD schema is further refined with additional scaling to assure compact structures and correct NPT ensemble.

Methods for constant temperature or pressure uses scaling factors  $\lambda$  or  $\mu$ , respectively, to compute scaled velocities,  $\mathbf{v}'(t)$ :

$$\mathbf{v}'(t + \frac{1}{2}\delta t) = \lambda \left( \mathbf{v}(t + \frac{1}{2}\delta t) + \mathbf{a}(t)\delta t \right). \quad (1.7)$$

New unconstrained coordinates  $\mathbf{r}'$  are then computed from scaled velocities:

$$\mathbf{r}'(t + \delta t) = \mathbf{r}(t) + \mathbf{v}'(t + \frac{1}{2}\delta t)\delta t. \quad (1.8)$$

Constraint algorithm is then applied on coordinates  $\mathbf{r}'$  to gain constrained coordinates,  $\mathbf{r}''$ . Velocities are then finally corrected:

$$\mathbf{v}''(t + \frac{1}{2}\delta t) = \frac{\mathbf{r}''(t + \delta t) - \mathbf{r}(t)}{\delta t}, \quad (1.9)$$

where  $\mathbf{v}''$  are corrected velocities.

And lastly whole simulation box and all atom coordinates are scaled according to pressure coupling with factor  $\mu$ :

$$\mathbf{b}(t + \delta t) = \mu \cdot \mathbf{b}(t), \quad (1.10)$$

$$\mathbf{r}(t + \delta t) = \mu \cdot \mathbf{r}''(t + \delta t), \quad (1.11)$$

where  $\mathbf{b}$  is a vector of box boundaries and  $\mathbf{r}(t+\delta t)$  are starting coordinates for next integration step. Forces are not usually scaled.

Constant temperature can be assured with several methods, like Berendsen weak coupling [71] to the external heat bath or Nosé-Hoover time step variation [72, 73].

Berendsen temperature coupling uses with velocity scaling scalar factor,  $\lambda$ ,

$$\lambda = \left[ 1 + \frac{\delta t}{\tau_T} \left\{ \frac{T_0}{T\left(t - \frac{\delta t}{2}\right)} - 1 \right\} \right]^{\frac{1}{2}}, \quad (1.12)$$

where  $T_0$  is temperature of the external heat bath,  $T$  is actual temperature of the system computed from equation (1.4) and  $\tau_T$  is a temperature-coupling time parameter.

Berendsen pressure coupling uses coordinates scaling tensor factor,  $\mu$ ,

$$\mu_{ij} = \delta_{ij} - \frac{\delta t}{3\tau_p} \beta_{ij} \{P_{0,ij} - P_{ij}(t)\}, \quad (1.13)$$

where  $\delta_{ij}$  is a Kronecker delta,  $\beta_{ij}$  is a tensor of system compressibility,  $P_{0,ij}$  is reference pressure,  $P_{ij}(t)$  is actual pressure and  $\tau_p$  is a pressure-coupling time parameter.

### 1.3.6.2 GROMACS

Gromacs [47, 74] is a package for molecular dynamics simulations. It is primarily designed for biochemical molecules like proteins and lipids that have a lot of complicated bonded interactions. It contains a fully automated topology builder for proteins, nucleotides, several sugars and lipids, and some special groups like hemes and

several small molecules. It also contains several possible algorithms for temperature or pressure coupling like Berendsen [71] or Nosé-Hoover [72, 73]. Constraints for bonds, angles and dihedrals can be solved by two-step LINCS [75] algorithm or by standard iterative SHAKE [76] algorithm. Gromacs can also use different force fields: united atom force fields like Gromacs (which is based on Gromos87 [77], with some modifications [78-82]) or Gromos96 [83], or all-atom force field OPLS-AA/L [84].

Tools for further trajectory analysis like cluster analysis; Ramachandran plots; essential analysis, *etc.* are also parts of the Gromacs package.

Gromacs is free software, available under the GNU General Public Licence at <http://www.gromacs.org> (last used 19.3.06)

### 1.3.7 Experimental binding assays

Binding assays are thoroughly used for determination of the affinity of the ligand to the receptor. There are basically two types of binding assays:

- Saturation assays for the determination of the receptor expression level and the affinity of the receptor to the specific ligand.
- Competition assays for the determination of the affinity of possible drug in comparison with standard labelled ligand.

Each type of the binding assay needs to be performed as precisely as possible. Radioactive labelling helps to watch for the picomolar concentrations of the ligands.

Binding in saturation assay is compiled from two main parts: selective binding to the receptor and nonselective adsorption to the membrane itself. This type of binding can be described using the following equation:

$$B = \frac{B_{\max} \cdot [\text{ligand}]}{K_d + [\text{ligand}] + K_{\text{nsp}} \cdot [\text{ligand}]}, \quad (1.14)$$

where B is an amount of bound radioligand in fmol.mg<sup>-1</sup>; B<sub>max</sub> is an amount of binding sites per mg of the membrane tissue or protein; K<sub>nsp</sub> is a constant for non-specific adsorption of the ligand; and K<sub>d</sub> is a dissociation equilibration constant.

B<sub>max</sub> value can be used as a measure of receptor expression. K<sub>d</sub> is a measure of a receptor affinity to the ligand and its value is roughly the concentration of the ligand that 50% of the ligand-binding sites are saturated. The higher value of the dissociation equilibration constant means lower affinity of the ligand to the receptor. Non-specific binding constant K<sub>nsp</sub> stands for adhesion of ligand to the membranes.

## 2 Goals of diploma thesis

Main goals of this diploma thesis are:

- Structural modelling of human melatonin MT2 receptor.
- Prediction of amino acid residues potentially involved in ligand binding for site-directed mutagenesis.
- Docking of the 2-iodomelatonin molecule into the predicted ligand binding site
- Participate in site-directed mutagenesis of human MT2 melatonin receptor.
- Test ligand binding affinity of created MT2 receptor mutants.
- Compare homology models of MT2 receptor with data obtained from site-directed mutagenesis.

## **3 Materials & Methods**

### **3.1 Theoretical part**

#### **3.1.1 Sequence**

Sequence NP\_005950 [33] from PubMed repository (Appendix 8.1) has been thoroughly used for modelling studies of human MT2 melatonin receptor.

#### **3.1.2 Template search**

Blastp 2.2.13 [85] on <http://www.ncbi.nlm.nih.gov/blast/> (last used 30.11.2005) was used for template search. PDB database [52] was used as a reference, while Conserved Domains search was done. Other parameters were: word length 3, expect value 10 and Blossum62 matrix.

#### **3.1.3 Trans membrane region prediction**

TMPred at [http://www.ch.embnet.org/software/TMPRED\\_form.html](http://www.ch.embnet.org/software/TMPRED_form.html) (last used 2.12.2005) was used for prediction with TMbase 25. Length of possible TM helices was set to be at least 17 amino acids and most 33 amino acids long.

For TopPred prediction at <http://bioweb.pasteur.fr/seqanal/interfaces/toppred.html> (last used 2.12.2005) was used GES hydrophobicity scale. Standard values were used with exception of organism, where eukaryote had been used instead of prokaryote.

TMHMM v. 2.0 was used at <http://www.cbs.dtu.dk/services/TMHMM-2.0/> (last used 2.12.2005).

#### **3.1.4 Homology modelling**

As a template we used bovine rhodopsin in the dark state from the protein PDB databank [52] (PDB access codes 1F88 [1] and 1U19 [25]), which is the only GPCR receptor with known 3D structure.

Sequence alignments were prepared using the program ClustalW [41] and modified using DeepView/SwissPDBViewer v3.7 program [86] or manually according to the literature [87].

Modelling of the hMT2 receptor was performed by DeepView/SwissPDBViewer v3.7 with connection to Swiss-MODEL server and by Modeller v 8.1 [44] in automatic all-hydrogen mode. Modeller produced ten models and model with the lowest pseudopotential function was brought into the comparison with SwissMODEL models.

### 3.1.5 Automated ligand docking

Autodock 3.05 in conjunction with AutoDockTools was used for automated docking. Models of the human MT2 melatonin receptors were repaired for missing hydrogen atoms and Kollman charges were added according to the residue list. Non-integral charge was spreaded over first amino acid and solvent parameters were added.

Parameter file for 2-iodomelatonin structure was prepared by PRODRG server [88] with full charges, chirality and energy mineralization at sketch mode on web address <http://davapc1.bioch.dundee.ac.uk/programs/prodrg/> (last used 4.12.2005) to obtain coordinate and topology file for automated docking with Autodock. Grid map types were CANOHI. At least 40 points in each direction with spacing 0.375 Å were used for AutoGrid mapping of the ligand-binding site (*e.g.* box of length at least 15 Å in each direction was used for mapping of the ligand-binding site of the receptor).

Combined genetic algorithm with local search was used for docking in prepared grid. 50 runs of Lamarckian genetic algorithm were used for each of 50 starts with maximum of 500 000 energy evaluation followed with local search with 500 iterations.

Results were clustered by positional root mean square deviation (RMSD) with cut-off 2.0 Å. The most populated cluster with the lowest binding energy was taken for further refinement with molecular dynamics simulation.

### 3.1.6 Molecular dynamics

Molecular dynamics simulations were performed with Gromacs 3.1.2 with standard Gromacs force field ffgmx with incorporated parameters for lipid molecules (obtained from Gromacs topology repository <http://www.gromacs.org/>) (browsed 5.12.2005) Changes in the force field are based on work of Tieleman group [89].

Starting system for MD simulation was an already equilibrated box of hydrated lipid bilayer build from 260 molecules of 1-palmitoyl-2-oleoyl-*sn*-glycero-3-phosphoethanolamine (POPE) whose coordinates and topologies were downloaded from Tieleman's site [90] <http://www.ucalgary.ca/~tieleman/download.html>, (last used 5.12.2005). Original box was extended to 9.5·9.5·10 nm and the membrane was further

equilibrated for 700 ps and the final structure has been used to construct the simulation system with the hMT2 melatonin receptor.

Melatonin coordinates were excluded from 2-iodomelatonin coordinates (result of automated docking) by deleting the iodine atom. Melatonin topology in Gromacs format was prepared from coordinates on PRODRG server with full charges and chirality but without energy minimization to obtain coordinate and topology files for Gromacs. Iodine was deleted because of lack of force field definition and partial charges deficiency for this atom on PRODRG server.

Protein model was rotated with a docked ligand so helix H4 was perpendicular to the membrane plane [26] and centred inside the simulation box into the equilibrated membrane. Overlapping lipids and waters were excluded from the simulation box. System contained one MT2 receptor-melatonin complex, 253 molecules of POPE, 13 chloride anions and 15143 molecules of water (approximately 62100 atoms)

Whole system was energy minimized by 750 steps of steepest-descent energy minimization (see Appendix 8.4.1). All heavy atoms of the MT2 receptor and melatonin molecule were positionally restrained and short 50 ps long MD run has been performed to relax the lipids and water molecules (see Appendix 8.4.2). System was then set completely free and equilibrated for additional 200 ps. Production run was 300 ps long (see Appendix 8.4.3).

Produced trajectories were analysed using clustering by root mean square deviation 0.15 Å with gromos algorithm [91]. Average structure of the MT2 receptor-melatonin complex from the greatest cluster was energy minimized with steepest descent energy minimization *in vacuo* (see Appendix 8.4.4), followed by finer energy minimization with conjugated gradients (see Appendix 8.4.5).



## 3.2 Experimental methods

### 3.2.1 Materials

A cDNA containing the coding sequence of the hMT2 receptor cloned into pcDNA3 vector was kindly gifted by DrS. M. Reppert. HEK293 cells were provided by American TypeCultureCollection. Cell culture media, supplements and sera were purchased from Sigma Aldrich (St Louis, MO, USA), 2-iodomelatonin (2000 Ci/mmol) was obtained from Amersham Biosciences (Piscataway, NJ, USA). Molecular biology reagents were purchased from New England Biolabs (Beverly, MA, USA) or Stratagene (La Jolla, CA, USA). Melatonin and general reagents were obtained from Sigma Aldrich. The anti-FLAG M2 monoclonal antibody was obtained from Sigma Aldrich (USA) and the horse fluorescein conjugated anti-mouse IgG antibody was purchased from Vector Laboratories (Burlingame, CA, USA)

### 3.2.2 Site directed mutagenesis of Gly121

*In vitro* site-directed mutagenesis using PCR is based on reannealing of the DNA with slightly different oligonucleotides. These short oligonucleotides are complementary to the template DNA except of one specified codon sequence. Thermostable DNA polymerase (*Taq*, *Pfu*) then starts to produce new DNA strains along the template with oligonucleotides as primers.

A PCR-based mutagenesis (QuikChange site-directed mutagenesis kit, Stratagene, USA) was performed using coding sequence for hMT2 in the plasmid pcDNA3 (Invitrogene, USA, see Appendix 8.2.1) as a template and oligonucleotides (synthesized by VBC-Genomics, Austria) introducing specific point mutations into the DNA of the receptor (Table 3.1). Following PCR program with mixture (Table 3.2) was used:

20 x	[	95 °C for 30 s	denaturation of double stranded DNA
		67 °C for 1 min	annealing of oligonucleotides with single stranded DNA
		72 °C for 12 min	synthesis of the new strand with <i>Pfu</i> polymerase
		4 °C until end	storing temperature.

1  $\mu\text{L}$  of solution with Dpn I enzyme (enzymatic activity 20  $\text{U}\cdot\mu\text{L}^{-1}$ , New England Biolabs, Canada) was added to the mixture to cleave the original methylated bacterial DNA. Mixture was then incubated for 2 hours at 37 °C for this purpose.

The presence of the mutations and the integrity of the rest of the gene were confirmed by automated DNA sequencing (ABI Prism, Amersham, USA).

**Table 3.1** – Oligonucleotides for mutation G121A (VBC-Genomics, Austria)

G121A up	5' - C AGC GCC TTT GTG ATG <b>GCC</b> CTG AGC GTC ATC GGC - 3' S A F V M A L S V I G
G121A down	5' - GCC GAT GAC GCT CAG GGC CAT CAC AAA GGC GCT G - 3'

**Table 3.2** – Composition of PCR mixture

Compound	Final concentration [nmol.dm <sup>-3</sup> ]	Volume [μL]
10 x concentrated <i>Pfu</i> buffer turbo	various*	5
cDNA template for hMT2 melatonin receptor	40	1.5
G121A up oligonucleotide	100	5
G121A down oligonucleotide	100	5
Mixture of deoxyribotriphosphonucleotides (dNTP)	4000	2
Water	55.6 · 10 <sup>9</sup>	30.5
<i>Pfu</i> polymerase turbo – activity 2.5 U.μL <sup>-1</sup>	-	1

\* *Pfu* buffer turbo composition: 0.1 M KCl, 0.1 M (NH<sub>4</sub>)<sub>2</sub>SO<sub>4</sub>, 0.2 M Tris-HCl (pH 8.8), 20 mM MgSO<sub>4</sub>, 1% Triton X-100, 1 g.cm<sup>-3</sup> BSA. *Pfu* polymerase kit from Stratagene, USA.

### 3.2.3 Transfection

HEK293 is the cell line which was generated by transformation of human embryonic kidney cell cultures with sheared adenovirus 5 DNA [92]. HEK 293 cells were grown as monolayers in Dulbecco's modified Eagle medium (DMEM) supplemented with 10% (v/v) fetal bovine serum, penicillin (50 U.mL<sup>-1</sup>) and streptomycin (50 μg.mL<sup>-1</sup>) in 95% O<sub>2</sub> / 5% CO<sub>2</sub> at 37 °C. Cultures at 90% confluence were transiently transfected using Lipofectamine 2000 transfection reagent (Invitrogene, USA). Cultures were transfected either with wild-type hMT2 melatonin receptor cDNA in pFLAG-CMV-2 plasmid (Sigma Aldrich, USA, see Appendix 8.2.2) or with the cDNA construct carrying desired mutations (*i.e.* pFLAG-hMT2-G121A).

For binding assays, the plates (100 mm) with cells were washed after 48 h with phosphate-buffered saline solution (PBS, pH 7.4) containing 5 mM EDTA and

harvested by gentle scraping. Cells were pelleted by centrifugation (1600 g, 6 min, 4°C) and dry pellets were stored in aliquots at -70°C.

For immunological studies, the cells were after 24 h trypsinized and reseeded onto poly L-lysine-treated cover slips and allowed to grow for an additional 24 h.

### **3.2.4 Binding assays**

Cell pellets were resuspended in binding buffer (50 mM Tris-HCl, pH 7.4) and in saturation assays incubated for 1.5 h at 37°C in final volume 150 µL with 2 – 1250 pM 2-iodomelatonin (approx. activity 2200 mCi/mL during experiment).

Non-specific binding was assessed in the presence of 1 µM melatonin and typically 2 - 6 µg of cell protein per tube was used for experiment as determined by the method of Bradford [93]. Incubation was terminated by addition of 3 mL of ice-cold binding buffer and bound and free ligands were separated by immediate vacuum filtration through Whatman GF/B filters. Radioactivity was measured by gamma counter with 55% efficiency (Packard Cobra, Perkin-Elmer, USA). Binding data were analyzed using the PRISM 4.0 program (GraphPad software, USA). Presented binding data represent results from triplicate experiments performed on two batches of transfected cells.

### **3.2.5 Immunocytochemistry**

Cells were rinsed briefly in PBS solution (pH 7.4) and then fixed for 15 min in 2% paraformaldehyde in PBS. To block non-specific binding, fixed cells were washed three times for 5 min with PBS and then incubated for 15 min at room temperature in antibody diluent (3% horse serum in PBS with 0.05% Tween 20). Cells were then incubated with anti-FLAG M2 monoclonal antibody (1 : 200, Sigma Aldrich, USA) for 1 h at 37°C. After that, the cells were washed three times for 5 min with PBS and incubated with horse anti-mouse fluorescein conjugated antibody for 1 h (1 : 200) at room temperature. Following three successive washes with PBS the cells were mounted in Vectashield medium (Vector Laboratories, USA) onto glass slides. Slides were viewed using Leica TCS 1-B laser scanning confocal microscope (Leica Microsystems, Germany).

# 4 Results

## 4.1 Result from theoretical part

### 4.1.1 Template search

First step in the process of model building was the search for the appropriate template structure. Blastp 2.2.13 program has been used to search for templates for homology modelling of human MT2 receptor. Blastp found 7 similar structures (PDB codes 1LN6, 1JFP, 1U19, and 1GZM, 1L9H, 1HZX and 1F88). All found structures were basically identical structures of bovine rhodopsin. Structures 1F88 and 1U19 were used for further modelling. Both 1F88 and 1U19 have suitable resolution for protein structure modelling - 2.80 Å and 2.20 Å, respectively. Structure 1U19 was used for modelling of possible disulphide bridge according to the literature [87].

### 4.1.2 Trans membrane predictions

Transmembrane segments of MT2 receptor were predicted using TMPred, TopPred and TMHMM programs. All these programs predicted 7 TM segments at very similar positions within the MT2 sequence.

Hydrophobicity profile confirmed 7 TM segments (Figure 4.1). This algorithm also suggests that the C-terminus might interact with the G-proteins through hydrophobic interactions.

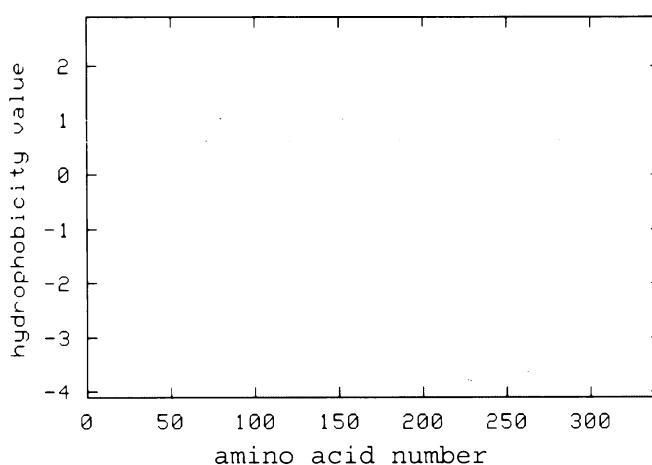


**Figure 4.1** – GES hydrophobicity profile of hMT2 sequence. Hydrophobicity peaks suggest 7 TM segments.

Program TMPred calculated two possible TM predictions (Figure 4.2); more plausible with the N-terminus located outside the cell and less probable with N-terminus predicted to be located inside the cell. Former prediction is in general agreement with the fact that N-terminus of GPCR is extracellular.

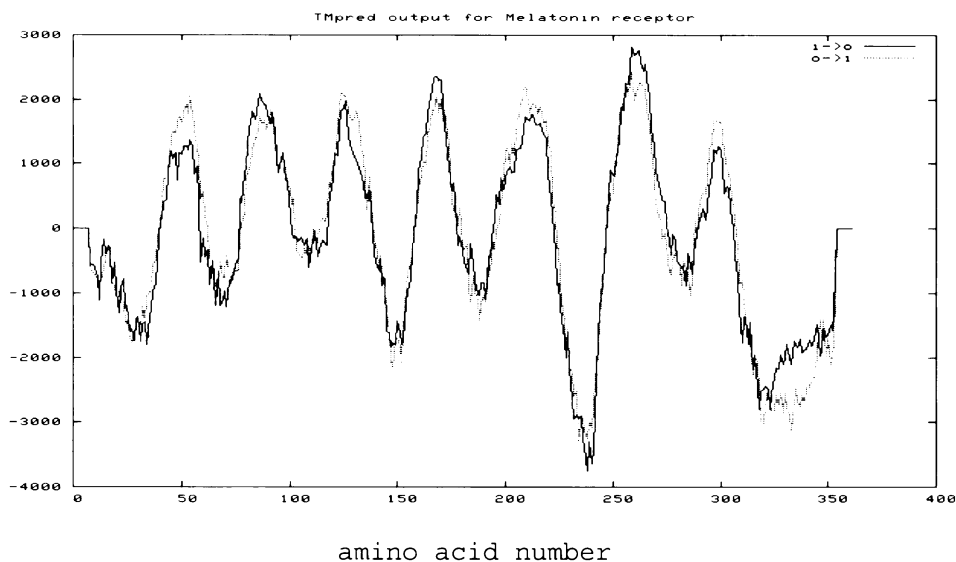


**Figure 4.2** – TMPred prediction results. Transmembrane segments are predicted within regions above zero level. Zero levels at the start and the end of hMT2 sequence are artefacts of the sliding window approach.

Program TopPred predicted slightly shifted TM positions, but confirmed extracellular N-terminus (Figure 4.3).

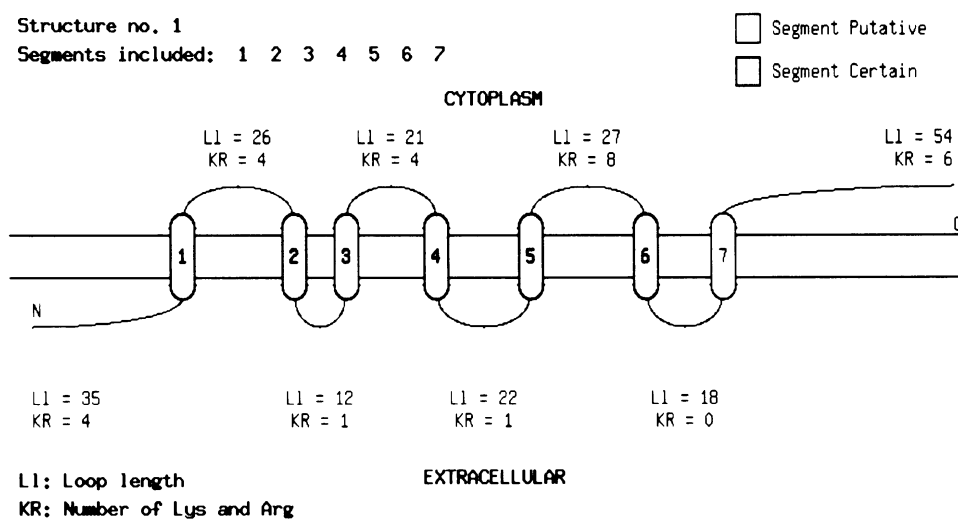


**Figure 4.3** – TopPred prediction results. Positive-inside rule is tracked by number of Lys and Arg in loops. Loops with higher numbers of positive residues are considered to be inside cell.[63]

Result obtained using the TMHMM program was also in a good agreement with other TM predictions (Figure 4.4).

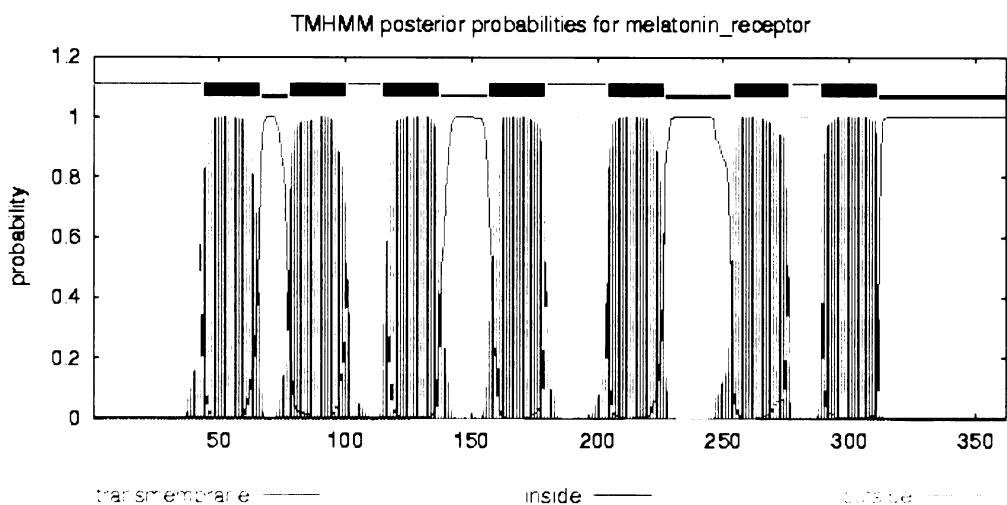


**Figure 4.4** – TMHMM prediction results. Prediction of HMM models for extracellular (violet), transmembrane (red) and cytosolic (blue) content for hMT2 receptor sequence.

### 4.1.3 Consensus TM prediction

Figure 4.5 shows consensus TM prediction, which was prepared as a superposition of previous transmembrane predictions.

```

MSENG SFANC CEAGG WAVRP GWSGA GSARP SRTPR PPWVA PALSA
VLIVT TAVDV VGNLL VILSV LRNRK LRNAG NLFLV SLALA DLVVA
FYPYP LILVA IFYDG WALGE EHCKA SAFVM GLSVI GSVFN ITAIA
INRYC YICHS MAYHR IYRRW HTPLH ICLIW LLTVV ALLPN FFVGS
LEYDP RIYSC TFIQT ASTQY TAAVV VIHFL LPIAV VSFCY LRIWV
LVLQA RRKAK PESRL CLKPS DLRSF LTMFV VEVIF AICWA PLNCI
GLAVA INPQE MAPQI PEGLF VTSYL LAYFN SCLNA IVYGL LNQNF
RREYK RILLA LWNPR HCIQD ASKGS HA EGL QSPAP PIIGV QHQAD AL

```

**Figure 4.5** – Consensus TM prediction. Amino acids in red colour have been predicted by all programs; underlined amino acids have been predicted by all predictions except one.

All calculated TM predictions were in relatively good agreement with membrane topology suggested for GPCR receptors in the literature [26]. All used programs predicted hydrophobic cores of all seven TM segments. Minor differences were in the prediction of the length of some TM segments (especially TM 5 and TM 6).

#### 4.1.4 Alignments

Success of the modelling process is closely related to the quality of the sequence alignment. Three different alignments have been generated based on following rules and assumptions:

**Alignment I** - This alignment is based on Clustal W pair-wise alignment of hMT2 receptor sequence with the sequence of bovine rhodopsine (see Appendix 8.3.1).

**Alignment II** - This alignment was created using the pseudopotential threading energy function [94] in program DeepView/SwissPDBViewer – (see Appendix 8.3.2).

**Alignment III** - Last alignment is based on the alignment recently published by Rivara *et al.* [87]. Main difference between Alignment III and Alignments I and II is in the regions around residues Cys113 and Cys190 of hMT2 receptor sequence. These cysteines residues are exactly matched with the residues Cys110 and Cys187, respectively, in the rhodopsin sequence. Residues Cys110 and Cys187 in bovine rhodopsin form disulphide bridge within the extracellular loop ECL2. Alignment according to Rivara *et al.* [87] tries to conserve this possible disulphide bridge in the model of hMT2 melatonin receptor – (see Appendix 8.3.3).

Table 4.1 summarizes quality of calculated Alignments I-III by their sequence identity and homology. Homologous residues are residues that match identical or similar residues in aligned sequence.

**Table 4.1** – Alignment quality table.

Model prediction quality is highly dependent on percentage of sequence identity with template. You can see slightly better conservation of residues in the TM segments. Alignment II has the highest number of identities, while alignment I has the best homology.

Alignment	Overall identities [%]	Overall homology [%]	Identities in TM segments [%]	Homology in TM segments [%]
I	19,0	<b>45,0</b>	<b>21,0</b>	<b>54,2</b>
II	<b>19,3</b>	41,7	<b>21,0</b>	50,0
III	17,7	43,4	19,9	53,0

## 4.1.5 Homology model building

First models were generated with DeepView/SwissPDBViewer in connection with SwissMODEL server using the structure 1F88 (resolution 2.80 Å) as a template. Since in 2004 another more complete crystal structure of bovine rhodopsin was solved (PDB access code 1U19, resolution 2.20 Å), the last model based on Alignment III (Rivara *et al.* (2005) [87]) was builded using this structure. However, the DeepView /SwissPDBViewer package was not able to model possible disulphide bridge [87, 95] between the Cys113 and Cys190 based on Alignment III. Therefore another modelling software (Modeller v8.1 package) has been employed to create another set of hMT2 receptor models where the model based on Alignment III contains predicted disulphide bridge. At the end 6 model structures have been obtained, 3 using the DeepView/SwissPDBViewer and 3 using the Modeller v8.1 package.

All 6 models have very similar structure of TM segments; the RMS deviation of C $\alpha$  in TM segments is between 0.29-0.80 Å (Table 4.2). Major structural variability can be seen in regions of the flexible loops where the sequence homology with the template is relatively low. Table 4.3 contains RMSDs between the models based on the same alignment but created using different programs. Main variations are caused by different loop building algorithms implemented in DeepView and Modeller programs.

**Table 4.2** – Comparison of models with 1U19 structure.

Positional RMSD in Å between models to the rhodopsine template. The most similar model to the bovine rhodopsin was Modeller model III.

Program	DeepView/SwissPDBViewer			Modeller		
	I	II	III	I	II	III
Alignment						
C $\alpha$ in TM segments [Å]	0.68	0.73	0.42	0.57	0.80	<b>0.29</b>
C $\alpha$ in whole protein [Å]	1.96	1.83	2.92	1.78	2.17	<b>0.86</b>

**Table 4.3** – Comparison of modelling programs.

This table shows positional RMSD between models based on the same alignment. Models were generated with SwissMODEL and Modeller. Please note very small differences in TM regions and between models based on Alignment I. The highest variability can be seen in loop regions between models based on Alignment III.

RMSD [Å]	Alignment I	Alignment II	Alignment III
C $\alpha$ in TM segments	<b>0.48</b>	0.63	<b>0.48</b>
C $\alpha$ in whole protein	<b>2.90</b>	3.78	3.99



#### 4.1.5.1 Models based on Alignment I



**Figure 4.6** – Comparison of models obtained using the Alignment I. Superimposition of models (in cartoon representation) calculated using Modeller (red) and SwissMODEL (green). Cysteines position (yellow) are described in more detail in Figure 4.7

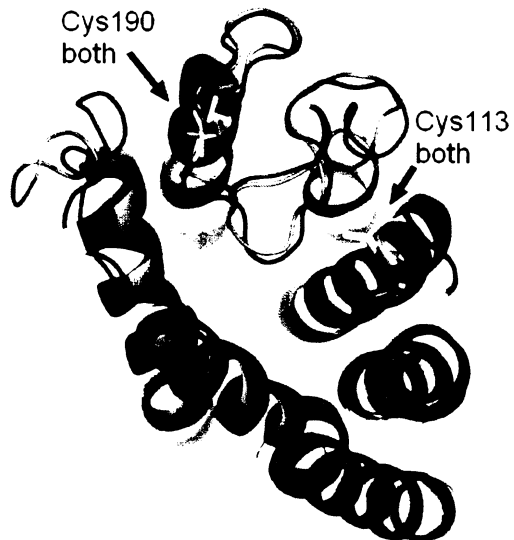


**Figure 4.7** – Position of cysteines in models based on Alignment I. Cysteines (yellow) have almost the same positions in both models, while not forming disulphide bridge.

Models were very similar even in loop regions as can be seen on Figure 4.6. Comparison of positional RMSD for alpha carbons (Table 4.3) also confirms high degree of similarity between models calculated on the basis of the same sequence alignment using two different programs. Cysteine residues potentially involved in disulphide bridge formation have almost the same position in both models. The distance between SH groups is too large to form the disulphide bridge (Figure 4.7).

Since these models are practically identical the model generated using the SwissMODEL has been arbitrary chosen for further study (Model I).

#### 4.1.5.2 Models based on Alignment II

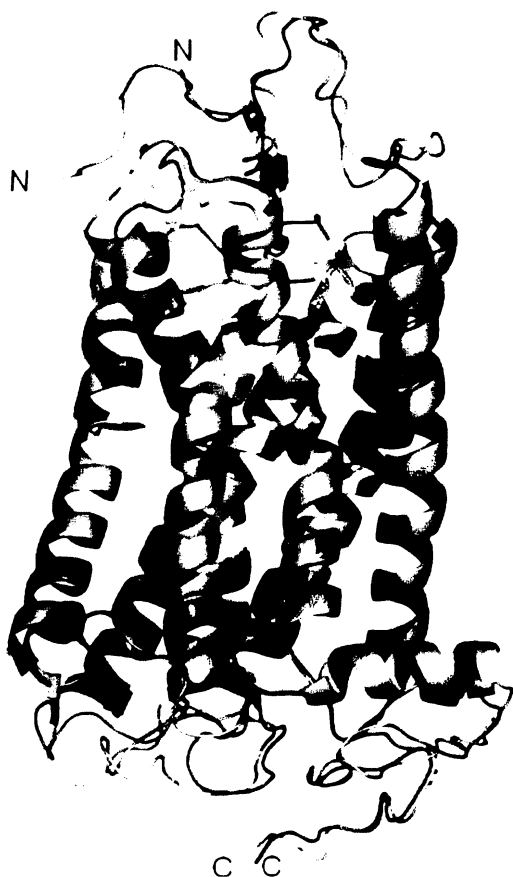


**Figure 4.8** - Comparison of models obtained using the Alignment II. Superimposition of models (in cartoon representation) calculated using Modeller (red) and SwissMODEL (green). Cysteine position (yellow) are described in more detail in Figure 4.9

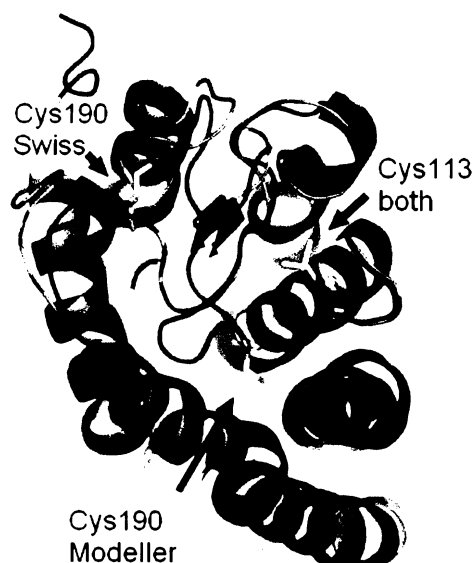


**Figure 4.9** - Position of cysteines in models based on Alignment II. Mark the changes of a position of Cys190 in extracellular loop ECL2 in both models. Modeller model Cys190 lies in proximity of its Cys113, while not forming disulphide bridge.

Models based on Alignment II differ from each other more significantly than models based on Alignment I (Figure 4.8). Position of Cys113 seems to be conserved in all models, while main difference can be seen in the conformation of ECL2 loop containing Cys190. Residue Cys190 in Modeller model is relatively close to the residue Cys113; but not close enough to form disulphide bridge. On the other hand, in SwissMODEL model residue Cys190 has almost the same position as Cys190 in models based on Alignment I (Figure 4.9).

Model generated using the SwissMODEL has been selected for further work (Model II) since this model was prepared by manual minimization of pseudopotential threading function implemented in DeepView package [86, 94].

### 4.1.5.3 Models based on Alignment III

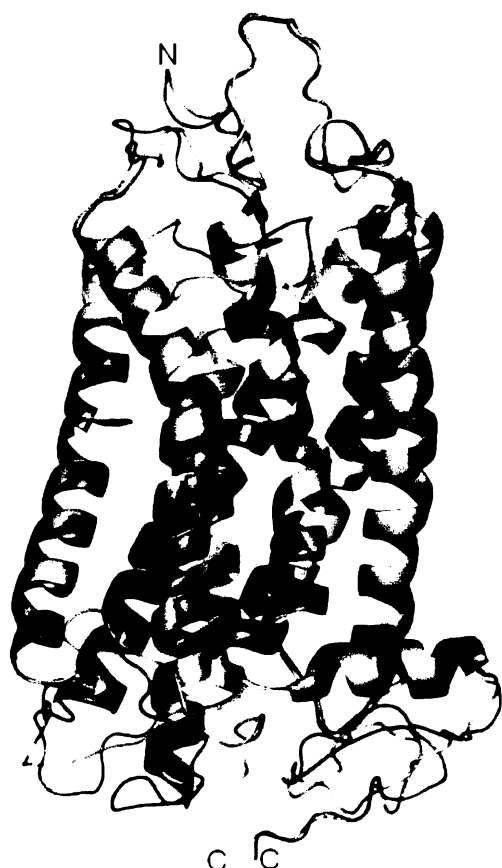


**Figure 4.10** - Comparison of models obtained using the Alignment III. Superimposition of models (in cartoon representation) calculated using Modeller (red) and SwissMODEL (green). Cysteine position (yellow) are described in more detail in Figure 4.9 Figure 4.11.

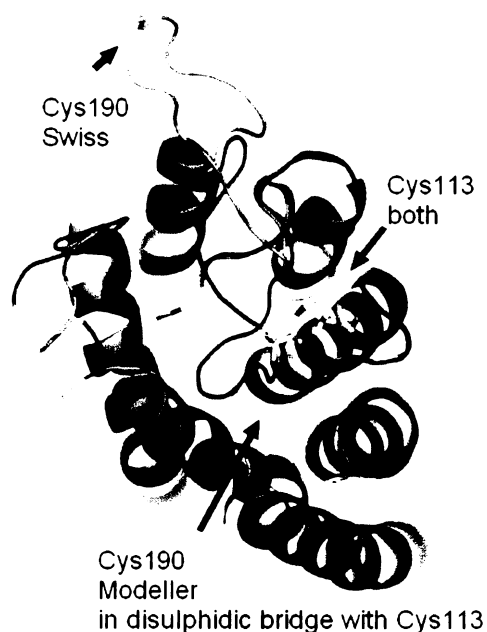


**Figure 4.11** - Position of cysteines in models based on Alignment III. Mark the difference in a position of Cys190 in loop ECL2 exposed to the extracellular environment in model from SwissMODEL, while Cys190 in model from Modeller made disulphide bridge with Cys193.

Models based on Alignment III differ mainly in the region of our interest (ECL2 loop), which is located in close proximity to proposed ligand-binding site (Figure 4.10). SwissMODEL-generated model predicted open conformation of this loop and residue Cys190 is exposed to the extracellular environment. By contrast, model generated using the Modeller package predicted formation of the disulphide bridge between residues Cys113 and Cys190 (Figure 4.11).

Although the existence of the disulphide bridge between residues Cys113 and Cys190 is still a hypothesis, the model calculated using the Modeller model was selected for further analysis (Model III).

#### 4.1.5.4 Short review of models selected for further work

Three different models have been selected for further analysis:

- **Model I:** SwissMODEL-generated model based on Alignment I.
- **Model II:** SwissMODEL-generated model based on Alignment II.
- **Model III:** Modeller-generated model based on Alignment III to conserve predicted disulphide bridge between residues Cys113 and Cys190.

#### 4.1.6 Docking of 2-iodomelatonin into the receptor

Program AutoDock 3.05 [45] has been used to predict the interactions between the ligand 2-iodomelatonin and the residues within the proposed ligand binding site of the human MT2 receptor. Ligand 2-iodomelatonin was docked into the ligand-binding site of all three selected models. Flexible docking of the 2-iodomelatonin revealed many possibilities of 2-iodomelatonin binding into the ligand-binding pocket located between helices H3, H4, H5, H6 and H7. In all models the ligand-binding pocket is closed from one side by ECL2 loop.

##### 4.1.6.1 Docking into the Model I

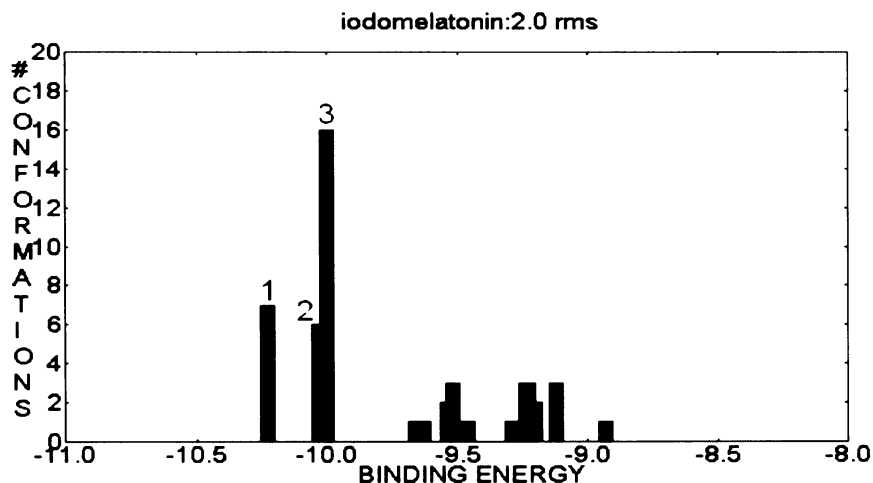


**Figure 4.12** – RMS histogram for docking results of 2-iodomelatonin into Model I. Each cluster contains complexes with similar geometry ( $\text{RMSD} \leq 2 \text{ \AA}$ ). Clusters are sorted according to the minimal binding energy of their members.

Cluster analysis in Figure 4.12 revealed three potential positions of 2-iodomelatonin in the ligand-binding site of the Model I of hMT2 melatonin receptor. Representative structures used for further analysis were the structures with minimal binding energy within the cluster.

Molecule of 2-iodomelatonin from the cluster with minimal binding energy (cluster 1) is located nearby residues Cys113 and Val291 (shown orange in Figure 4.13). The position of the structure from the cluster with second lowest binding energy (cluster 2) is shifted towards residue His208 (shown in green in Figure 4.13). Cluster 3 was the most populated cluster and the indole group of 2-iodomelatonin is very close to the side-chain of residue His208 while the N-acetyl group potentially interacts with residue Asn268 (shown in blue in Figure 4.13).

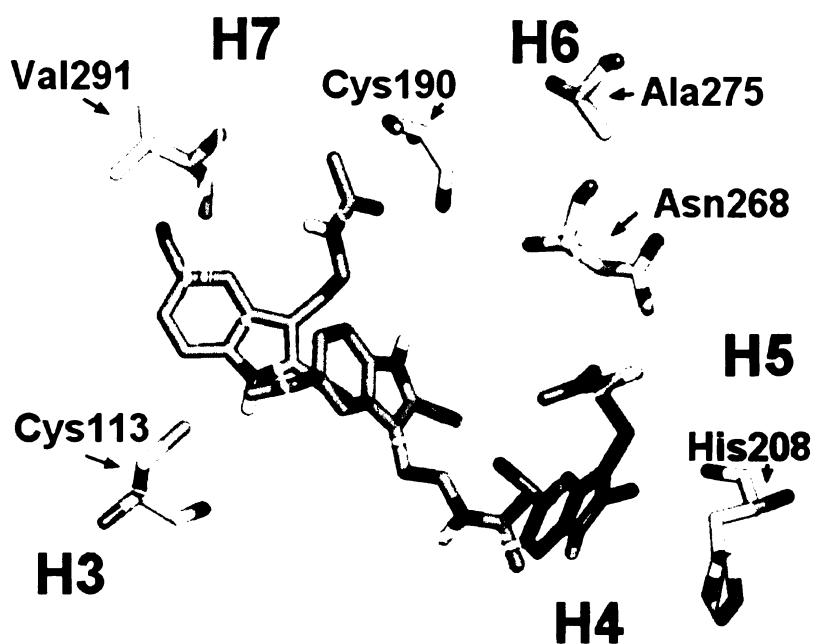


**Figure 4.13** – Prediction of 2-iodomelatonin binding into the pocket of Model I. Positions of the 2-iodomelatonin are shown together with residues Cys113, Cys190, His208, Asn268, Ala275 and Val291 of human MT2 receptor. Structures with minimal energies from each cluster are shown: cluster 1 in orange, cluster 2 in green and cluster 3 in blue.

Structure from the cluster 3 have been selected for further work because: (1) it is the most populated cluster, (2) it is in an agreement with findings published by Grol and Jansen [96, 97] who suggested that His208 plays a critical role in melatonin binding.

#### 4.1.6.2 Docking into the Model II

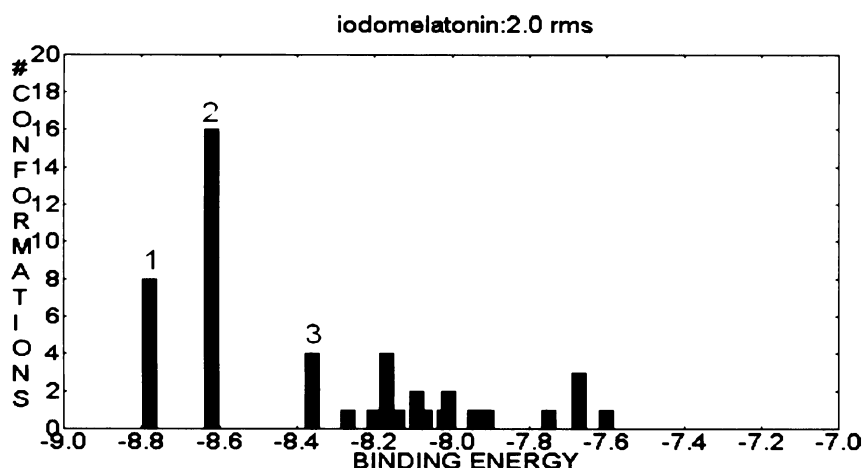


**Figure 4.14** – RMS histogram for docking results of 2-iodomelatonin into Model II. Each cluster contains complexes with similar geometry ( $\text{RMSD} \leq 2 \text{ \AA}$ ). Clusters are sorted according to the minimal binding energy of their members.

Cluster analysis in Figure 4.14 revealed three positions of 2-iodomelatonin in the ligand-binding site of the Model II of human MT2 melatonin receptor. Representative structures used for further analysis were the structures with minimal binding energy within the cluster.

Molecule of 2-iodomelatonin from the cluster with the minimal binding energy (cluster 1) is very close to the residues Cys113 and Tyr188. It is not located nearby any critical residue as shown in orange in Figure 4.15. Cluster 2 was the most populated and position of 2-iodomelatonin (shown in green in Figure 4.15) is in better agreement with experimental data, *i.e.* ligand has close contact with residues Cys113, Cys190, Val291 and Ala275. However, it has no contact with critical residues His208 and Asn268. Ligand molecule from the last cluster (cluster 3) displays contacts with more critical or involved amino acids (shown in blue in Figure 4.15), *i.e.* it has predicted close interaction between methoxy group of 2-iodomelatonin and side-chain of residue His208. Moreover it also interacts with residue Tyr298.

Structure from the cluster 3 has been selected for further refinement because: (1) it has contact with critical residue His208 [96, 97] and (2) this position is in relatively good agreement with other mutational binding data.

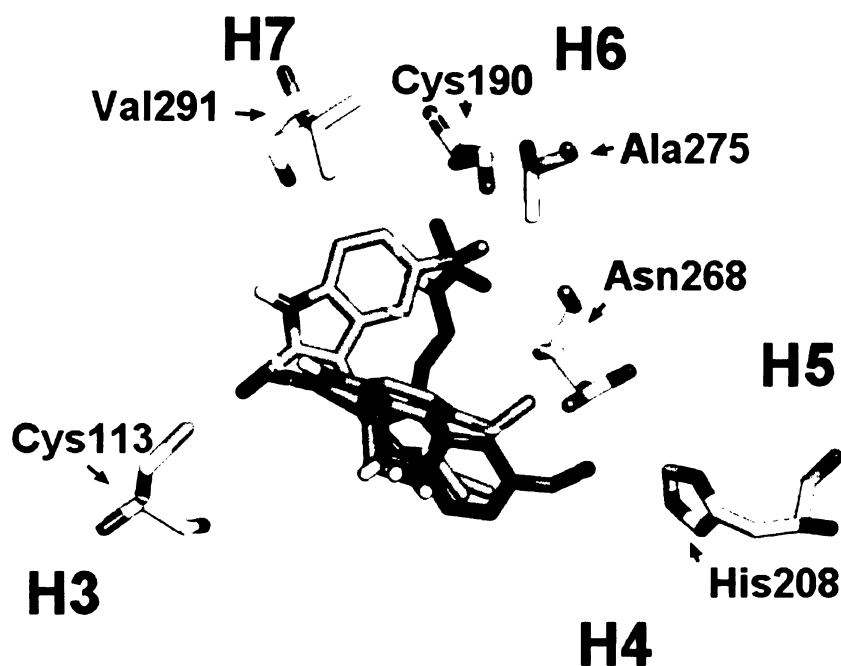


**Figure 4.15** – Prediction of 2-iodomelatonin binding into the pocket of Model II. Positions of the 2-iodomelatonin are shown together with residues Cys113, Cys190, His208, Asn268, Ala275 and Val291 of human MT2 receptor. Structures with minimal energies from each cluster are shown: cluster 1 in orange, cluster 2 in green and cluster 3 in blue.

#### 4.1.6.3 Docking into the Model III

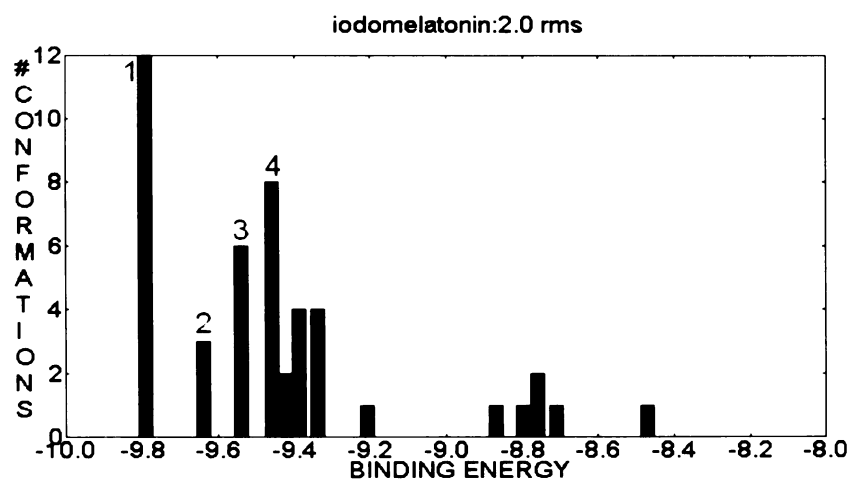


**Figure 4.16** – RMS histogram for docking results of 2-iodomelatonin into Model III. Each cluster contains complexes with similar geometry ( $\text{RMSD} \leq 2 \text{ \AA}$ ). Clusters are sorted according to the minimal binding energy of their members.

Cluster analysis in Figure 4.16 revealed four likely positions of 2-iodomelatonin in the ligand-binding site of the Model III of hMT2 melatonin receptor. Representative structures used for further analysis were the structures with minimal binding energy within the cluster.

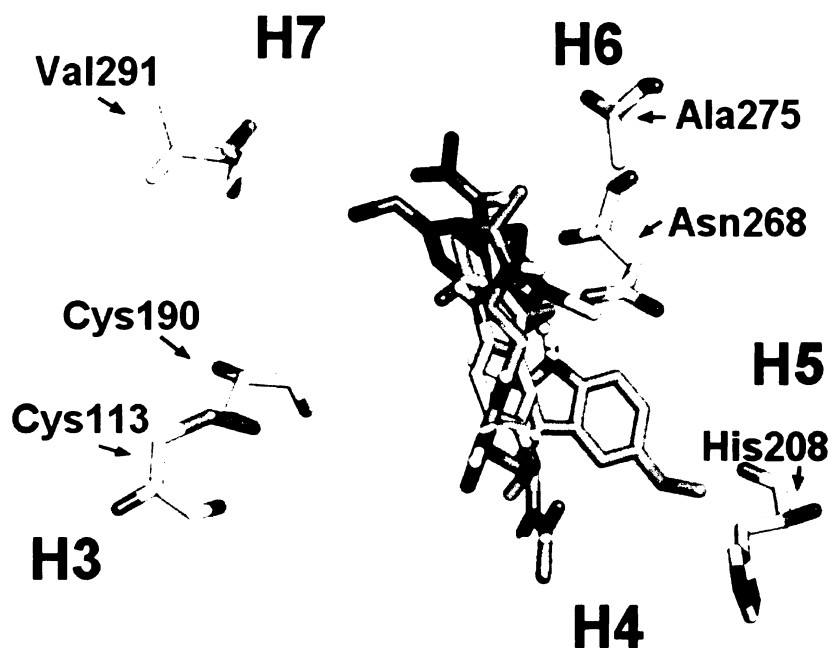


**Figure 4.17** – Prediction of 2-iodomelatonin binding into the pocket of Model III. Positions of the 2-iodomelatonin are shown together with residues Cys113, Cys190, His208, Asn268, Ala275 and Val291 of human MT2 receptor. Structures with minimal energies from each cluster are shown: cluster 1 in orange, cluster 2 in blue, cluster 3 in green and cluster 4 in cyan.

Molecule of 2-iodomelatonin from the cluster with the minimal binding energy (cluster 1) is in vicinity to the residue His208. Cluster 1 was also the most populated cluster (shown in orange in Figure 4.17). Indole group of 2-iodomelatonin is located nearby another critical residue Asn268 while N-acetyl group is in a close contact with the residue Gly121. In cluster 2, molecule of 2-iodomelatonin is located nearby residues Ala275 and Asn268 as shown in blue in Figure 4.17. Position of docked 2-iodomelatonin molecule in cluster 3 is similar to the position of ligand from cluster 2, but it is completely turned. Methoxy group is in proximity of the residue Ala275, while the N-acetyl group is in a close contact with the residue Gly121 (shown in green in Figure 4.17). N-Acetyl group of 2-iodomelatonin molecule from the last cluster (cluster 4) is in contact with the residue Asn268 as shown in cyan colour in Figure 4.17.

Ligand position from the cluster 1 have been selected for further refinement because: (1) cluster 1 is the most populated cluster and (2) molecule of 2-iodomelatonin is in a contact with residues His208 and Asn268 known to be critical for melatonin binding [96, 97].



#### 4.1.6.4 Short review of selected ligand-receptor complexes

Three different complexes has been selected for refinement by molecular dynamics simulation mainly on the basis of experimental data published by Grol & Jansen (1996) [96, 97], and Gerdin *et al.* (2003) [28]:

- **Complex I:** Model I with docked 2-iodomelatonin from the cluster 3.
- **Complex II:** Model II with docked 2-iodomelatonin from the cluster 3.
- **Complex III:** Model III with docked 2-iodomelatonin from the cluster 1.

#### 4.1.7 Molecular dynamics

In order to obtain more realistic models of MT2 receptor I have performed series of MD simulations with MT2 receptor embedded in fully hydrated lipid bilayer.

##### 4.1.7.1 Setup of MD simulation

First, systems containing only the hydrated lipid bilayer were created and simulated for total time of 700 ps. Figure 4.18 shows the snapshot of this system from the end of the equilibration run.

Three simulation systems were then created by insertion of protein–ligand complexes (Complex I-III) into the middle of the lipid bilayer as can be seen in Figure 4.19. Orientation of the receptors in the membrane was defined using the helix H4, which was oriented perpendicular to the plane of the membrane (based on crystal structure of bovine rhodopsine) [1, 26]. Iodine atom in 2-iodomelatonin molecule was removed due to the force field deficiency (2-iodomelatonin was changed into the melatonin) [88].

All three simulation systems with Complexes I-III were then energy minimized using the method of conjugated gradients.

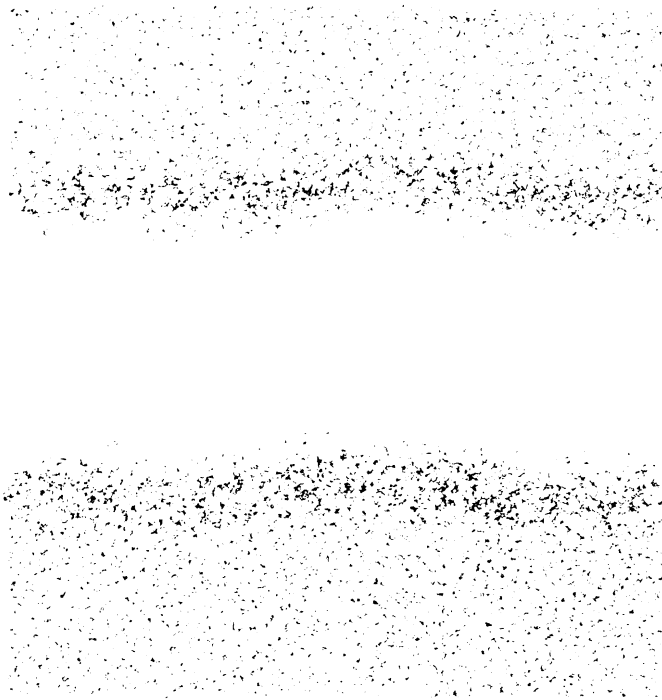


**Figure 4.18** – Snapshot of the end of lipid bilayer re-equilibration. Lipids (cyan) and water (red) molecules are shown. Simulation box has 9.5x9.5x10 nm.

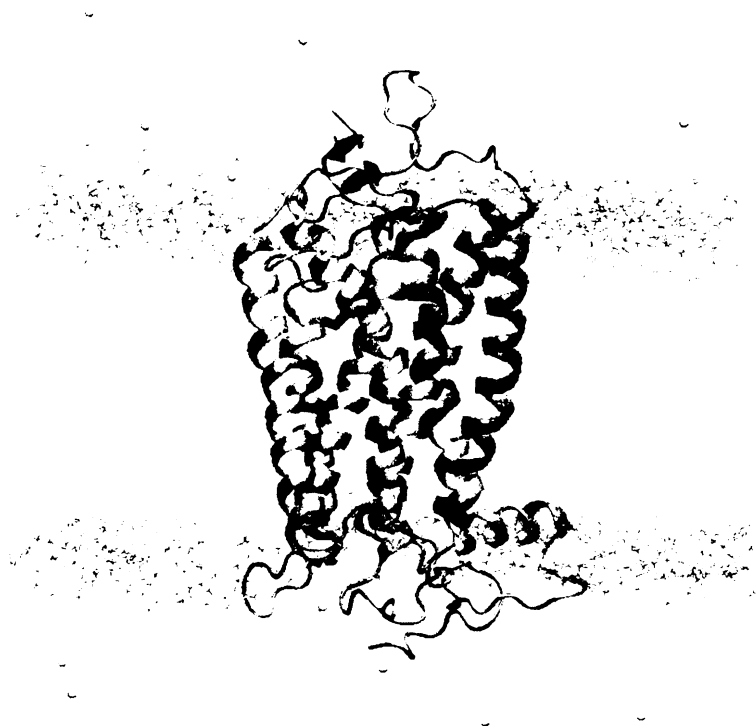


**Figure 4.19** – Snapshot of the simulation system with Complex I. Snapshot has been taken after energy minimization of the system. Protein is shown in cartoon representation; melatonin (dark blue) is docked into the protein. Chloride anions (yellow) and POPE lipids (cyan) are shown. Water molecules are not shown for better clarity.

50 ps-long MD runs with positional restrains on heavy-atoms of the complex were used to close the vacuum gaps between the protein and lipids (vacuum gaps were created by removal of lipid molecules sterically overlapping with the complex). These pre-run simulations quickly re-equilibrated the system and filled the gaps around the protein molecule (compare Figure 4.20 with Figure 4.21).

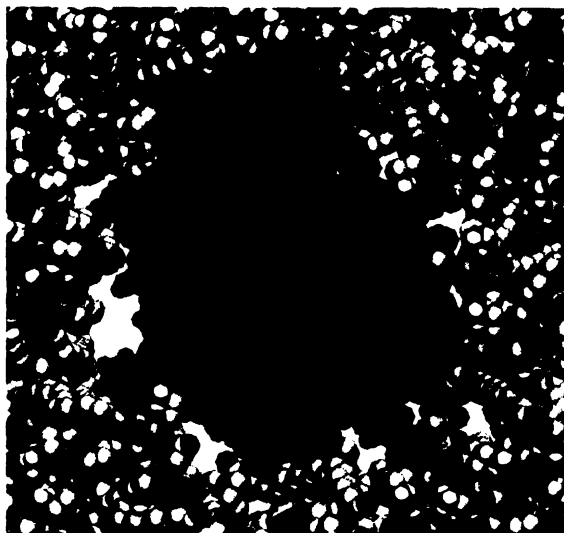


**Figure 4.20** – Complex I after the energy minimization seen from above  
Receptor (dark blue) is surrounded with lipids (other colours) and the vacuum hole can be seen (white)

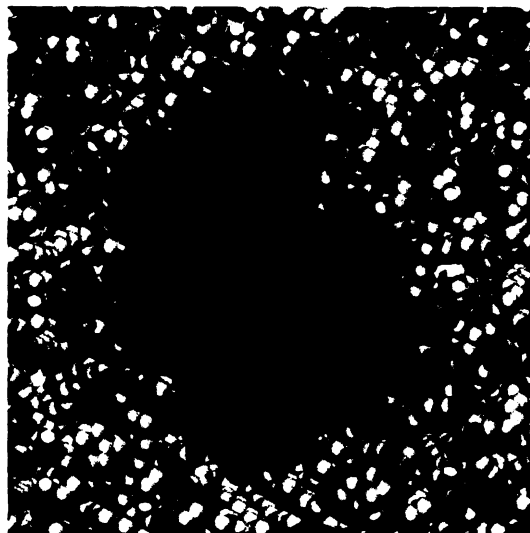


**Figure 4.21** – Complex I after pre-run MD simulation seen from above  
Receptor (dark blue) is surrounded with lipids (other colours) and vacuum hole disappeared.

#### 4.1.7.2 Production run

After the preparation of all three simulation systems the unrestrained 500 ps-long trajectories have been calculated. As can be seen on potential energy and positional RMSD profiles (Figure 4.22), the systems needed additional 200 ps to become equilibrated and stable. Trajectories between 200 to 500 ps were used to collect data. Since the energy and RMSD profiles were essentially the same for all three systems, only the profiles for MD simulation of Complex I are shown.

Analysis of calculated trajectories revealed, that secondary and tertiary structure of the human MT2 receptor did not change significantly during the simulation. The melatonin molecule remained in the ligand-binding pocket as can be seen on Figure 4.23. Structures of the MT2 receptor with bound melatonin obtained from the equilibrated MD simulation trajectories were clustered [91].

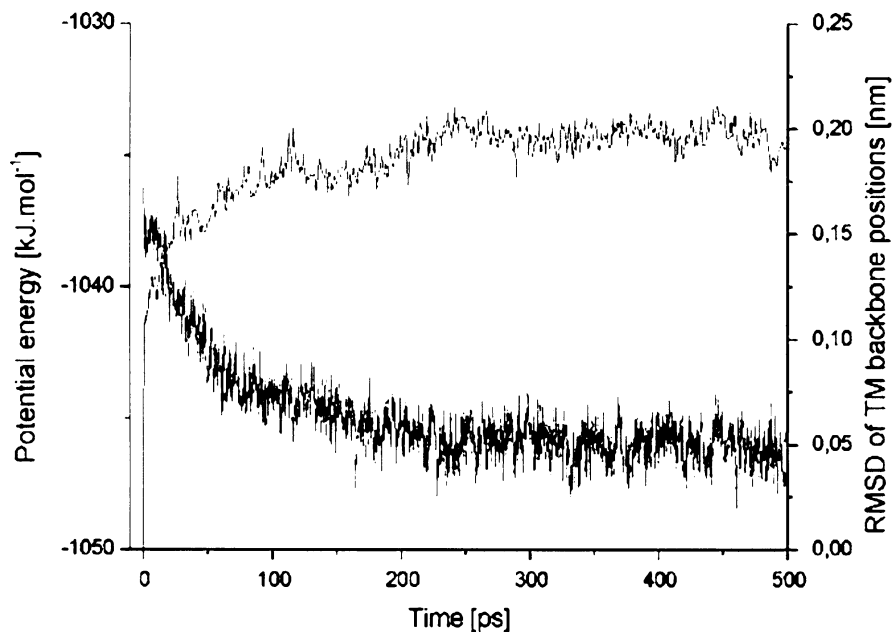


**Figure 4.22** – Energy and RMSD profiles of system with Complex I. Potential energy of the system (blue) and positional RMSD of receptor TM backbone (black) during full MD simulation run. As can be seen, system was equilibrated after initial 200 ps.

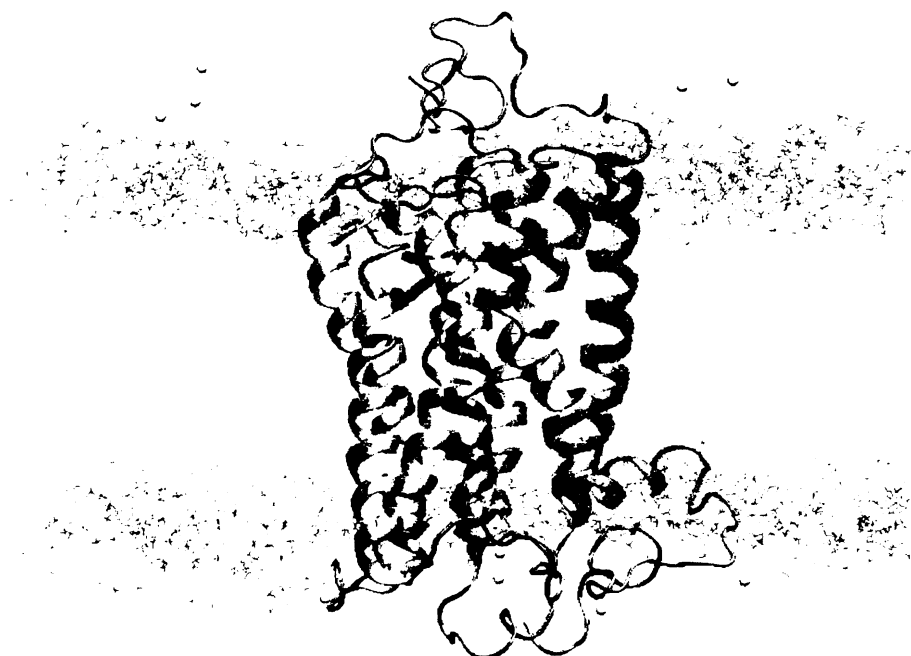


**Figure 4.23** – Snapshot taken from the end of MD production run with Complex II. Protein is shown in the cartoon representation; melatonin (dark blue) is docked into the protein. Chloride anions (yellow) and POPE lipids (cyan) are shown. Water molecules are not shown for better clarity.

## 4.1.8 Analysis of the MD results

For all three simulations the average structure of the complex from the most populated cluster was calculated and energy minimized.

### 4.1.8.1 Simulation I:

The results of MD Simulation I with Complex I are shown on Figure 4.24 and Figure 4.25. As a result of MD the melatonin molecule rotated slightly along its indole ring.

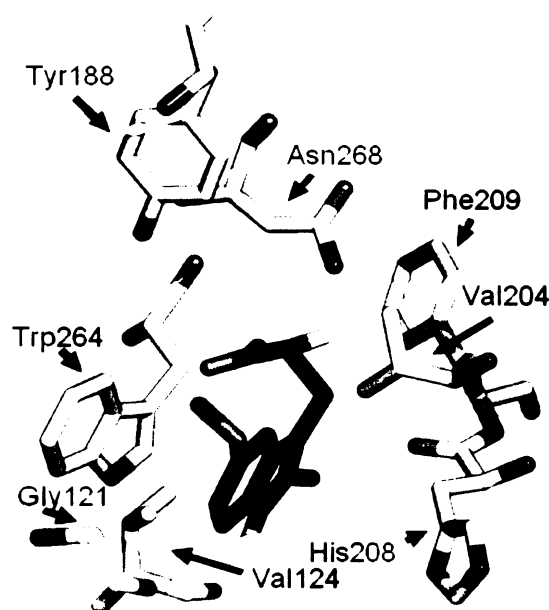


**Figure 4.24** – Ligand-binding site of Complex I before MD simulation  
2-iodomelatonin (dark blue) is docked into the ligand-binding site (light grey).

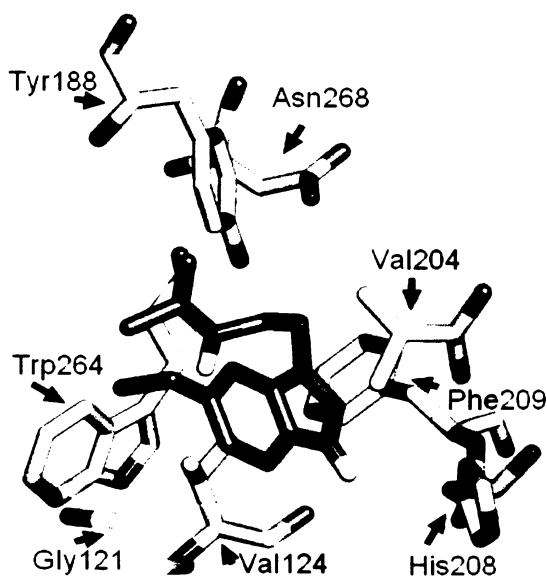


**Figure 4.25** – Ligand-binding site of Complex I after MD simulation  
Melatonin (violet) is docked into the relaxed ligand-binding site (light grey).

Aromatic residues Tyr188 or Phe209, and Trp 264 seem to interact with the ligand through the unspecific hydrophobic interactions and are now much closer to the melatonin.

Melatonin also seems to interact with residues Val124, Val204, Phe209, and Trp264. Moreover melatonin interacts with residue His208, which is located close to the indole group of melatonin. N-Acetyl group of melatonin is in vicinity of polar residue Asn 268. Simulation I also suggests possible conformational change in the region of residues Met120, Val291, Leu295, and Tyr298 that form a tunnel connecting the ligand-binding site with the extracellular environment.

#### 4.1.8.2 Simulation II:

The MD Simulation II shows that melatonin molecule in Complex II is in closer contact with residues His208 and Asn268 (Figure 4.26 and Figure 4.27).

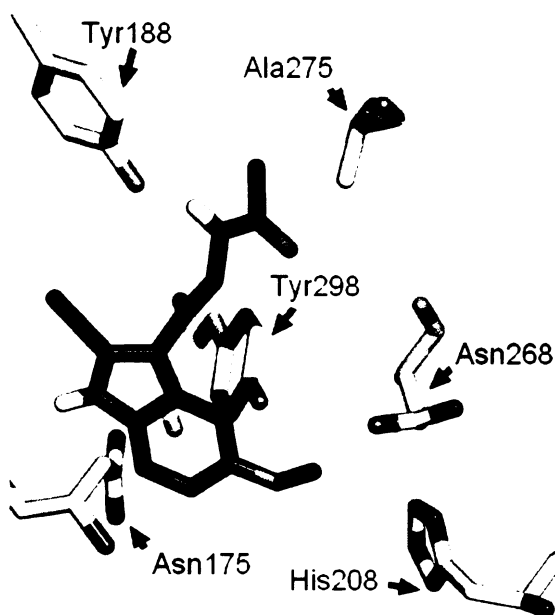


**Figure 4.26** – Ligand-binding site of Complex II before MD simulation  
2-iodomelatonin (dark blue) is docked into the ligand-binding site (light grey).  
Asn268 is buried below 2-iodomelatonin – His208 plane.

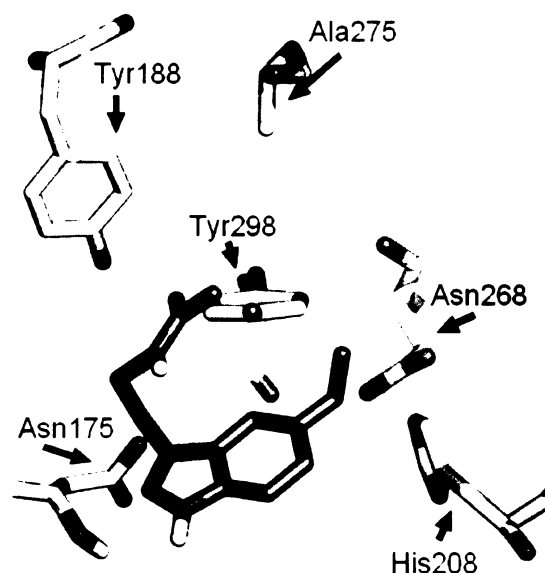


**Figure 4.27** – Ligand-binding site of Complex II after MD simulation  
Melatonin (violet) is docked into the relaxed ligand-binding site (light grey).  
Asn268 is buried below melatonin plane.

Hydrogen bond between methoxy group of melatonin and the side-chain of the residue His208 is preserved during the simulation only in this model. Residues Asn 175, Tyr188 and Tyr298 also form hydrogen bonds with melatonin. Residue Gly121 seems to help to enlarge the cavity for the ligand.

All possibly involved proline and some cysteine residues (Pro174, Pro212, and Pro266, Cys113, Cys140, Cys219, Cys263, and Cys302) likely restrain the shape of TM helices in favour of close interactions with melatonin molecule. Serine residues in helix H3 stabilize another helices with hydrogen bonds to backbone carbonyl group of Phe299 in H7 (Ser124) or with side-chain carbonyl group from Asp86 in H2 (Ser127).

Residue Cys190 in connection with residues Tyr188 and Val291 probably forms a tunnel enclosure. Interestingly tunnel is probably located between H6 and H7 in this complex.

### 4.1.8.3 Simulation III:

Simulation III shows that molecule of melatonin is shifted away from the vicinity of the residue His208 (Figure 4.28 and Figure 4.29).

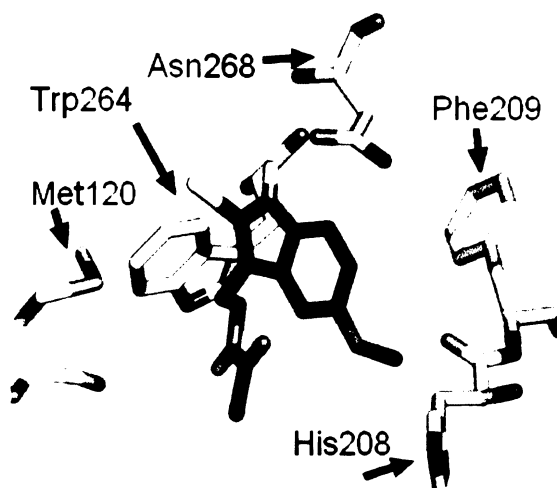


**Figure 4.28** – Ligand-binding site of Complex III before MD simulation. 2-iodomelatonin (dark blue) is docked into the ligand-binding site (light grey).

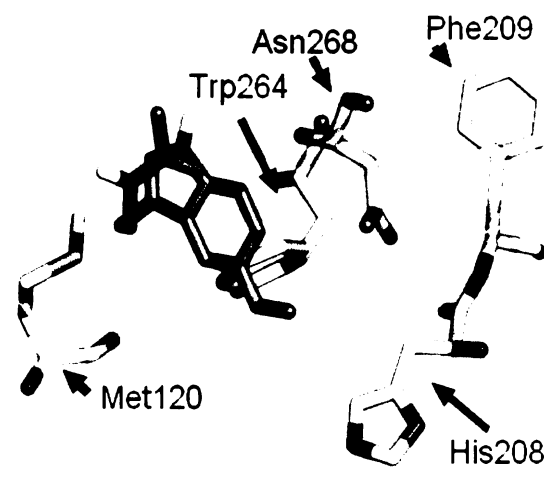


**Figure 4.29** – Ligand-binding site of Complex III after MD simulation. Melatonin (violet) is docked into the relaxed ligand-binding site (light grey).

Residues Cys113 and Cys190 form in disulphide bond. Residue Asn268 is in close contact with methoxy group of melatonin. The role of residue Ala275 is much trickier – it can be part of a tunnel between helices H6 and H7, but other residues (Val291, Leu295 and Leu295) more likely form the tunnel between helices H3 and H7. Residue Ala275 is then a part of the turn between helix H6 and extracellular loop ECL3.

Residue Trp264 is located nearby of the indole group of melatonin, while residue Asn175 interacts with N-acetyl group of the melatonin molecule.

Shaping role of prolines is confirmed especially for residue Pro266 that stabilizes kink in helix H7.

## 4.2 Experimental results

Experimental part of this diploma thesis was done in collaboration with the group of Ing. Jan Teisinger, PhD from Institute of Physiology, AS CR. Residues for mutagenesis were selected on the basis of combination of Complex I and Complex II during year 2003 and mutational data from this collaboration were published [98, 99]. I have performed the site-directed mutagenesis of MT2 receptor residue Gly121 (mutation to alanine) and characterized this mutant using the saturation-binding assay.

### 4.2.1 Plasmid preparation

Mutation of the human MT2 melatonin receptor residue 121 from glycine to alanine was accomplished by site-directed mutagenesis of the plasmid pcDNA3 containing cDNA of hMT2 receptor. Figure 4.30 shows sequencing chromatogram with the region containing the point mutation of Gly121Ala.

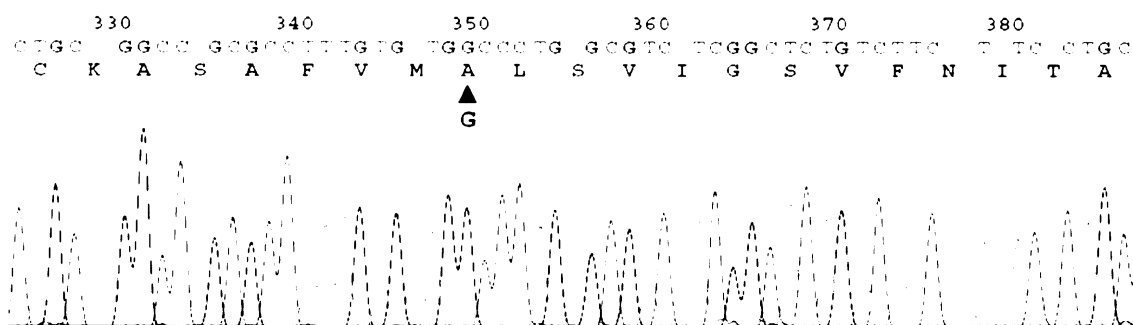


**Figure 4.30** – Sequencing of the DNA of hMT2 melatonin receptor. Codon GGC (Gly121) was exchanged for GCC (Ala121).

Mutated cDNA of hMT2 receptor was then transferred from the plasmid pcDNA3 into the pFLAG-CMV-2 plasmid using the Hind III and Eco RI cleavage sites (performed by Ing. Teisinger, CSc.).

### 4.2.2 Binding assay

Plasmid pFLAG-hMT2 was transfected into the HEK cell culture Part of the HEK cells were used for saturation binding assays. Other part of the cell tissue was used to determine non-specific binding of radiolabeled 2-iodomelatonin in presence of at least 1000x greater concentration of non-labelled melatonin. RNDr. Petr Mazna, PhD, used last batch of cells for immunocytochemical identification of expression. According to



the microscopy, all mutant hMT2 receptors were localised in cell membranes.

Mutation of Gly121 to alanine depressed both affinity and expression of the hMT2 receptor (compare slope at Figure 4.31 with slope at Figure 4.32)

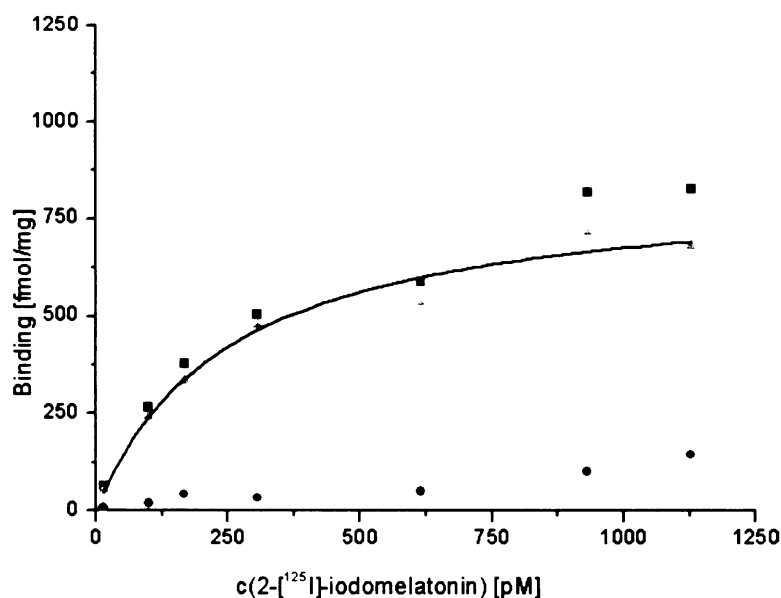


**Figure 4.31** – Saturation binding assay for G121A mutant receptor  
Total (black squares) and non-specific binding (red circles) of 2-[<sup>125</sup>I]-iodomelatonin was determined and receptor-specific binding (green triangles) was computed from the difference. The non-linear fit to the equation (1.14) showed  $K_D = 192 \pm 18$  pM,  $B_{max} = 854 \pm 164$  fmol/mg and  $K_{nsp} = 117 \pm 9$  mL/g.

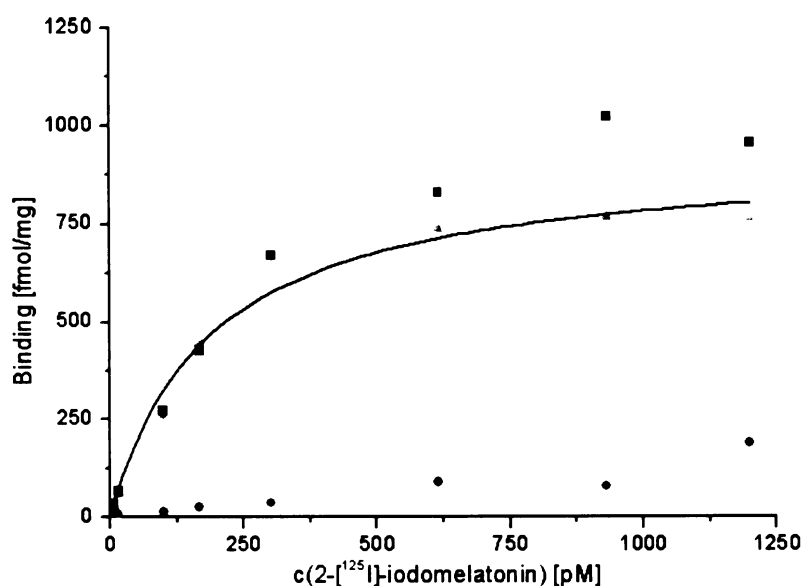


**Figure 4.32** – Saturation binding assay for Wild-type receptor  
Total (black squares) and non-specific binding (red circles) of 2-[<sup>125</sup>I]-iodomelatonin was determined and receptor-specific binding (green triangles) was computed from the difference. The non-linear fit to the equation (1.14) showed  $K_D = 145 \pm 25$  pM,  $B_{max} = 1182 \pm 350$  fmol/mg and  $K_{nsp} = 133 \pm 12$  mL/g.

## 5 Discussion

Melatonin receptors are the main research topic of several groups around the world. We have attempted to compare the worldwide mutational data with our models to understand the mechanism of ligand recognition of the human MT2 melatonin receptor. For this purpose, we have prepared compilation from various available sources of mutational data:

- Grol and Jansen prepared first pharmacophoric model of melatonin receptors. [96, 97]
- Mutational data from GPCRDB [16] were brought from Gerdin [28].
- Mseeh et al focused on cysteines in the receptor [95].
- Our group focused on residues in TM 3, 5, 6, 7 and in ECL2 loop [98-100].

Data were critically clustered into several classes according to their importance. Residues were sorted by an affinity of mutated human MT2 melatonin receptor. As “**critical**” were assumed residues where mutation significantly diminished binding to the receptor. Mutation of “**involved**” residues lead to the depression of binding and also expression of the receptor was lowered. Mutation of the “**folding**” residues resulted mainly in worse expression of the receptor. Mutations with high error-rate binding assays with minor binding changes were noted as “**involved(?)**”. Residues where mutation changed nothing were noted as “**not involved**”. “**Positive**” residues were residues where mutation made ligand binding easier.

### 5.1 Summary of mutational data

All hMT2 melatonin receptor amino acids studied for their possible significance to the specificity and affinity to the ligand and their possible interaction with the ligand are contained in Table 5.1. The most specific interactions with the ligand are hydrogen bonds. Two or three hydrogen bonds were detected in Simulation II, while in Simulation I there are only one or two hydrogen bonds and in Simulation III is the only hydrogen bond formed with residue Tyr200. Rivara *et al.* also reported theoretic specific interaction with this residue based on their model [87]. Unfortunately, no experimental data are known for this residue.

**Table 5.1** – Residues potentially involved in ligand binding.

Residues were described by their possible interactions with ligand or with specific TM helix noted with helix number. As “**steric**” are labelled residues, whose mutation sterically disallows ligand insertion. “**Shape**” residues are involved in formation of TM helix shape. Especially proline residues may be a part of “**kinks**” in helical topology. “**Tunnel**” residues are thought to be a part of a ligand way into the ligand-binding site. Exposed residues are designated as “**outside**”.

Model	Model 1		Model 2		Model 3	
	Before MD	After MD	Before MD	After MD	Before MD	After MD
<b>Critical</b>						
H208	polar	polar	H-bond	H bond	polar	polar
N268	polar	polar	shape 6	polar	polar	polar
A275	shape 6	shape 6.	nonpolar	tunnel, shape 6	shape 6	shape 6
<b>Involved</b>						
C113	tunnel	tunnel	shape	shape ECL2	SS bridge	SS bridge
G121	steric	steric	steric	steric	steric	polar
Y188	tunnel	H-bond	H-bond	H-bond	outside	outside
C190	outside	outside	tunnel	tunnel	SS bridge	SS bridge
V204	nonpolar	nonpolar	nonpolar	nonpolar	nonpolar	nonpolar
L272	outside	outside	nonpolar	nonpolar	outside	outside
V291	tunnel	tunnel	tunnel	tunnel	tunnel	tunnel
L295	tunnel	tunnel	nonpolar	nonpolar	tunnel	tunnel
Y298	tunnel	tunnel	stacking	H-bond	tunnel	tunnel
<b>Folding</b>						
M120	tunnel	tunnel	steric	shape ECL2	-	polar
S123	shape 3	shape 3	shape 3	H-bond 7	shape 3	shape 3
V124	shape 6	nonpolar	nonpolar	nonpolar	nonpolar	nonpolar 7
S127	shape 7	shape 3	shape 3	H-bond 2	shape 3	shape 3
C140	outside	outside	outside	outside	outside	outside
F209	outside	nonpolar	outside	outside	stacking	outside
C219	shape 5	shape 5	shape 5	shape 5	shape 5	shape 5
C263	shape 6	shape 6	outside	outside	shape 6	shape 6
W264	nonpolar	outside	kink 7	kink 7	stacking	stacking
C302	outside	shape 5	shape 7	shape 7	outside	outside
<b>Involved(?)</b>						
I125	nonpolar	nonpolar	nonpolar	nonpolar	nonpolar	nonpolar
P174	kink 4	kink 4	kink 4	kink 4	shape 4	shape 4
N175	H bond	polar	polar	polar	polar	polar
V205	outside	nonpolar	outside	outside	outside	outside
P212	kink 5-	kink 5-	kink 5	kink 5	kink 5	kink 5
P266	kink 6	kink 6	shape 6	kink 6	shape 6	shape 6
<b>Posit4e</b>						
F257	generally disallows closer contact between H6 and H7					
S293	shape 6	shape 6	outside	outside	outside	outside

### 5.1.1 Potential role of His208

Grol and Jansen proposed that residue His208 is involved in hydrogen bond with methoxy group of melatonin [96, 97]. Rivara *et al.* proposed T-shape interaction of His208 imidazole ring with  $\pi$ -electronic cloud of ligand aromatic ring [87].

Mutagenesis data confirmed that His208 is probably present in ligand-binding site [28]. Mutation of this residue resulted in the depression of the affinity of the hMT2 melatonin receptor to the 2-iodomelatonin, while the mutation of its neighbour Phe209 does not changed binding but decreased the level of functional receptor in a membrane.

Grol and Jansen findings are not in agreement by our Complex I where methoxy group interacts with residue Gly121. On the other hand, melatonin and residue His208 form a polar interaction supported by T-shape stacking interaction with residue Phe209.

The most correct model is Complex II in which hydrogen bond between His208 and methoxy group of melatonin was detected, while residue Phe209 is turned outside and is involved in hydrophobic contacts with lipids.

Such potential role for residue His208 is not confirmed in the Complex III, where melatonin is shifted away from His208.

### 5.1.2 Is disulphide bridge between Cys113 and Cys190 present?

Mseeh *et al.* (2002) proposed presence of disulphide bridge between residues Cys113 and Cys190 [95]. Their evidence was based on two different approaches – (1) mutation of Cys113 and Cys190 to alanines which led to the specific-binding loss, however measurable residual binding was detected; and (2) expression of wild-type human MT2 melatonin in presence of thiol-reducing agent which depressed receptor expression but binding to 2-iodomelatonin was not much affected.

Model I predicted that residue Cys113 is involved in formation of a tunnel to the extracellular space, which could be altered with its mutation to the alanine, but gives no similar prediction for Cys190 exposed to the extracellular environment.

Model II had different roles for each of cysteines: Cys113 is part of helix H3; Cys190 in connection with other residues is a part of tunnel between H6 and H7.

Model III was prepared to contain a disulphide bridge between Cys113 and Cys190 and its weak point lies in minimal agreement with other data; especially it cannot explain the loss of binding after the mutation of residue Tyr188 to the phenylalanine.

### 5.1.3 Tunnel presence

Many of the mutated residues had impact on the binding ability of the receptor, while they are not present in the ligand-binding site. It has been speculated that they form a dynamical tunnel providing a passage to the ligand-binding site. This hypothesis is also supported by the fact that ligand-binding site is buried in the core of human MT2 melatonin receptor. However there are two possible areas for tunnel formation (Figure 5.1):

Model I and Model III suggested that the tunnel is placed between helices H3 and H7 based on residues (Cys113 in Model I), Met120, Val291, Leu295 and Tyr298.

Model II proposed another tunnel position between helices H6 and H7 and ECL2 loop (containing key residues Tyr188 and Cys190). ECL2 loop should be more flexible in absence of disulphide bond between Cys113 and Cys190 and where mutation of Ala275 to the bigger residue disabled loop opening.

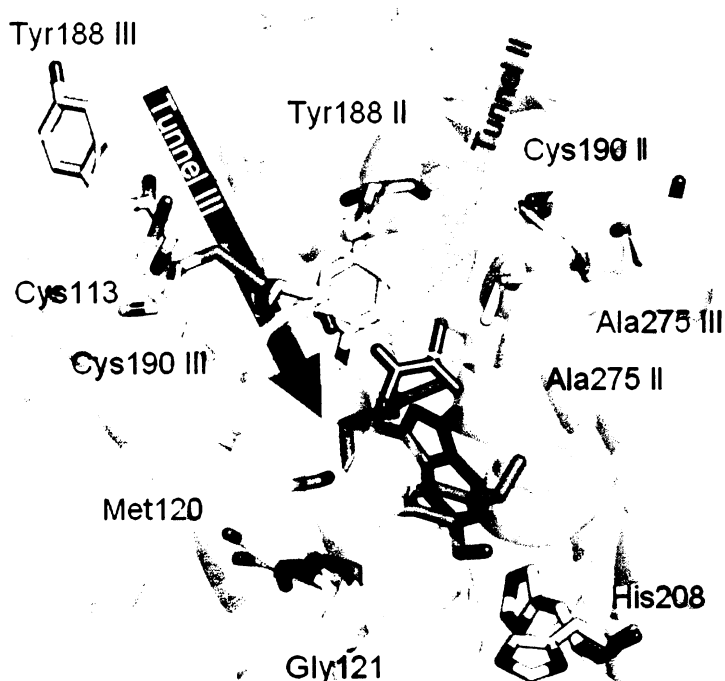


**Figure 5.1** – Possible tunnel positions proposed for Complexes I and III. Complex II (melatonin in green and hMT2 receptor in yellow) has active residues Tyr188 II, Cys190 II, Ala275 II and Tyr298 (not shown) located between helices H6 and H7. Complex III has active residues Cys113, Met120, Cys190, Val291, Leu295 and Tyr298 between helices H3 and H7.

## 5.2 Final model

The model showing the best agreement with mutational data is the Model II, in spite of absence of the disulphide bridge. The Model II proposes other roles for mentioned cysteine residues Cys113 and Cys190. Model II also as the only model contains hydrogen bond between His208 and methoxy group of melatonin.

Figure 5.2 shows cartoon representation of the final model II in complex with melatonin and Figure 6.1 shows the ligand-binding site of the human MT2 melatonin receptor.

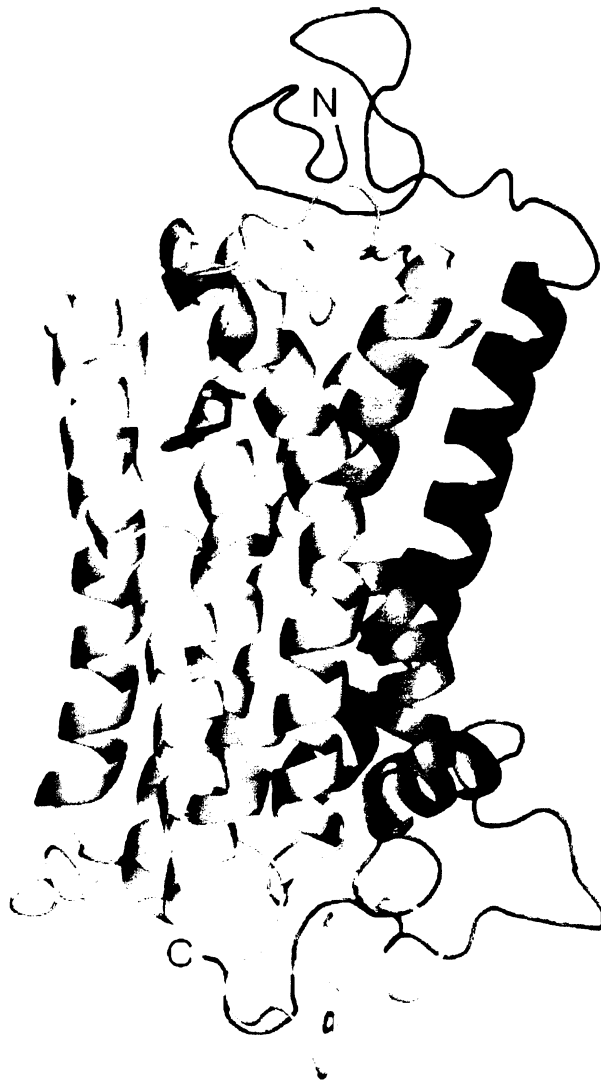


**Figure 5.2** – Final model of the human MT2 melatonin receptor  
Model II in complex with melatonin was selected as a final model with the best agreement with the experimental data. Cartoon representation shows 7 TM helices from dark blue (H1, at the right side behind plane) via green (H4, at the left) to red (H7, right). Melatonin is in its docked and refined position.

## 6 Conclusion

- (1) Structural model of human MT2 melatonin receptor has been prepared.
- (2) Amino-acid residues potentially involved in the ligand binding were selected for mutagenesis experiments.
- (3) Ligand 2-iodomelatonin has been docked into the selected models of the human MT2 melatonin receptor.
- (4) Structures of receptor-ligand complexes were refined using MD simulations.
- (5) Site-directed mutagenesis of the residue Gly121 in human MT2 melatonin receptor was performed and the mutant was characterised by the binding assay of 2- $^{125}$ I-iodomelatonin.
- (6) Obtained models were confronted with available experimental data on mutagenesis of melatonin receptors.
- (7) Final model of the human MT2 melatonin receptor has been selected and can be seen on Figure 5.2 and its ligand-binding site on Figure 6.1.

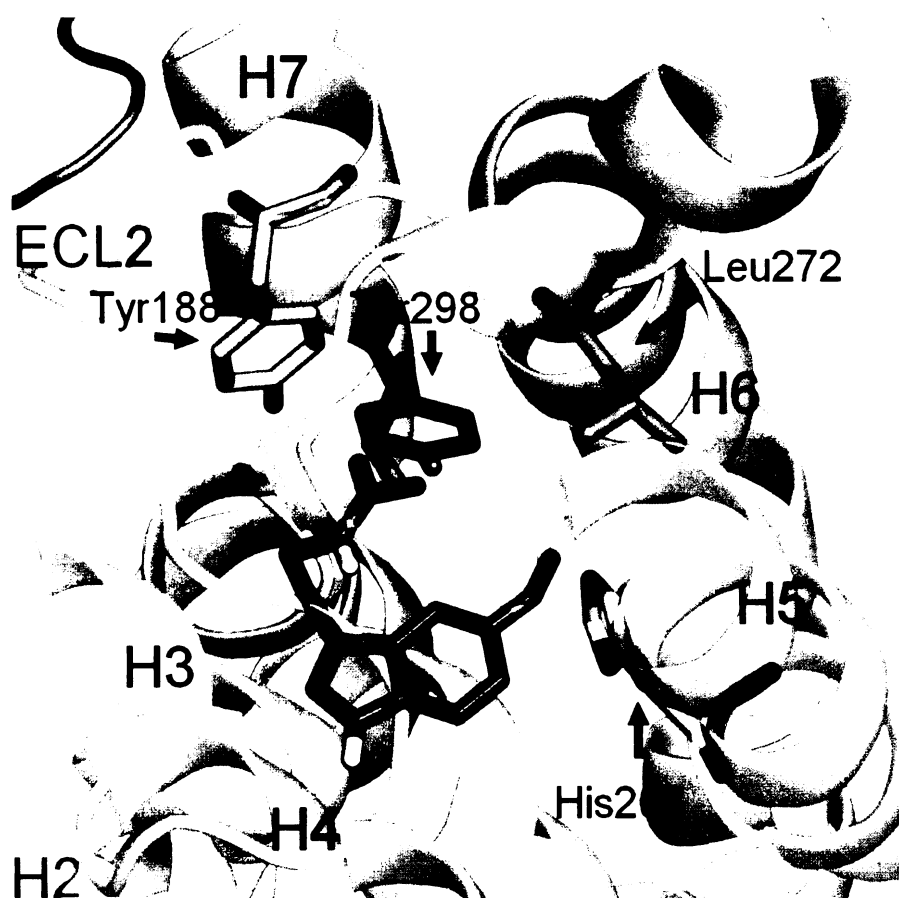


**Figure 6.1** – Ligand-binding site of the human MT2 melatonin receptor

## 7 References

1. Palczewski, K. et al. Crystal structure of rhodopsin: A G protein-coupled receptor. *Science* **289**, 739-45 (2000).
2. Lerner, A., Case, J., Takahashi, Y., Lee, T. and Morei, W. Isolation of melatonin, the pineal gland factor that lightens melanocytes. *J Am Chem Soc* **80**, 2587 (1958).
3. Brzezinski, A. Melatonin in humans. *N Engl J Med* **336**, 186-95 (1997).
4. Wang, L.M., Suthana, N.A., Chaudhury, D., Weaver, D.R. and Colwell, C.S. Melatonin inhibits hippocampal long-term potentiation. *Eur J Neurosci* **22**, 2231-7 (2005).
5. Zhdanova, I.V. Melatonin as a hypnotic: pro. *Sleep Med Rev* **9**, 51-65 (2005).
6. Romero, M.P., Osuna, C., Garcia-Perganeda, A., Carrillo-Vico, A. and Guerrero, J.M. The pineal secretory product melatonin reduces hydrogen peroxide-induced DNA damage in U-937 cells. *J Pineal Res* **26**, 227-35 (1999).
7. Gavella, M. and Lipovac, V. Antioxidative effect of melatonin on human spermatozoa. *Arch Androl* **44**, 23-7 (2000).
8. Acuna-Castroviejo, D. et al. Melatonin, mitochondria, and cellular bioenergetics. *J Pineal Res* **30**, 65-74 (2001).
9. Mazzucchelli, C. et al. The melatonin receptor in the human brain: cloning experiments and distribution studies. *Brain Res Mol Brain Res* **39**, 117-26 (1996).
10. Pandi-Perumal, S.R., Zisapel, N., Srinivasan, V. and Cardinali, D.P. Melatonin and sleep in aging population. *Exp Gerontol* **40**, 911-25 (2005).
11. Wang, J.Z. and Wang, Z.F. Role of melatonin in Alzheimer-like neurodegeneration. *Acta Pharmacol Sin* **27**, 41-9 (2006).
12. Wu, Y.H. and Swaab, D.F. The human pineal gland and melatonin in aging and Alzheimer's disease. *J Pineal Res* **38**, 145-52 (2005).
13. Turgut, M., Uysal, A., Pehlivan, M., Oktem, G. and Yurtseven, M.E. Assessment of effects of pinealectomy and exogenous melatonin administration on rat sciatic nerve suture repair: an electrophysiological, electron microscopic, and immunohistochemical study. *Acta Neurochir (Wien)* **147**, 67-77; discussion 77 (2005).
14. Quinn, J. et al. Chronic melatonin therapy fails to alter amyloid burden or oxidative damage in old Tg2576 mice: implications for clinical trials. *Brain Res* **1037**, 209-13 (2005).
15. Pierce, K.L., Premont, R.T. and Lefkowitz, R.J. Seven-transmembrane receptors. *Nat Rev Mol Cell Biol* **3**, 639-50 (2002).
16. Horn, F. et al. GPCRDB information system for G protein-coupled receptors. *Nucleic Acids Res* **31**, 294-7 (2003).
17. Rios, C.D., Jordan, B.A., Gomes, I. and Devi, L.A. G-protein-coupled receptor dimerization: modulation of receptor function. *Pharmacol Ther* **92**, 71-87 (2001).
18. Overton, M.C. and Blumer, K.J. Use of fluorescence resonance energy transfer to analyze oligomerization of G-protein-coupled receptors expressed in yeast. *Methods* **27**, 324-32 (2002).
19. Overton, M.C. and Blumer, K.J. G-protein-coupled receptors function as oligomers in vivo. *Curr Biol* **10**, 341-4 (2000).



20. Breitwieser, G.E. G protein-coupled receptor oligomerization: implications for G protein activation and cell signaling. *Circ Res* **94**, 17-27 (2004).
21. Ballesteros, J.A. and Weinstein, H. Integrated methods for the construction of three dimensional models and computational probing of structure-function relations in G-protein coupled receptors. *Methods Neurosci.* **25**, 366-428 (1995).
22. Teller, D.C., Okada, T., Behnke, C.A., Palczewski, K. and Stenkamp, R.E. Advances in determination of a high-resolution three-dimensional structure of rhodopsin, a model of G-protein-coupled receptors (GPCRs). *Biochemistry* **40**, 7761-72 (2001).
23. Okada, T. et al. Functional role of internal water molecules in rhodopsin revealed by X-ray crystallography. *Proc Natl Acad Sci U S A* **99**, 5982-7 (2002).
24. Li, J., Edwards, P.C., Burghammer, M., Villa, C. and Schertler, G.F. Structure of bovine rhodopsin in a trigonal crystal form. *J Mol Biol* **343**, 1409-38 (2004).
25. Okada, T. et al. The retinal conformation and its environment in rhodopsin in light of a new 2.2 Å crystal structure. *J Mol Biol* **342**, 571-83 (2004).
26. Fanelli, F. and De Benedetti, P.G. Computational modeling approaches to structure-function analysis of G protein-coupled receptors. *Chem Rev* **105**, 3297-351 (2005).
27. Ramachandran, G.N. and Sasisekharan, V. Conformation of polypeptides and proteins. *Adv Protein Chem* **23**, 283-438 (1968).
28. Gerdin, M.J., Mseeh, F. and Dubocovich, M.L. Mutagenesis studies of the human MT2 melatonin receptor. *Biochem Pharmacol* **66**, 315-20 (2003).
29. Kokkola, T. and Laitinen, J.T. Melatonin receptor genes. *Ann Med* **30**, 88-94 (1998).
30. Reppert, S.M., Weaver, D.R. and Ebisawa, T. Cloning and characterization of a mammalian melatonin receptor that mediates reproductive and circadian responses. *Neuron* **13**, 1177-85 (1994).
31. Browning, C., Beresford, I., Fraser, N. and Giles, H. Pharmacological characterization of human recombinant melatonin mt(1) and MT(2) receptors. *Br J Pharmacol* **129**, 877-86 (2000).
32. Dubocovich, M.L. and Markowska, M. Functional MT1 and MT2 melatonin receptors in mammals. *Endocrine* **27**, 101-10 (2005).
33. Reppert, S.M. et al. Molecular characterization of a second melatonin receptor expressed in human retina and brain: the Mel1b melatonin receptor. *Proc Natl Acad Sci U S A* **92**, 8734-8 (1995).
34. Dubocovich, M.L., Masana, M.I., Iacob, S. and Sauri, D.M. Melatonin receptor antagonists that differentiate between the human Mel1a and Mel1b recombinant subtypes are used to assess the pharmacological profile of the rabbit retina ML1 presynaptic heteroreceptor. *Naunyn Schmiedebergs Arch Pharmacol* **355**, 365-75 (1997).
35. Dubocovich, M.L., Yun, K., Al-Ghoul, W.M., Benloucif, S. and Masana, M.I. Selective MT2 melatonin receptor antagonists block melatonin-mediated phase advances of circadian rhythms. *Faseb J* **12**, 1211-20 (1998).
36. Sumaya, I.C., Masana, M.I. and Dubocovich, M.L. The antidepressant-like effect of the melatonin receptor ligand luzindole in mice during forced swimming requires expression of MT2 but not MT1 melatonin receptors. *J Pineal Res* **39**, 170-7 (2005).
37. Dubocovich, M.L. Melatonin receptors: are there multiple subtypes? *Trends Pharmacol Sci* **16**, 50-6 (1995).
38. Molinari, E.J., North, P.C. and Dubocovich, M.L. 2-[125I]iodo-5-

- methoxycarbonylamino-N-acetyltryptamine: a selective radioligand for the characterization of melatonin ML2 binding sites. *Eur J Pharmacol* **301**, 159-68 (1996).
39. Mailliet, F. et al. Characterization of the melatonergic MT(3) binding site on the NRH:quinone oxidoreductase 2 enzyme. *Biochem Pharmacol* **71**, 74-88 (2005).
  40. Altschul, S.F., Gish, W., Miller, W., Myers, E.W. and Lipman, D.J. Basic local alignment search tool. *J Mol Biol* **215**, 403-10 (1990).
  41. Thompson, J.D., Higgins, D.G. and Gibson, T.J. CLUSTAL W: improving the sensitivity of progressive multiple sequence alignment through sequence weighting, position-specific gap penalties and weight matrix choice. *Nucleic Acids Res* **22**, 4673-80 (1994).
  42. Wallner, B. and Elofsson, A. All are not equal: a benchmark of different homology modeling programs. *Protein Sci* **14**, 1315-27 (2005).
  43. Schwede, T., Kopp, J., Guex, N. and Peitsch, M.C. SWISS-MODEL: An automated protein homology-modeling server. *Nucleic Acids Res* **31**, 3381-5 (2003).
  44. Fiser, A. and Sali, A. Modeller: generation and refinement of homology-based protein structure models. *Methods Enzymol* **374**, 461-91 (2003).
  45. Morris, G.M. et al. Automated Docking Using a Lamarckian Genetic Algorithm and an Empirical Binding Free Energy Function. *J Comput Chem* **19**, 1639 - 1662 (1998).
  46. van Gunsteren, W.F. and Mark, A.E. Validation of molecular dynamics simulation. *J. Chem. Phys.* **108**, 6109-6116 (1998).
  47. Lindahl, E., Hess, B. and van der Spoel, D. GROMACS 3.0: a package for molecular simulation and trajectory analysis. *J Mod Model* **7**, 306-317 (2001).
  48. Case, D.A. et al. The Amber biomolecular simulation programs. *J Comput Chem* **26**, 1668-88 (2005).
  49. Brooks, B.R. et al. CHARMM: A Program for Macromolecular Energy, Minimization, and Dynamics Calculations,. *J. Comp. Chem.* **4**, 187-217 (1983).
  50. Phillips, J.C. et al. Scalable molecular dynamics with NAMD. *J Comput Chem* **26**, 1781-802 (2005).
  51. Thornton, J.M., Todd, A.E., Milburn, D., Borkakoti, N. and Orengo, C.A. From structure to function: approaches and limitations. *Nat Struct Biol* **7 Suppl**, 991-4 (2000).
  52. Berman, H.M. et al. The Protein Data Bank. *Acta Crystallogr D Biol Crystallogr* **58**, 899-907 (2002).
  53. Cserzo, M., Wallin, E., Simon, I., von Heijne, G. and Elofsson, A. Prediction of transmembrane alpha-helices in prokaryotic membrane proteins: the dense alignment surface method. *Protein Eng* **10**, 673-6 (1997).
  54. Hirokawa, T., Boon-Chieng, S. and Mitaku, S. SOSUI: classification and secondary structure prediction system for membrane proteins. *Bioinformatics* **14**, 378-9 (1998).
  55. Hofmann, K. and Stoffel, W. TMbase - A database of membrane spanning proteins segments. *Biol. Chem. Hoppe-Seyler* **374**, 166 (1993).
  56. Rost, B., Casadio, R., Fariselli, P. and Sander, C. Transmembrane helices predicted at 95% accuracy. *Protein Sci* **4**, 521-33 (1995).
  57. Tusnady, G.E. and Simon, I. The HMMTOP transmembrane topology prediction server. *Bioinformatics* **17**, 849-50 (2001).
  58. Krogh, A., Larsson, B., von Heijne, G. and Sonnhammer, E.L. Predicting

- transmembrane protein topology with a hidden Markov model: application to complete genomes. *J Mol Biol* **305**, 567-80 (2001).
59. Sonnhammer, E.L., von Heijne, G. and Krogh, A. A hidden Markov model for predicting transmembrane helices in protein sequences. *Proc Int Conf Intell Syst Mol Biol* **6**, 175-82 (1998).
  60. Jones, D.T., Taylor, W.R. and Thornton, J.M. A model recognition approach to the prediction of all-helical membrane protein structure and topology. *Biochemistry* **33**, 3038-49 (1994).
  61. Persson, B. and Argos, P. Prediction of membrane protein topology utilizing multiple sequence alignments. *J Protein Chem* **16**, 453-7 (1997).
  62. Claros, M.G. and von Heijne, G. TopPred II: an improved software for membrane protein structure predictions. *Comput Appl Biosci* **10**, 685-6 (1994).
  63. von Heijne, G. Membrane protein structure prediction. Hydrophobicity analysis and the positive-inside rule. *J Mol Biol* **225**, 487-94 (1992).
  64. Kyte, J. and Doolittle, R.F. A simple method for displaying the hydrophobic character of a protein. *J Mol Biol* **157**, 105-32 (1982).
  65. Engelman, D.M., Steitz, T.A. and Goldman, A. Identifying nonpolar transbilayer helices in amino acid sequences of membrane proteins. *Annu Rev Biophys Biophys Chem* **15**, 321-53 (1986).
  66. Dayhoff, M.O., Schwartz, R.M. and Orcutt, B.C. *A model of evolutionary change in proteins*, 345-352 (Nat. Biomed. Res. Found., Washington D.C., 1978).
  67. Henikoff, S. and Henikoff, J.G. Amino acid substitution matrices from protein blocks. *Proc Natl Acad Sci U S A* **89**, 10915-9 (1992).
  68. Peitsch, M.C. ProMod and Swiss-Model: Internet-based tools for automated comparative protein modelling. *Biochem Soc Trans* **24**, 274-9 (1996).
  69. Luthy, R., Bowie, J.U. and Eisenberg, D. Assessment of protein models with three-dimensional profiles. *Nature* **356**, 83-5 (1992).
  70. Nezbeda, I., Kolafa, J. and Kotrla, M. *Úvod do počítačových simulací - Metody Monte Carlo a molekulární dynamiky*, 205 (Karolinum, Praha, 2002).
  71. Berendsen, H.J.C., Postma, J.P.M., van Gunsteren, W.F., DiNola, A. and Haak, J.R. Molecular dynamics with coupling to an external bath. *J Chem Phys* **81**, 3684-3690 (1984).
  72. Nosé, S. A molecular dynamics method for simulations in the canonical ensemble. *Mol Phys* **52**, 255-268 (1984).
  73. Hoover, W.G. Canonical dynamics: Equilibrium phase-space distributions. *Phys. Rev. A* **31**, 1695-1697 (1985).
  74. Van Der Spoel, D. et al. GROMACS: fast, flexible, and free. *J Comput Chem* **26**, 1701-18 (2005).
  75. Hess, B., Bekker, H., Berendsen, H.J.C. and Fraaije, J.G.E.M. LINCS: A linear constraint solver for molecular simulations. *J. Comp. Chem.* **18**, 1463-1472 (1997).
  76. Ryckaert, J.P., Ciccotti, G. and Berendsen, H.J.C. Numerical integration of the cartesian equations of motion of a system with constraints; molecular dynamics of n-alkanes. *J. Comp. Phys.* **23**, 327-341 (1977).
  77. van Gunsteren, W.F. and Berendsen, H.J.C. *Gromos-87 manual* (AG Groningen, The Netherlands, Biomos BV Nijenborgh 49747, 1987).
  78. van Buuren, A.R., Marrink, S.J. and Berendsen, H.J.C. A molecular dynamics study of the decane/water interface. *J. Phys. Chem.* **97**, 9206-9212 (1993).
  79. Mark, A.E., van Helden, S.P., Smith, P.E., Janssen, L.H.M. and van Gunsteren,

- W.F. Convergence properties of free energy calculations: alpha-cyclodextrin complexes as a case study. *J. Am. Chem. Soc.* **116**(1994).
80. Jorgensen, W.L., Chandrasekhar, J., Madura, J.D., Impey, R.W. and Klein, M.L. Comparison of simple potential functions for simulating liquid water. *J. Chem. Phys.* **79**, 926–935 (1983).
  81. Van Buuren, A.R. and Berendsen, H.J. Molecular dynamics simulation of the stability of a 22-residue alpha-helix in water and 30% trifluoroethanol. *Biopolymers* **33**, 1159-66 (1993).
  82. Liu, H., Müller-Plathe, F. and van Gunsteren, W.F. A force field for liquid dimethyl sulfoxide and liquid properties of liquid dimethyl sulfoxide calculated using molecular dynamics simulation. *J. Am. Chem. Soc.* **117**, 4363–4366 (1995).
  83. van Gunsteren, W.F. et al. *Biomolecular Simulation: The GROMOS96 manual and user guide*, (Hochschulverlag AG an der ETH Zürich, Zürich, Switzerland: , 1996).
  84. Kaminski, G.A., Friesner, R.A., Tirado-Rives, J. and Jorgensen, W.L. Evaluation and Reparametrization of the OPLS-AA Force Field for Proteins via Comparison with Accurate Quantum Chemical Calculations on Peptides. *J. Phys. Chem. B* **105**, 6474-6487 (2001).
  85. Altschul, S.F. et al. Gapped BLAST and PSI-BLAST: a new generation of protein database search programs. *Nucleic Acids Res* **25**, 3389-402 (1997).
  86. Guex, N. and Peitsch, M.C. SWISS-MODEL and the Swiss-PdbViewer: an environment for comparative protein modeling. *Electrophoresis* **18**, 2714-23 (1997).
  87. Rivara, S. et al. Analysis of structure-activity relationships for MT2 selective antagonists by melatonin MT1 and MT2 receptor models. *J Med Chem* **48**, 4049-60 (2005).
  88. Schuttelkopf, A.W. and van Aalten, D.M. PRODRG: a tool for high-throughput crystallography of protein-ligand complexes. *Acta Crystallogr D Biol Crystallogr* **60**, 1355-63 (2004).
  89. Tieleman, D.P., Marrink, S.J. and Berendsen, H.J. A computer perspective of membranes: molecular dynamics studies of lipid bilayer systems. *Biochim Biophys Acta* **1331**, 235-70 (1997).
  90. Tieleman, D.P. and Berendsen, H.J. A molecular dynamics study of the pores formed by Escherichia coli OmpF porin in a fully hydrated palmitoylcholine bilayer. *Biophys J* **74**, 2786-801 (1998).
  91. Daura, X. et al. Peptidfaltung: Wenn die Simulation das Experiment erreicht. *Angew. Chem. Int. Ed.* **111**, 249 - 253 (1999).
  92. Graham, F.L., Smiley, J., Russell, W.C. and Nairn, R. Characteristics of a human cell line transformed by DNA from human adenovirus type 5. *J Gen Virol* **36**, 59-74 (1977).
  93. Bradford, M.M. A rapid and sensitive method for the quantitation of microgram quantities of protein utilizing the principle of protein-dye binding. *Anal Biochem* **72**, 248-54 (1976).
  94. Sippl, M.J., Hendlich, M. and Lackner, P. Assembly of polypeptide and protein backbone conformations from low energy ensembles of short fragments: Development of strategies and construction of models for myoglobin, lysozyme, and thymosin p4. *Protein Science* **I**, 625-640 (1992).
  95. Mseeh, F., Gerdin, M.J. and Dubocovich, M.I. Identification of cysteines involved in ligand binding to the human melatonin MT(2) receptor. *Eur J*

- Pharmacol* **449**, 29-38 (2002).
96. Grol, C.J. and Jansen, J.M. The high affinity melatonin binding site probed with conformationally restricted ligands--II. Homology modeling of the receptor. *Bioorg Med Chem* **4**, 1333-9 (1996).
  97. Jansen, J.M. et al. The high affinity melatonin binding site probed with conformationally restricted ligand--I. Pharmacophore and minireceptor models. *Bioorg Med Chem* **4**, 1321-32 (1996).
  98. Mazna, P. et al. Molecular modeling of human MT2 melatonin receptor: the role of Val204, Leu272 and Tyr298 in ligand binding. *J Neurochem* **91**, 836-42 (2004).
  99. Mazna, P. et al. Ligand binding to the human MT2 melatonin receptor: the role of residues in transmembrane domains 3, 6, and 7. *Biochem Biophys Res Commun* **332**, 726-34 (2005).
  100. Berka, K. et al. Molecular determinants of the agonist binding site of human MT2 melatonin receptor. *Materials Structure* **12**, 26 (2005).
  101. Wiesner, J. Modeling the Enzyme-substrate Complex: Cytochrome P450 3A4-ellipticine. *Diploma thesis*, Charles University in Prague (2004).
  102. Šilhán, J. Studium konformace C-terminálního segmentu 14-3-3ζ proteinu. *Diplomová práce*, Charles University in Prague (2005).
  103. Bouřa, E. Studium interakcí C-konce DNA vazebné domény proteinu AFX (FoxO4) s DNA. *Diplomová práce*, Charles University in Prague (2005).
  104. Pabiánová, A. Studium interakcí mezi DNA vazebnou doménou forkhead transkripčního faktoru FoxO4 a 14-3-3 proteinem. *Diplomová práce*, Charles University in Prague (2005).

# 8 Appendixes

## 8.1 Human MT2 melatonin receptor sequence

```

1 msengsfanc ceaggwavrp gwsgagsarp srtprppwva palsavlivt tadvvgnll
61 vilsvlrnrk lrnagnlflv slaladlvva fypyplilva ifydgwalge ehckasafvm
121 glsvigsvfn itaiainryc yichsmayhr iyrrwhtplh icliwlltvv allpnffvgs
181 leydpriysc tfigtastqy taavvvihfl lpiavvsfcy lriwvvlvqa rrkakpesrl
241 clkpsdlrsf ltmfvvfivf aicwaplnci glavainpge mapqipeglf vtsyllayfn
301 sclnaivygl lnqnrreyk rillalwnpr hciqdaskgs haegllqspap piigvqhqd
361 al

```

Figure 8.1 - The complete sequence of MT2 melatonin receptor (NP\_005950) [33]

## 8.2 Maps of plasmids

### 8.2.1 pcDNA3

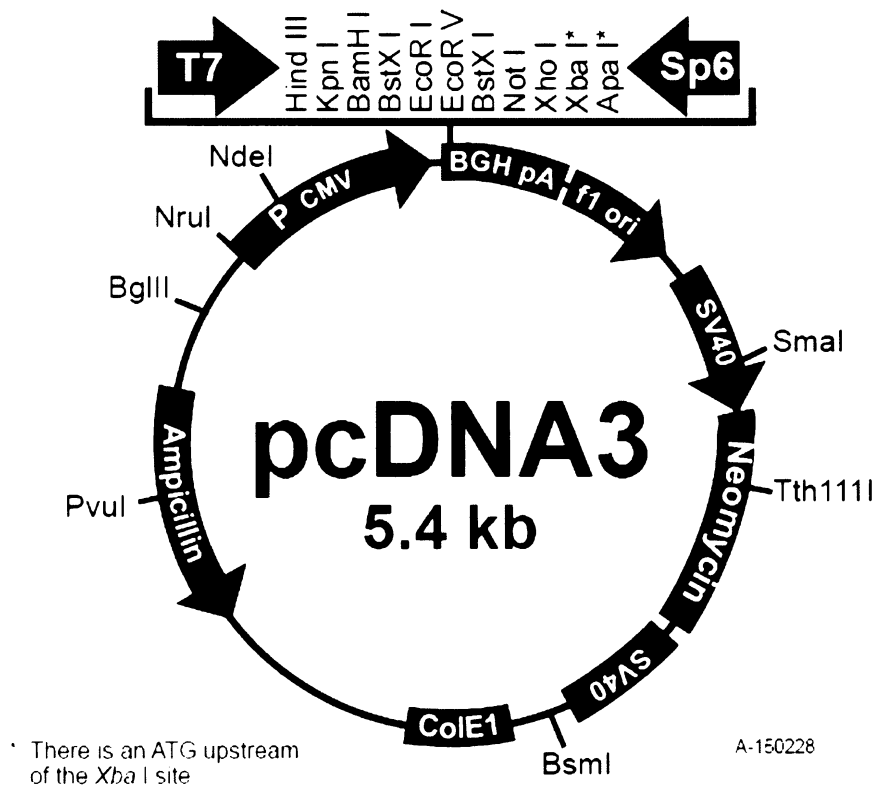
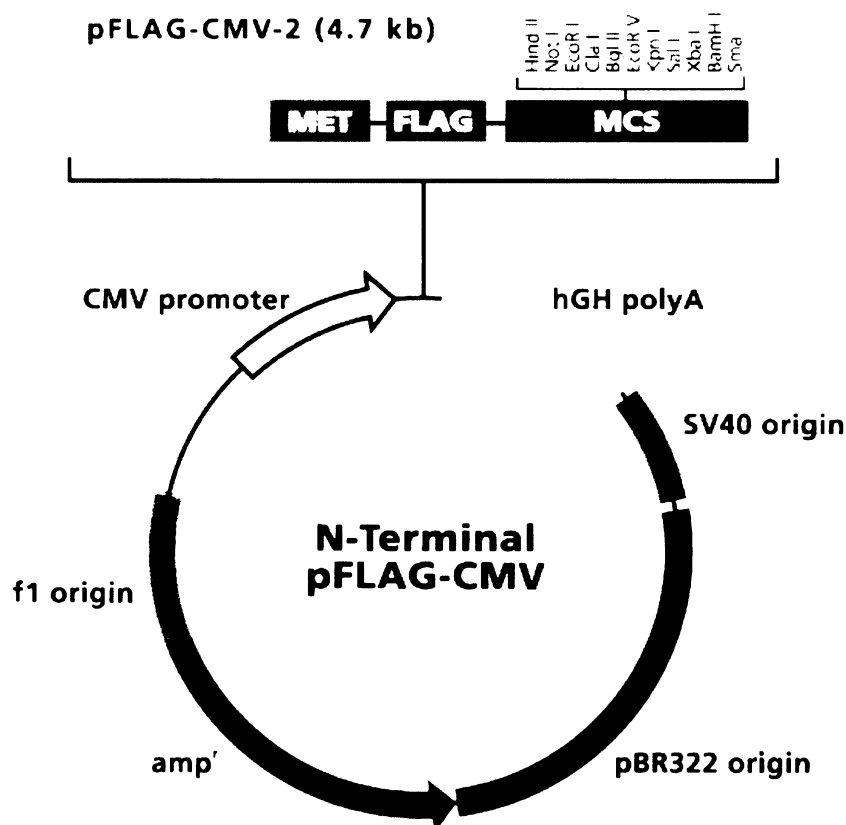


Figure 8.2 – map of the vector pcDNA3 (Invitrogen, USA)

Plasmid provides ampicillin and neomycin resistance. Sequence for human MT2 melatonin receptor was cloned into the multiple cloning site. Multiple cloning site contains also Hind III and Eco RI sites for respective restriction endonucleases.

## 8.2.2 pFLAG-CMV-2

In order to efficiently visualise the expression of MT2 receptor in eukaryotic cells the cDNA encoding the human MT2 melatonin receptor from pcDNA3 (Invitrogene, USA) was mutated and inserted into the pFLAG-CMV-2 plasmid (Sigma Aldrich, USA) with restriction endonucleases Hind III and Eco RI by Ing. Teisinger, CSc.. Using this vector we were able to express human MT2 melatonin receptor with N-terminally fused FLAG epitope for immunological visualization of receptor expression using confocal microscopy. FLAG-tag is a short peptide fused to the receptor, which is recognisable by specific anti-FLAG antibody connected with visualisation system (fluorescence probe).



### Multiple Cloning Site

FLAG Peptide Sequence																		
Met*	Asp	Tyr	Lys	Asp	Asp	Asp	Asp	Lys			Not I	EcoR I						
AUG	GAC	UAC	AAA	GAC	GAC	GAC	GAC	AAG	GII	GCG	GCC	GCG	AAI	TCA				
TAC	CCG	ATG	TTT	CCG	CCA	CCG	CTG	CCC	GAA	CGC	CGG	CGC	TTA	AGT				
Hind III																		
			Cla I		Bgl II		EcoR V		Kpn I		Sal I		Xba I		BamH I		Sma I	
TCG	ACA	GAT	CTG	ATA	TCG	GTA	CCA	GTC	GAC	TCT	AGA	GGA	TCC	CGG	GT			
AGC	TAI	CIA	GAC	IAT	AGC	CAT	GGT	CAG	CTG	AGA	TCI	CCT	AGG	GCC	CA			

**Figure 8.3** - map of the vector pFLAG-CMV-2 (Sigma Aldrich, USA) Plasmid contains ampicillin resistance. Multiple cloning site starts with Hind III restriction site followed by Eco RI restriction site. Inserted

## 8.3 Alignments

### 8.3.1 Alignment I

mel1b 1	MSENGSFANC	CEAGGWAVRP	GWGAGSARP	SRTPRPPWVA	PALSAVLIVT
1f88A 1	M NGTEGPN	FYVP-FSNKT	GVVRSPEAP	QYYLAEPWQF	SMLAAYMFL
	** . .	. . . .	* . . *	** . .	. * . * . .
mel1b 51	<u>TAVDVVGNLL</u>	VILSVLRNRK	LRNAGNLFV	SLALADLVVA	FYPYPLILVA
1f88A 48	<u>IMLGFPINFL</u>	TLYVTVQHKK	LRTPLNYILL	NLAVADLFMV	FGGFTTTLYT
	. ** .	. . . . *	** . * . *	. *** . *** .	* . . * .
mel1b 101	<u>IFYDGWALGE</u>	EHCKASAFVM	GLSVIGSVFN	ITAIAINRYC	YICHSMAYHR
1f88A 98	<u>SLHGYFVFGP</u>	TGCNLEGFFA	TLGGEIALWS	LVVLAIERVY	VVCKPMSNFR
	. . *	* . . *	* . . . .	. . *** . ***	. * . * . *
mel1b 151	<u>IYRRWHTPLH</u>	<u>ICLIWLLTVV</u>	<b>ALLPNFFVGS</b>	LEYDPR----	----IYSCTF
1f88A 148	FG-ENHAIMG	VAFVWVMAA	CAAP-PLVGW	SRYIPEGMQC	SCGIDYYTPH
	. * . .	. . * . . .	* . **	* *	*
mel1b 193	IQTASTQYTA	AVVVIHFLLP	IAVVSFCYLR	IWVLVLQARR	KAKPESRLCL
1f88A 196	EETNNEFVI	YMFVVHFIIP	LIVIFFCYGQ	LVFTVKEAAA	-----SATT
	. * . .	. * . *** . *	. * . *** .	. * . *	
mel1b 243	KPSDLRSFLT	MFVVFVIFAI	CWAPLNCIGL	AVAINPQEMA	PQIPEGLFVT
1f88A 244	QKAEKEVTRM	VIIMVIAFLI	CWLPYAGVAF	YIFTHQ---G	SDFGPIFMTI
	. .	. . . . * *	** * . . .	. . . . .	. . . . .
mel1b 293	<u>SYLLAYFN</u> SC	<u>LNAIVYGLLN</u>	QNFRRYKRI	LLALWNPRHC	IQDASKGSHA
1f88A 291	<u>PAFFAKTSAV</u>	YNPVIYIMMN	KQFRNCMVT	LCCGKNP---	---STTVSKT
	. . . * . .	* . . * . *	**	* **	. . * .
mel1b 343	EGLQSPAPPI	IGVQHQADAL			
1f88A 341	ETSQVAPA -				
	* * . . .				

**Figure 8.4 - Alignment I**

Pair-wise alignment between hMT2 receptor sequence and bovine rhodopsin sequence (1F88) was generated using ClustalW [41]. Identical amino acids are noted with stars, while similar amino acids are noted with points. Underlined amino acids were predicted to be a part of TM segments. Bold amino acid is situated in TM 4 region and has not its mirror in template.

### 8.3.2 Alignment II

mel1b 1	MSENGSFANC	CEAGGWAVRP	GWGAGSAR-	PSRTPR----	PPWVAPALSA
1F88 1	MNG	TEGPNFYV-P	FSNKTGVVRS	PFEAPQYYLA	EPWQFSMLAA
	*	* . * *	. . * *	* . *	** . * . *
mel1b 46	<u>VLI</u> TTAVDV	VGNLLVILSV	LRNRKLRNAG	NLFLVSLALA	DLVVAFYYP
1F88 43	<u>YM</u> LLIMLGF	PINFLTLYVT	VQHKKLRTPL	NYILLNLAVA	DLFMVFGGFT
	. . .	* . * .	. . . . *** .	* . * . * . * . *	** . * .
mel1b 96	<u>LILVAIF</u> YDG	WALGEEHCKA	<u>SAFVMGLSVI</u>	GSVFNITAI	INRYCYICH
1F88 93	<u>TTLYT</u> SLHGY	FVFGPTGCNL	EGFFATLGGE	IALWSLVVLA	IERVYVVKCP
	* . .	* * .	* * .	. . . . *	* . * . * . *
mel1b 146	MAYHRIYRRW	HTPLHICLIW	LLTVVALLPN	<b>FFVGS</b> LEYDP	RIYSCT----
1F88 143	MSNFR-FGEN	HAIMGVAFTW	VMALACAAPP	L-VGWSRYIP	EGMQCSCGID
	* . * .	* . . . . *	. . . .	* . ** * *	* .



```

mel1b 192 -FI---QTAS TQYTAAVVVI HFLLPIAVVS FCYLRIWVLV LQARRKAKPE
1F88 191 YYTPHEETNN ESFVIYMFVV HFIIPLIVIF FCYGQL-VFT VKEAAA----
      . . * . . . * . * . * . * . * . * . * .
mel1b 238 SRLCLKPS-D LRSFLTMFVV FVIFAICWAP LNCIGLAVAI NPQEMAPQIP
1F88 240 SATTQKA--- ---EKEVTRM VIIMVIAFLI CWLPYAGVAF YIFTHQGSDF
      * * * . . . * * . * . * .
mel1b 287 EGLFVTSYLL AYFNSCLNAI VYGLLNQNFR REYKRILLAL WNPRHCIQDA
1F88 284 GPIFMTIPAF FAKTSAVYNP VIYIMMNKQF RNCMVTTLCC GKNP-----
      . * . * . * . * . * . * . * .
mel1b 337 SKGSHAEGLQ SPAPPIIGVQ HQADAL
1F88 334 STTVSKTETS QV-APA
      * . *

```

**Figure 8.5 - Alignment II**

Pair-wise alignment between hMT2 receptor sequence and bovine rhodopsin sequence (1F88) was generated using pseudopotential threading function in program DeepView / SwissPDBViewer 3.7 [86, 94]. Identical amino acids are noted with stars, while similar amino acids are noted with points. Underlined amino acids were predicted to be a part of TM segments. Bold amino acids are situated in transmembrane regions TM 4 and TM 5 and have not their mirrors in template.

### 8.3.3 Alignment III

```

mel1b 1 MSENSFANC CEAGGWAVRP GWSGAGSARP SRTPRPPWVA PALSAVLIVT
1F88 1 MNGTEGP NFYVPFSNKT GVVRSPFEAP QYLAEPWQF SMLAAYMFLL
      . . . * . * . * . * . * . * . * .
mel1b 51 TAVDVVGNLL VILSVLRNRK LRNAGNLFLV SLALADLVVA FYPYPLILVA
1F88 48 IMLGFPINFL TLYVTVQHKK LRTPLNYILL NLAVADLFMV FGFTTTLYT
      . * . * . * . * . * . * . * . * . * .
mel1b 101 IFYDGWALGE EHCKASAFVM GLSVIGSVFN ITAIAINRYC YICHSMAYHR
1F88 98 SLHGYFVFGP TGCNLEGFFA TLGGEIALWS LVVLAIERYV VVCKPMS-NF
      . * . * . * . * . * . * . * . * . * .
mel1b 151 IYRRWHTPLH ICLIWLLTVV ALLPNFFVGS LEYDPRIY-S CT---FI---
1F88 147 RFGENHAIMG VAFTWVMALA CAAPPLVGWS RYIPEGMQCS CGIDYYTPHE
      . * . * . * . * . * . * . * . * . * .
mel1b 194 QTASTQYTAA VVVIHFLLPI AVVSFCYLRI WVLVLQARRK AKPESRLCLK
1F88 197 ETNNESFVIY MFVVHFIIPL IVIFFCYGQL VFTVKEAAA- ----SATTQ
      . * . * . * . * . * . * . * . * . * .
mel1b 244 PSDLRSFLTM FVVVFIFAIC WAPLNCIGLA VAINPQEMAP QIPEGLFVTS
1F88 245 KAEKEVTRMV IIMVIAFLIC WLPYAGVAFY IFTHQGSD-- -FGPIFMTIP
      . . . * . * . * . * . * . * . * . * .
mel1b 294 YLLAYFNSCL NAIVYGLLNQ NFRREYKRIL LALWNPRHCI QDASKGSHAE
1F88 292 AFFAKTSAVY NPVIYIMMNK QFRNCMVTTL CCGKNP---- --STTVSKTE
      . * . * . * . * . * . * . * . * . * .
mel1b 344 GLQSPAPPII GVQHQADAL
1F88 342 TSQVAPA
      * . . .

```

**Figure 8.6 - Alignment III**

Pair-wise alignment between hMT2 receptor sequence and bovine rhodopsin sequence (1U19) was generated on the basis of published alignment by Rivara *et al.* [87]. Identical amino acids are noted with stars, while similar amino acids are noted with points. Underlined amino acids were predicted to be a part of TM segments.

## 8.4 Gromacs run scripts

### 8.4.1 Energy minimization

```
define      = -DFLEX_SPC    ; flexible SPC water instead of SPC
constraints= none
integrator  = steep        ; steepest descent energy minimization
nstcomm     = 1           ; [steps] frequency of centre of mass removal
ns_type     = grid        ; grid search for neighbour list
nstlist     = 10          ; [steps] frequency of neighbour list update
;
;      Energy minimization parameters
nsteps      = 750         ; [steps] maximum number of minimisation steps
emtol       = 1000        ; [kJ.mol-1.nm-1] maximum force to converge
emstep      = 0.01        ; [nm] initial step size
;
;      Electrostatics
rlist       = 0.9         ; [nm] distance for the neighbour list cut-off
coulombtype= PME          ; Particle-Mesh Ewald sum electrostatics
rcoulomb    = 0.9         ; [nm] distance for the Coulomb cut-off
rvdw        = 1.0         ; [nm] distance for the LJ cut-off
fourierspacing=0.12; [nm] max grid space for FFT grid
pme_order   = 4           ; interpolation order for PME
optimize_fft= yes        ; optimization of FFT grid at the start of MD
;
;      Couplings
Tcoupl      = no          ; temperature coupling is off
Pcoupl      = no          ; pressure coupling is off
gen_vel     = no          ; velocities are not generated
```

### 8.4.2 Pre-run with positional restraints

```
define      = -DPOSRES      ;positional restraint on protein and
melatonin
constraints= all-bonds
integrator  = md            ; leap-frog Verlet integrator
dt          = 0.002        ; [ps] integration time step
nsteps      = 25000        ; [steps] total time 50 ps.
nstcomm     = 1            ; see 8.4.1
nstxout     = 250          ; [steps] coordinates each 0.5 ps
nstvout     = 1000         ; [steps] velocities each 2 ps
nstfout     = 0            ; [steps] output forces never
nstenergy   = 10           ; [steps] energy output
nstlist     = 10           ; see 8.4.1
ns_type     = grid         ; see 8.4.1
rlist       = 0.9          ; see 8.4.1
;
;      Electrostatics
coulombtype = PME          ; see 8.4.1
rcoulomb    = 0.9          ; see 8.4.1
rvdw        = 0.9          ; see 8.4.1
fourierspacing = 0.12     ; see 8.4.1
```

```

ewald_rtol      = 1e-5      ; see 8.4.1
pme_order      = 6          ; interpolation order for PME
optimize_fft   = yes        ; see 8.4.1
;
;   Couplings
Tcoupl         = berendsen  ;
tc-grps        = Protein DRG POPE SOL CL  ;
tau_t          = 0.1        0.1 0.1 0.1 0.1 ;
ref_t          = 300        300 300 300 300 ;
;energy monitoring
; Berendsen temperature coupling given by equation (1.12) of five
molecular groups to ref_t with relaxation time tau_t.
;
;   Energy monitoring of groups
energygrps     = Protein DRG POPE SOL CL ;

; Berendsen pressure coupling given by equation (1.13) is on
pcoupl         = berendsen
pcoupltype     = anisotropic ; box remains rectangular
tau_p          = 10 ; pressure coupling time parameter
compressibility = 4.5e-5 4.5e-5 4.5e-5 0 0 0 ;compressibility
xx, yy, zz, xy, xz, yz
ref_p          = 1.0 1.0 1.0 1.0 1.0 1.0 ;reference pressure for
each direction
;
; Velocities are generated by Maxwell distribution at the
temperature gen_temp 300 K with random seed gen_seed.
gen_vel        = yes
gen_temp       = 300.0
gen_seed       = 173529

```

### 8.4.3 Full production run

```

constraints= all-bonds
integrator   = md          ; leap-frog Verlet integrator
dt          = 0.002       ;[ps] integration time step
nsteps      = 250 000    ;[steps] total time 500 ps
nstcomm     = 1          ; see 8.4.1
nstxout     = 500        ;[steps] coordinates each 1 ps
nstvout     = 10000     ;[steps] velocities each 20 ps
nstfout     = 0          ;[steps] output forces never
nstlog      = 100       ;[steps] log output each 0.5 ps
nstenergy   = 100       ;[steps] energy output each 0.5 ps
nstlist     = 10        ; see 8.4.1
ns_type     = grid       ; see 8.4.1
rlist       = 0.9        ; see 8.4.1
;
;   Electrostatics
coulombtype  = PME        ; see 8.4.1
rcoulomb     = 0.9        ; see 8.4.1
rvdw         = 1.0        ; see 8.4.1
fourierspacing = 0.12    ; see 8.4.1
ewald_rtol   = 1e-5      ; see 8.4.1
pme_order    = 4          ; interpolation order for PME
optimize_fft = yes        ; see 8.4.1

```

```

;
; Couplings
; Berendsen temperature coupling given by equation (1.12) of five
molecular groups to ref_t with relaxation time tau_t.
Tcoupl = berendsen ;
tc-grps = Protein DRG POPE SOL CL ;
tau_t = 0.1 0.1 0.1 0.1 0.1 ;
ref_t = 300 300 300 300 300 ;
; Energy monitoring of groups:
energygrps = Protein DRG POPE SOL CL ;
;
; Berendsen pressure coupling given by equation (1.13) is on
pcoupl = berendsen
pcoupltype = anisotropic ; box remains rectangular
tau_p = 10 ; pressure coupling time parameter
compressibility = 4.5e-5 4.5e-5 4.5e-5 0 0 0 ;compressibilities
xx, yy, zz, xy, xz, yz
ref_p = 1.0 1.0 1.0 1.0 1.0 1.0 ;reference pressure for
each direction
;
; Velocities are generated by Maxwell distribution at the
temperature gen_temp 300 K with random seed gen_seed.
gen_vel = yes
gen_temp = 300.0
gen_seed = 173529

```

## 8.4.4 Steepest descent minimization of average structure

```

constraints= none ;all constraints are off
integrator = steep; steepest descent energy minimization
nsteps = 3000 ;[steps] maximum number of minimisation steps
;
; Energy minimizing stuff
emtol = 200 ;[kJ.mol-1.nm-1] maximum force to converge
emstep = 0.01 ;[nm] initial step size

nstcomm = 1 ;[steps] frequency of centre of mass removal
ns_type = grid ; grid search for neighbour list
morse = no ; harmonic potential
rlist = 1.2 ;
;
; Electrostatics
coulombtype= Shift ; Shifted Coulomb potential
vdw_type = Shift ; Shifted van der Waals potential
rcoulomb = 1.2 ;[nm] distance for the Coulomb cut-off
rcoulomb_switch = 1.0 ;[nm] distance to start forces decay to
zero at rcoulomb distance
rvdw = 1.2 ;[nm] distance for the LJ cut-off
rvdw_switch= 1.0 ;[nm] distance to start forces decay to zero at
rvdw distance
epsilon_r = 6.0 ; dielectric constant changed
;
; Couplings
Tcoupl = no ; temperature coupling is off
Pcoupl = no ; pressure coupling is off

```

```
gen_vel = no ; velocities are not generated
```

## 8.4.5 Conjugated gradient minimization

```
integrator = cg ; conjugated gradients
nsteps = 3000 ;[steps] maximum number of minimisation steps
;
; Energy minimizing stuff
emtol = 100 ;[kJ.mol-1.nm-1] maximum force to converge
emstep = 0.01 ;[nm] initial step size
nstcgsteep = 1000 ;frequency of addition of 1 steepest
descent step .
```

```
nstcomm = 1 ;[steps] frequency of centre of mass removal
ns_type = grid ; grid search for neighbour list
morse = no ;harmonic potential
rlist = 1.2
;
; Electrostatics
coulombtype= Shift ; Shifted Coulomb potential
vdw_type = Shift ; Shifted van Der Waals potential
rcoulomb = 1.2 ;[nm] distance for the Coulomb cut-off
rcoulomb_switch = 1.0 ;[nm] distance to start forces decay to
zero at rcoulomb distance
rvdw = 1.2 ;[nm] distance for the LJ cut-off
rvdw_switch= 1.0 ;[nm] distance to start forces decay to zero at
rvdw distance
epsilon_r = 6.0 ; dielectric constant changed
;
; Couplings
Tcoupl = no ; temperature coupling is off
Pcoupl = no ; pressure coupling is off
gen_vel = no ; velocities are not generated
```

## 8.5 Site-directed mutagenesis data

Mutagenesis data for evaluation of models were gained from various data:

- data from our group measured by Mazna and published in [98, 99],
- unpublished data from our group,
- data from combined computational and pharmacophoric studies by Grol [96]
- data from GPCRDB from site-directed mutagenesis by Gerdin [28]
- data from site-directed mutagenesis and chemical modifications by Mseeh [95]

Table 8.1 – Binding data of 2-[<sup>125</sup>I]-iodomelatonin to the mutated hMT2 melatonin receptor from various sources. WT means wild-type, mutations are described by the notation XyyyZ, where X is wild type amino acid at position yyy, which was mutated to Z. K<sub>d</sub> is dissociation equilibration constant and B<sub>max</sub> is a number of binding sites per mg of membrane tissue and can be used as a measure of expression

Mutation	K <sub>d</sub> [pM]	B <sub>max</sub> [fmol/mg]	$\frac{K_d}{K_{d,WT}}$	$\frac{B_{max}}{B_{max,WT}}$	Mutation Result	Publication
WT	145 ± 25	1182 ± 350	100 ± 34	100 ± 59		Mazna [99]
WT	128 ± 15	1085 ± 133	100 ± 23	100 ± 25		Mazna [98]
WT	128 ± 61	2440 ± 130	100 ± 95	100 ± 11		Mseeh [95]
WT	130 ± 10	1706 ± 534	100 ± 15	100 ± 63		Gerdin [28]
P41A	Binding, no data		N.A.	N.A.	Not involved	Unpublished
P93A	Binding, no data		N.A.	N.A.	Not involved	Unpublished
P95A	Binding, no data		N.A.	N.A.	Not involved	Unpublished
C113A	Not binding		N.A.	N.A.	<b>Involved</b>	Mseeh [95]
M120A	165 ± 34	428 ± 135	114 ± 43	36 ± 22	Folding	Mazna [99]
G121A	192 ± 18	854 ± 164	132 ± 35	72 ± 35	<b>Involved</b>	Mazna [99]
G121I	180 ± 22	1367 ± 378	124 ± 37	116 ± 66	Involved?	Mazna [99]
S123	Not binding				Involved?	Grol [96]
S123A	100 ± 30	337 ± 103	77 ± 29	20 ± 12	Folding	Gerdin [28]
V124A	169 ± 30	152 ± 43	117 ± 41	13 ± 7	Folding	Mazna [99]
I125A	165 ± 23	911 ± 286	114 ± 35	77 ± 47	Involved?	Mazna [99]
S127	Not binding				Involved?	Grol [96]
S127A	90 ± 10	621 ± 153	69 ± 13	36 ± 20	Folding	Gerdin [28]
C140A	185±148	110 ± 20	145 ± 185	5 ± 1	Folding	Mseeh [95]
C143A	117 ± 59	4500 ± 64	91 ± 90	184 ± 12	Not involved	Mseeh [95]
P174A	Not binding				Involved?	Unpublished
P174G	Not binding				Involved?	Unpublished
N175A	170 ± 20	1054 ± 204	131 ± 25	62 ± 31	Involved?	Gerdin [28]
Y188A	Not binding				<b>Involved</b>	Mazna [99]
Y188F	Not binding				Involved	Mazna [99]
C190A	Not binding				<b>Involved</b>	Mseeh [95]
V204A	Not binding				Involved	Mazna [98]
V205A	159 ± 35	1388 ± 252	124 ± 42	128 ± 39	Involved?	Mazna [98]
H208	Not binding				Critical	Grol [96]
H208A	290 ± 10	1867 ± 256	223 ± 25	109 ± 49	<b>Critical</b>	Gerdin [28]
F209A	180 ± 37	256 ± 60	141 ± 45	24 ± 8	Folding	Mazna [98]

P212A	Not binding					Involved?	Unpublished
P212G	Not binding					Involved?	Unpublished
C219A	158±127	520 ± 90	123 ± 158	21 ± 5	Folding	Mseeh [95]	
F257A	90 ± 10	2576 ± 343	69 ± 13	151 ± 67	Positive	Gerdin [28]	
C263A	174 ± 68	80 ± 10	136 ± 118	3 ± 1	Folding	Mseeh [95]	
W264A	60 ± 10	75 ± 16	46 ± 11	4 ± 2	Folding	Gerdin [28]	
P266A	Not binding					Involved?	Unpublished
P266G	Not binding					Involved?	Unpublished
N268A	Not binding					<b>Critical</b>	Mazna [99]
N268D	Not binding					Involved	Mazna [99]
N268L	Not binding					Involved	Mazna [99]
N268Q	175 ± 37	1942 ± 384	121 ± 46	164 ± 81	Rescue	Mazna [99]	
G271T	Not saturable						Mazna [98]
L272A	Not binding					Involved	Mazna [98]
A275I	Not binding					<b>Critical</b>	Mazna [99]
A275V	194 ± 41	1711 ± 560	134 ± 51	145 ± 90	Rescue	Mazna [99]	
P278A	Binding, no data					Not involved	Unpublished
P286A	Binding, no data					Not involved	Unpublished
V291A	Not binding					<b>Involved</b>	Mazna [99]
V291I	Not binding					Involved	Mazna [99]
S293A	100 ± 30	1878 ± 312	77 ± 29	110 ± 53	Positive	Gerdin [28]	
L295A	Not binding					<b>Involved</b>	Mazna [99]
L295I	Not binding					Involved	Mazna [99]
L295V	Not binding					Involved	Mazna [99]
Y298A	Not binding					<b>Involved</b>	Mazna [98]
Y298F	Not binding					Involved	Unpublished
C302A	112 ± 44	630 ± 130	88 ± 76	26 ± 7	Folding	Mseeh [95]	

**Positive** - Mutation made binding easier.

**Not involved** - Mutation did not changed binding or production of the receptor.

**Folding** - Mutation depressed expression of the receptor in the membrane.

**Involved** - Binding into the receptor depressed by at least 30%, data usually supported by lower expression of the receptor.

**Involved?** - No binding data unconfirmed by other groups or only light changes in binding or expression

**Critical** - Binding of the receptor diminished.

**Rescue** – Mutation to the similar group rescued at least partly binding.

## 8.6 Author's publications

## Molecular modeling of human MT2 melatonin receptor: the role of Val204, Leu272 and Tyr298 in ligand binding

Petr Mazna,\* Veronika Obsilova,\* Irena Jelinkova,\* Ales Balik,\* Karel Berka,† Zofie Sovova,‡ Rüdiger Ettrich,‡ Petr Svoboda,\*§ Tomas Obsil† and Jan Teisinger\*

\*Institute of Physiology, Academy of Sciences of the Czech Republic, Prague, Czech Republic

†Department of Physical and Macromolecular Chemistry, Faculty of Science, Charles University, Prague, Czech Republic

‡Laboratory of High Performance Computing, Institute of Physical Biology USB and Institute of Landscape Ecology AS CR, Zamek, Nove Hradky, Czech Republic

§Department of Physiology, Faculty of Natural Sciences, Charles University, Prague, Czech Republic

### Abstract

A model of the helical part of the human MT2 melatonin (hMT2) receptor, a member of the G protein-coupled receptors superfamily has been generated, based on the structure of bovine rhodopsin. Modeling has been combined with site-directed mutagenesis to investigate the role of the specific amino acid residues within the transmembrane domains (TM) numbers V, VI and VII of hMT2 receptor in the interaction with 2-iodomelatonin. Saturation binding assays with 2-iodomelatonin demonstrated that the substitution V204A (TMV) resulted in total loss of binding while the mutation V205A had no effect. The replacement of F209 with alanine led to a significant decrease in the Bmax value of receptor binding while

mutations V205A and F209A also within TM V did not significantly change binding properties of the hMT2 receptor. In the case of TM VI, the substitution G271T caused substantial decrease in 2-iodomelatonin binding to the hMT2 receptor. The change L272A (TM VI) as well as mutation Y298A within TM VII completely abolished ligand binding to the receptor. These data suggest that several new amino acid residues within TM V, VI and VII are involved in ligand–MT2 receptor interaction.

**Keywords:** homology modeling, 2-iodomelatonin, melatonin, MT2 melatonin receptor, site-directed mutagenesis.

*J. Neurochem.* (2004) **91**, 836–842.

The pineal hormone melatonin is present in all vertebrate species including humans. Aside from being an important regulator of seasonal reproduction and circadian rhythms Bartness *et al.* (1993), melatonin was reported to be a potentially important immunomodulator (Maestroni 1993), a powerful free radical scavenger (Reiter 1996) and a substance exerting oncostatic activity (Molis *et al.* 1995). Hormone effects are mediated via activation of G protein-coupled receptors (GPCRs), designated as MT1, MT2 and Mel1c, which modulate a wide range of intracellular messengers, e.g. cAMP or  $[Ca^{2+}]_i$  (reviewed in Vanecek 1998; Dubocovich *et al.* 2003). The MT1 and MT2 melatonin receptors are expressed in mammals whereas the Mel1c subtype has been found only in lower vertebrates (Ebisawa 1994; Reppert *et al.* 1994, 1995a, 1995b). Both mammalian receptors are 60% identical in amino acid sequence and bind 2-iodomelatonin with high affinities (Reppert *et al.* 1994, 1995a). The expression of the MT2 subtype was observed mainly in brain and retina (Reppert *et al.* 1995a).

Similar to other GPCRs, melatonin receptors contain seven putative transmembrane domains (TMs) connected by three extracellular and three intracellular loops. It is widely accepted that TMs are involved in specific interactions with ligand (Baldwin 1994; Ballesteros 2001). Still very little is known about the actual arrangement of TMs in the majority of GPCRs, as with the exception of light receptor rhodopsin (Palczewski 2000), their structures at the atomic level are unknown.

Received March 26, 2004; revised manuscript received June 29, 2004; accepted July 15, 2004.

Address correspondence and reprint requests to Jan Teisinger, Institute of Physiology, Academy of Sciences of the Czech Republic, Videnska 1083, 142 20 Prague 4, Czech Republic. E-mail: teisingr@biomed.cas.cz

**Abbreviations used:**  $[Ca^{2+}]_i$ , intracellular calcium; 3-D, three-dimensional; GPCR, G protein-coupled receptor; h, human; HEK, human embryonic kidney; 2-iodomelatonin, 2-[ $^{125}I$ ]-iodomelatonin; 4P-PDOT, (4-phenyl-2-propionamidotetralin); luzindole, (2-benzyl-*N*-acetyltryptamine); RMS, root mean square; TM, transmembrane domain; WT, wild-type.



So far, existing models of the melatonin binding site were generated by using the known MT1 and Mel<sub>1c</sub> receptor primary structures fitted into a 3-D structure of bacteriorhodopsin or into a low-resolution structure of bovine rhodopsin (Sugden *et al.* 1995; Grol and Jansen 1996; Navajas *et al.* 1996). Validity of these models has been tested in studies using site-directed mutagenesis (reviewed in Barrett *et al.* 2003). The observation that conserved histidine in TMV is critical for melatonin binding to both mammalian receptor subtypes (Conway *et al.* 1997; Kokkola *et al.* 2003; Gerdin *et al.* 2003) confirmed basic conceptions of these two models (Grol and Jansen 1996; Navajas *et al.* 1996). Some other mutations revealed structural differences between the MT1 and MT2 receptors, as demonstrated by distinct tolerance to changes in conserved serines in TM III (Gerdin *et al.* 2003; Conway *et al.* 2001).

In order to further characterize the interactions between melatonin receptors and their ligands, we decided to study the structure of the ligand binding site of the hMT2 receptor. The lack of detailed structure of the mammalian melatonin receptor led us to construct 3-D models of both human MT2 (hMT2) and human MT1 (hMT1) receptors using the X-ray structure of bovine rhodopsin as a template (Okada *et al.* 2002). Based on these models we have mutated six residues within TM V (V204A, V205A and F209A), TM VI (G271T and L272A) and TM VII (Y298A) of the hMT2 receptor. The wild type and mutants of the hMT2 receptor were transiently expressed in HEK293 cells and their binding properties were characterized using radiolabeled melatonin. Our results suggest that amino acid residues V204, L272 and Y298 are part of the ligand binding site of the hMT2 receptor.

## Materials and methods

### Materials

A cDNA containing the coding sequence of the hMT2 receptor cloned into pcDNA3 vector was kindly gifted by Dr S. M. Reppert. HEK293 cells were provided by American Type Culture Collection. Cell culture media, supplements and sera were purchased from Sigma Aldrich (St Louis, MO, USA). 2-iodomelatonin (2000 Ci/mmol) was obtained from Amersham Biosciences (Piscataway, NJ, USA). Molecular biology reagents and enzymes were purchased from New England Biolabs (Beverly, MA, USA) or Stratagene (La Jolla, CA, USA). Melatonin and general reagents were obtained from Sigma Aldrich. Luzindole (2-benzyl-*N*-acetyltryptamine) and 4P-PDOT (4-phenyl-2-propionamidotetralin) were purchased from Tocris (Bristol, UK). The anti-FLAG M2 monoclonal antibody was obtained from Sigma Aldrich and the horse fluorescein conjugated anti-mouse IgG antibody was purchased from Vector Laboratories (Burlingame, CA, USA).

### FLAG epitope tagging and generation of human MT2 receptor mutants

A cDNA encoding the hMT2 receptor was subcloned from pcDNA3 into the plasmid pFLAG-CMV-2 (Sigma Aldrich) to produce the

vector pFLAG-hMT2 containing the complete coding sequence of the human MT2 receptor N-terminally fused with FLAG epitope. A PCR-based mutagenesis (QuikChange site-directed mutagenesis kit; Stratagene) was performed using pFLAG-hMT2 as the template and the oligonucleotides (synthesized by VBC-Genomics) introducing specific point mutations. The presence of the mutations and the integrity of the rest of the gene were confirmed by automated DNA sequencing (ABI Prism).

### Cell culture and transfection

HEK293 cells were grown as monolayers in Dulbecco's modified Eagle's medium (DMEM) supplemented with 10% (v/v) fetal bovine serum, penicillin (50 U/mL) and streptomycin (50 µg/mL) in 95% O<sub>2</sub>/5% CO<sub>2</sub> at 37°C. Cultures at 90% confluence were transiently transfected either with wild-type receptor cDNA (pFLAG-hMT2) or with the above-listed cDNA constructs carrying desired mutations using Lipofectamine 2000 transfection reagent (Invitrogen). For binding assays, after 48 h, the plates (100 mm) with cells were washed with PBS solution (pH 7.4) containing 5 mM EDTA and harvested by gentle scraping. Cells were pelleted by centrifugation (1600 × g, 6 min, 4°C) and dry pellets were stored in aliquots at -70°C. For immunological studies, the cells were after 24 h trypsinized and reseeded onto poly L-lysine-treated coverslips (diameter 15 mm) and allowed to grow for an additional 24 h.

### Binding assays

Cell pellets were resuspended in binding buffer (50 mM Tris-HCl, pH 7.4) and in saturation assays incubated for 1.5 h at 37°C in final volume 150 µL with 2–1250 pM 2-iodomelatonin. In the case of competitive assays, MT2 receptor ligands of various concentration (0.1 pM to 10 µM) were incubated with samples and 2-iodomelatonin at a fixed concentration ~ 130 pM. Nonspecific binding was assessed in the presence of 1 µM melatonin and typically 2–6 µg of cell protein per tube was used for experiment as determined by the method of Bradford (1976). Incubation was terminated by addition of 3 mL of ice-cold binding buffer and bound and free ligands were separated by immediate vacuum filtration through Whatman GF/B filters. Radioactivity was measured by gamma counter with 55% efficiency (Packard Cobra). Binding data were analyzed using the PRISM 4.0 program (GraphPad software). Statistical significances were determined by Student's *t*-test. Presented binding data represent results from at minimum triplicate experiments performed on at least two batches of transfected cells.

### Immunocytochemistry

Cells were rinsed briefly in phosphate-buffered saline (PBS; pH 7.4) and then fixed for 15 min in 2% paraformaldehyde in PBS. To block non-specific binding, fixed cells were washed three times for 5 min with PBS and then incubated for 15 min at room temperature in antibody diluent (3% horse serum in PBS with 0.05% Tween 20). Cells were then incubated with anti-FLAG M2 monoclonal antibody (1 : 200) for 1 h at 37°C. After that, the cells were washed three times for 5 min with PBS and incubated with horse anti-mouse fluorescein conjugated antibody for 1 h (1 : 200) at room temperature. Following three successive washes with PBS the cells were mounted in Vectashield medium (Vector Laboratories) onto glass slides. Slides were viewed using Leica TCS 1-B laser scanning confocal microscope.

### Molecular modeling

Models of the hMT2 and hMT1 receptors were built by using homology modeling from the published X-ray structure of bovine rhodopsin solved at 2.6 Å resolution (PDB access code 1L9H) (Okada *et al.* 2002). The sequence alignment was performed using CLUSTALX (Thompson *et al.* 1997). The slow-accurate mode with a gap opening penalty of 10 and a gap extensions penalty of 0.1 for the local alignment was used, as well as the Gonnet 250 protein weight matrix and hydrophobic penalties for the amino acids GPSNDQEKR. 3-D models comprising all non-hydrogen atoms were generated by the MODELLER6 package (Sali and Overington 1994). The stereochemical quality of all models was checked with PROCHECK (Laskowski *et al.* 1993). Structures of 2-iodomelatonin, 4P-PDOT and luzindole were built with the sketcher module of InSight II v2000.1 (Accelrys Inc., San Diego, CA, USA) and geometry-optimized using the DISCOVER force field cvff. In order to obtain receptor–ligand complexes, ligands were manually fitted into the binding site of the hMT2 receptor. The starting point for 2-iodomelatonin docking was the orientation proposed by Grol and Jansen (1996). Ligands were positioned by avoiding severe steric overlaps with the receptor, trying to keep the hydrophobic parts close to the hydrophobic side chains. Resulting complexes were minimized *in vacuo* using SANDER with the ff99 force field included in AMBER 7.0 (Case *et al.* 2002). Figure 2 was generated using Pymol v0.93 (<http://www.pymol.org>).

## Results

### Molecular modeling of hMT2 receptor

The model of the helical part of hMT2 receptor was generated by homology to the known crystal structure of bovine rhodopsin resolved at 2.6 Å resolution (Okada *et al.* 2002). The starting point for manual docking of the 2-iodomelatonin molecule into the ligand binding site of hMT2 was the orientation proposed by Grol and Jansen (1996) with the methoxy group oriented towards H208 from TM V. As we have used a different and more appropriate template (bovine rhodopsin) to build the homology model of hMT2 receptor, our model differs from the model of Grol and Jansen (1996) who used bacteriorhodopsin structure as a template. Therefore the orientation of 2-iodomelatonin molecule had to be refined in order to avoid steric overlaps with residues within the ligand binding pocket. We also tried to keep the hydrophobic indole ring of 2-iodomelatonin close to the hydrophobic side chains within the ligand binding site. Figure 1 shows the schematic diagram of proposed orientation of 2-iodomelatonin molecule with respect to the transmembrane helices of the hMT2 receptor. In the final orientation with no steric overlaps between the ligand and the receptor, the 5-methoxy group of the melatonin is located close to H208 (TM V) with the methoxy-oxygen atom in the hydrogen bond distance (about 3 Å) from the hydroxyl group of Y298 from TM VII (Fig. 2a). The location of the 5-methoxy group of 2-iodomelatonin close to H208 is in agreement with data published by Conway *et al.* (1997), who suggested interaction between

H211 of ovine Mel<sub>1aB</sub> receptor and 5-methoxy group of melatonin. Our model of hMT2 with docked 2-iodomelatonin also suggests that the indole ring of the ligand interacts with hydrophobic side chains of L272 from TM VI and V204 from TM V (Fig. 2a). Other residues found in the relative proximity (but not in direct contact) of 2-iodomelatonin molecule were V205, F209 (TM V), G271 (TM VI), and several other residues from TM III (M120, G121, V124, and I125).

We have also performed manual docking of two hMT2 antagonists 4P-PDOT and luzindole used in this study in competition binding assays. Docking suggested that both antagonists interact with hMT2 ligand binding site predominantly through unspecific hydrophobic interactions. The tetralin ring of 4P-PDOT was placed between side chains of residues I125, Y183 and L272, and its phenyl group was located between the side chains of L181, L272 and A275 (Fig. 2b). Luzindole was oriented in a similar way to 2-iodomelatonin, where its imidazole ring interacts with side chains of L272 and A275 and the benzyl ring interacts with L181 (Fig. 2c).

In order to compare the structure of the ligand binding sites of the MT1 and MT2 receptors, we have also generated the homology model of human MT1 receptor. Final models of hMT1 and hMT2 can be superimposed with root mean square (RMS) deviation of 0.83 Å over 287 C $\alpha$  atoms. Figure 2(d) shows comparison of the ligand binding sites of both receptors. As amino acid residues studied in this work are conserved among both melatonin receptor subtypes, it is not surprising that they are located at very similar positions within the modeled structures.

### Ligand binding to hMT2 receptor

Based on our model of hMT2, six residues participating in putative melatonin binding site within TM V, TM VI and

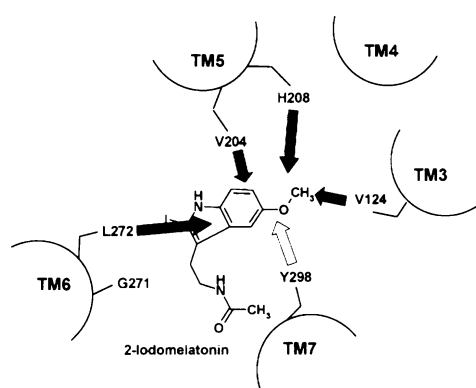


**Fig. 1** Schematic diagram showing proposed orientation of the 2-iodomelatonin molecule with respect to the transmembrane helices of the hMT2 receptor. The white arrow indicates a possible hydrogen bond between hydroxyl group of Y298 and 5-methoxy group of 2-iodomelatonin. Black arrows indicate predicted hydrophobic interactions between 2-iodomelatonin and residues located within modeled ligand binding site of the hMT2 receptor.

TM VII of the hMT2 receptor were mutated. FLAG-tagged hMT2 receptor (wild type) or each of six mutant receptors was transiently transfected into HEK293 cells. After 48–56 h, the expression of constructs was confirmed by immunocytochemical localization of N-terminal FLAG epitope of the hMT2 receptor (Fig. 3). The saturation binding experiments with 2-iodomelatonin provided data summarized in Table 1 and Fig. 4. It has been found that alanine substitution of the amino acids V205 and F209 in TM V did not significantly change  $K_d$  (equilibrium dissociation constant) value of the hMT2 receptor when compared with the  $K_d$  value obtained for the wild type, but the mutation in position 209 resulted in a significant decrease in the  $B_{max}$  value (maximum binding capacity) of receptor binding (Table 1, Fig. 4.). The replacement of

V204 with alanine led to a complete loss of binding. The substitution of G271 for threonine in TM VI led to a severe change in receptor's binding affinity, which showed no saturation up to  $\sim 1250$  pM of 2-iodomelatonin. The mutation of L272 in TM VI as well as the replacement of Y298 in TM VII completely abolished melatonin binding to the receptor. Immunocytochemical localization confirmed that hMT2 receptors containing mutations V204A, L272A, and Y298A, respectively, are expressed at levels comparable with wild-type receptor (Fig. 3). Therefore it is reasonable to assume that loss of specific binding observed for these mutants is caused by the inhibition of the ligand binding presumably because of structural changes within the ligand binding site. Taken together these results suggest the involvement of amino

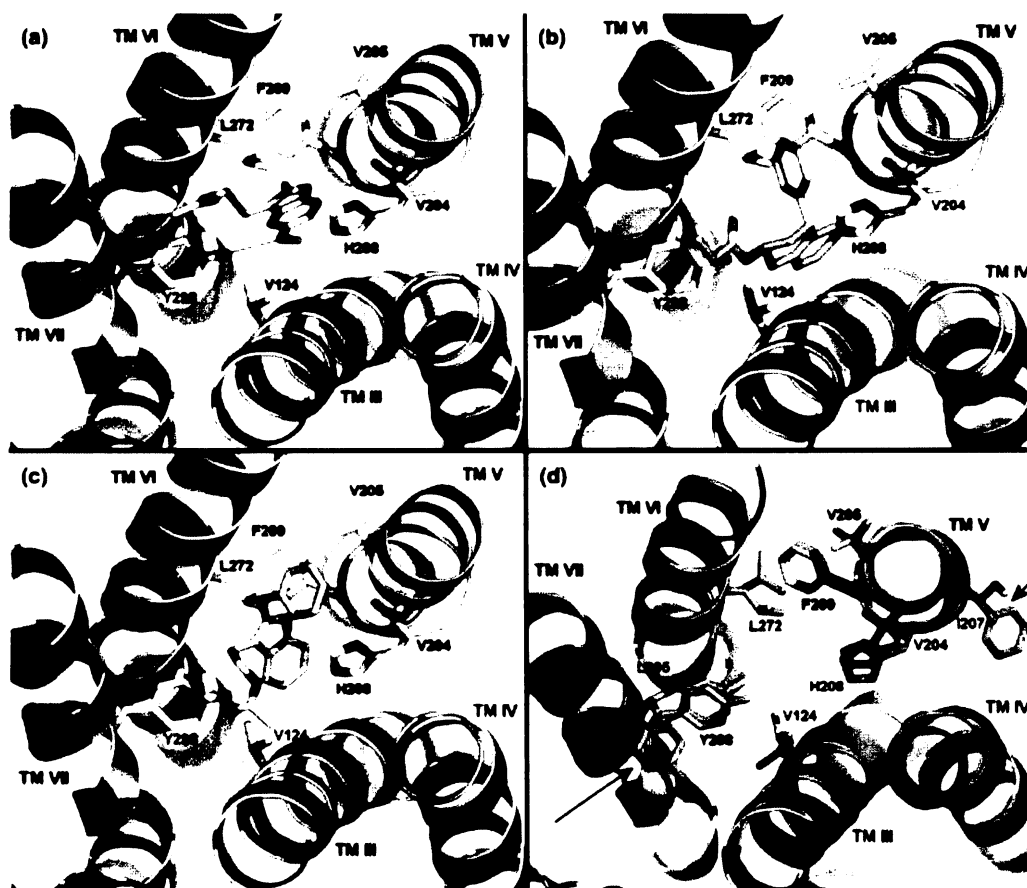


**Fig. 2** Model of the human MT2 melatonin receptor. (a) Model of the MT2 receptor with docked 2-iodomelatonin. Only the amino acid residues studied in this work (V204, V205, H208, F209, L272, Y298) are shown. Our model suggests that amino acid residues V204, H208, L272, and Y298 are directly involved in the 2-iodomelatonin–receptor interaction. The black line indicates possible hydrogen bond between hydroxyl group of Y298 and methoxy-oxygen of the 2-iodomelatonin. Part of TM III has been removed for better view into the ligand binding site. (b) Model of the MT2 receptor with docked antagonist 4P-PDOT (4-phenyl-2-propionamidotetraolin). (c) Model of the MT2 receptor with

docked antagonist luzindole (2-benzyl-*N*-acetyltryptamine). (d) Superimposition of molecular models of human MT2 (green) and MT1 (orange) receptors. These two models can be superimposed with a root mean square (RMS) deviation of 0.83 Å over 287 C $\alpha$  atoms. Only the amino acid residues of hMT2 receptor are labeled. Amino acid residues V124, V204, V205, I207, H208, F209, L272, L295, Y298 of hMT2 correspond to V111, V191, V192, F194, H195, F196, L259, Y282, Y285 of hMT1, respectively. Black arrows indicate main differences between the ligand binding site of hMT1 and hMT2 receptor models.



**Fig. 3** Immunocytochemical analysis of expression of FLAG-tagged wild-type hMT2 receptor and selected mutants. Only the mutants where complete loss of specific ligand binding has been observed (V204A, L272A, Y298A) are shown. Non-permeabilized HEK293 cells were immunostained with an anti-FLAG M2 monoclonal antibody and a horse anti-mouse fluorescein conjugated antibody. The scale bar represents 5  $\mu\text{m}$ .

acid residues V204 (TM V), L272 (TM VI), and Y298 (TM VII) in 2-iodomelatonin binding.

In addition, we have also performed competition binding experiments with melatonin and two hMT2 receptor antagonists 4P-PDOT and luzindole (Dubocovich *et al.* 1997) on

receptors containing mutations at positions 205 and 209 (which retains its ability to bind 2-iodomelatonin). These experiments showed no significant differences in  $K_i$  values (equilibrium dissociation constant of the competitor) compared with the wild-type receptor (Table 1).

### Discussion

The main aim of this study was to investigate the structure of the ligand binding site of the hMT2 receptor. Therefore we have generated a 3-D homology model of hMT2 receptor using the crystal structure of bovine rhodopsin as a template followed by manual docking of the 2-iodomelatonin molecule into the predicted ligand binding site. In our model of the hMT2 ligand binding site (Figs 1 and 2), both residues V204 in TM V and L272 in TM VI are located in the neighborhood of the indole ring of the 2-iodomelatonin molecule. This location indicates that these residues can participate in hydrophobic interactions with the indole group of the ligand. Such an interaction has been previously suggested by Sugden *et al.* (1995) and Navajas *et al.* (1996) in the case of the Mel1c and MT1 melatonin receptors for playing a role in the orientation and/or stabilization of the melatonin molecule in its binding pocket. Our results also confirmed the contribution of G271 (G258 in the hMT1 receptor) to high-affinity melatonin binding to the hMT2 receptor in agreement with data reported for the MT1 melatonin receptor (Gubitza and Reppert 2000; Conway *et al.* 2000). It is possible that this substitution of small and conformationally flexible G271 for polar and bulkier threonine can alter the proper orientation of adjacent L272 in the hMT2 receptor binding pocket, thus affecting melatonin binding.

**Table 1** 2-iodomelatonin binding to FLAG-tagged hMT2 and mutant receptors. Saturation and competitive binding experiments with [ $^{125}\text{I}$ ]Mel were performed on membrane preparations from HEK293 cells transiently transfected with the FLAG-tagged WT hMT2 and point-mutated receptors as described under Materials and methods. Values represent the mean  $\pm$  SEM of 3–5 experiments per construct performed on at least two batches of transfected cells. Each sample was determined in triplicate

Construct	Saturation assays			Competitive assays		
	Equivalent residue in hMT1	$K_d$ (pM)	$B_{\text{max}}$ (fmol/mg protein)	Ligand's $K_i$		
				Melatonin (pM)	Luzindole (pM)	4P-PDOT (pM)
Wild type hMT2		128 $\pm$ 15	1085 $\pm$ 133	501 $\pm$ 49	7759 $\pm$ 560	805 $\pm$ 97
V204A (TMV)	V191	No specific binding	–	–	–	–
V205A (TMV)	V192	159 $\pm$ 35	1388 $\pm$ 252	–	–	–
F209A (TMV)	F196	180 $\pm$ 37	256 $\pm$ 60**	658 $\pm$ 70	8359 $\pm$ 1056	1009 $\pm$ 143
G271T (TMVI)	G258	Not saturable	–	–	–	–
L272A (TMVI)	L259	No specific binding	–	700 $\pm$ 68	5381 $\pm$ 980	1081 $\pm$ 435
Y298A (TMVII)	Y285	No specific binding	–	–	–	–

\*\*Significantly different ( $p < 0.01$ ) from FLAG-tagged hMT2 receptor.  $K_d$  represents the equilibrium dissociation constant,  $B_{\text{max}}$  represents the maximum binding capacity,  $K_i$  represents the equilibrium dissociation constant of the competitor.

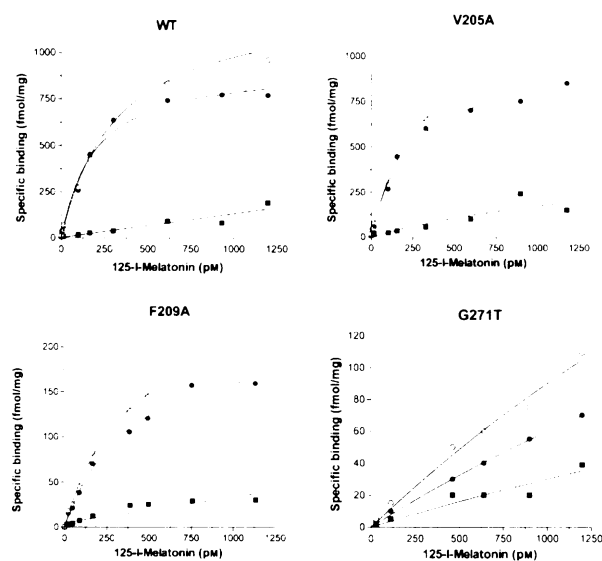


**Fig. 4** Representative binding isotherms of FLAG-tagged hMT2 receptor (WT) and receptors with introduced mutations at positions 205, 209 and 271. Specific  $K_d$  and  $B_{max}$  values for WT and all mutants are given in Table 1.  $\circ$ , total binding;  $\bullet$ , specific binding;  $\blacksquare$ , non-specific binding.

The mutation of V205 (V192 in hMT1 receptor) in TM V left binding parameters of the receptor unaffected, which is in agreement with our model where this residue is relatively away from docked ligand (about 6 Å) and is oriented towards the membrane. However, this observation is in discrepancy with previously published data for the ovine MT1 receptor by Conway *et al.* (1997), who found an approximate twofold increase in the receptor's  $K_d$  value after the mutation of the corresponding valine (V192 in hMT1 receptor). To compare the structure of hMT2 and hMT1 receptors we built a homology model of hMT1 receptor using the same procedure as in the case of hMT2. The comparison of these two models reveals that both subtypes have very similar ligand binding sites. However, we do see some differences in the close vicinity of the ligand binding site, in particular at positions 207 and 295 (in hMT2 numbering, see Fig. 2d). The hMT1 subtype contains phenylalanine at position 194 and tyrosine at position 282 which corresponds to I207 and L295, respectively, in the sequence of hMT2 receptor. As residue I207 is close to V205, the presence of different side chain at this position could be one of the reasons for observed differences between MT2 and MT1 subtypes.

Possible involvement of histidine residue(s) in melatonin interaction with its binding site was reported by Kosar *et al.* (1994). Previous melatonin receptor models proposed the participation of H208 (H195 in hMT1 receptor) in TM V in specific interaction with the 5-methoxy group of melatonin (Grol and Jansen 1996; Navajas *et al.* 1996). The role of

H208 in melatonin binding was subsequently confirmed using site-directed mutagenesis, which demonstrated substantial increase in the receptor's  $K_d$  value of both mammalian receptor subtypes carrying mutation in H208 (Conway *et al.* 1997; Gerdin *et al.* 2003; Kokkola *et al.* 2003). The substitution of the neighboring residue F209 for alanine described here does not affect the receptor's  $K_d$  for 2-iodomelatonin, which is in a good agreement with our model, where the position of this residue (about 8 Å from docked melatonin) does not indicate any specific interaction with the ligand (Fig. 2). However, the mutation of F209 caused significant decrease in the receptor's  $B_{max}$ , implicating possible impairment of receptor trafficking and/or cell membrane expression.

The contribution of particular residues in TM VII to melatonin binding has been already suggested by Navajas *et al.* 1996) who proposed the involvement of conserved serine (S280 in hMT1 receptor) in specific hydrogen bonding with the carbonyl oxygen of the N-acetyl group of the melatonin. However, Kokkola *et al.* (2003) reported that this residue in the MT1 receptor is not critical for specific receptor–ligand interactions. The same result has been observed recently in the case of the hMT2 receptor (Gerdin *et al.* 2003). Our hMT2 receptor model predicted that other residues within TM VII could be close to the docked 2-iodomelatonin molecule, namely Y298. The replacement of Y298 by alanine caused complete inhibition of 2-iodomelatonin binding to the receptor. We propose that this effect could be the result of a missing hydrogen bond between Y298 and the 5-methoxy group of the 2-iodomelatonin, because the Y298 hydroxyl group is in hydrogen bond distance (about 3 Å) and oriented towards the methoxy-oxygen atom.

In conclusion, the 3-D model of the hMT2 melatonin receptor has been generated using the crystal structure of bovine rhodopsin as a template. It has been suggested that V204 in TM V, L272 in TM VI, and Y298 in TM VII can play an important role in the high-affinity 2-iodomelatonin binding to the hMT2 receptor. Our data also confirmed the participation of G271 in the hMT2 receptor–2-iodomelatonin interaction similar to its counterpart G258 in hMT1 (Gubitza and Reppert 2000). These data indicate the involvement of several residues in TM V, VI and VII in ligand binding pocket of the hMT2 receptor as well as those amino acids residues in close proximity to the binding domain. This study also hints at the potential structural differences between the MT1 and MT2 receptors.

#### Acknowledgements

This research was supported by the Grant Agency of the Czech Republic (grant numbers 309/02/1479, 309/04/0496, 204/03/0714), Internal Grant Agency of Academy of Sciences (grants numbers A5011103, A5011408, and B5011308), by the Academy of Sciences

of the Czech Republic (research project number AVOZ 501 1922) and the Ministry of Education of the Czech Republic (grant number LN00A141 and MSM 113100001).

## References

- Baldwin J. M. (1994) Structure and function of receptors coupled to G proteins. *Curr. Opin. Cell Biol.* **6**, 180–190.
- Ballesteros J. A., Shi L. and Javitch J. A. (2001) Structural mimicry in G protein-coupled receptors: implications of the high-resolution structure of rhodopsin for structure-function analysis of rhodopsin-like receptors. *Mol. Pharmacol.* **60**, 1–19.
- Barrett P., Conway S. and Morgan P. J. (2003) Digging deep: structure–function relationships in the melatonin receptor family. *J. Pineal Res.* **35**, 221–230.
- Bartness T. J., Powers J. B., Hastings M. H., Bittman E. L. and Goldman B. D. (1993) The timed infusion paradigm for melatonin delivery: what has it taught us about the melatonin signal, its reception, and the photoperiodic control of seasonal responses? *J. Pineal Res.* **15**, 161–190.
- Bradford M. M. (1976) A rapid and sensitive method for the quantitation of microgram quantities of protein utilizing the principle of protein-dye binding. *Anal. Biochem.* **72**, 248–254.
- Case D. A., Pearlman D. A., Caldwell J. W. *et al.* (2002) *AMBER 7*. University of California, San Francisco.
- Conway S., Canning S. J., Barrett P., Guardiola-Lemaitre B., Delagrangé P. and Morgan P. J. (1997) The roles of valine 208 and histidine 211 in ligand binding and receptor function of the ovine Mella beta melatonin receptor. *Biochem. Biophys. Res. Commun.* **239**, 418–423.
- Conway S., Drew J. E., Mowat E. S., Barrett P., Delagrangé P. and Morgan P. J. (2000) Chimeric melatonin mtl1 and melatonin-related receptors: identification of domains and residues participating in ligand binding and receptor activation of the melatonin mtl1 receptor. *J. Biol. Chem.* **275**, 20 602–20 609.
- Conway S., Mowat E. S., Drew J. E., Barrett P., Delagrangé P. and Morgan P. J. (2001) Serine residues 110 and 114 are required for agonist binding but not antagonist binding to the melatonin MT(1) receptor. *Biochem. Biophys. Res. Commun.* **282**, 1229–1236.
- Dubocovich M. L., Masana M. I., Jacob S. and Sauri D. M. (1997) Melatonin receptor antagonists that differentiate between the human Mella and Mellb recombinant subtypes are used to assess the pharmacological profile of the rabbit retina ML1 presynaptic heteroreceptor. *Naunyn Schmiedeberg's Arch. Pharmacol.* **355**, 365–375.
- Dubocovich M. L., Rivera-Bermudez M. A., Gerdin M. J. and Masana M. I. (2003) Molecular pharmacology, regulation and function of mammalian melatonin receptors. *Front. Biosci.* **8**, 1093–1108.
- Ebisawa T., Karne S., Lerner M. R. and Reppert S. M. (1994) Expression cloning of a high-affinity melatonin receptor from *Xenopus* dermal melanophores. *Proc. Natl. Acad. Sci. USA* **91**, 6133–6137.
- Gerdin M. J., Mseeh F. and Dubocovich M. L. (2003) Mutagenesis studies of the human MT2 melatonin receptor. *Biochem. Pharmacol.* **66**, 315–320.
- Grol C. J. and Jansen J. M. (1996) The high affinity melatonin binding site probed with conformationally restricted ligand. I. Pharmacophore and minireceptor models. *Bioorg. Med. Chem.* **4**, 1333–1339.
- Gubitza A. K. and Reppert S. M. (2000) Chimeric and point-mutated receptors reveal that a single glycine residue in transmembrane domain 6 is critical for high affinity melatonin binding. *Endocrinology* **141**, 1236–1244.
- Kokkola T., Foord S. M., Watson M. A., Vakkuri O. and Laitinen J. T. (2003) Important amino acids for the function of the human MT1 melatonin receptor. *Biochem. Pharmacol.* **65**, 1463–1471.
- Kosar E., Teisinger J., Vyskocil F. and Vanecek J. (1994) Chemical modifications of melatonin receptors in chicken brain. *J. Neurochem.* **63**, 662–670.
- Laskowski R. A., McArthur M. W., Moss D. S. and Thornton J. M. (1993) PROCHECK – a program to check the stereochemical quality of the protein structures. *J. Appl. Crystallogr.* **26**, 283–289.
- Maestroni G. J. (1993) The immunoneuroendocrine role of melatonin. *J. Pineal Res.* **14**, 1–10.
- Molis T. M., Spriggs L. L., Jupiter Y. and Hill S. (1995) Melatonin modulation of estrogen-regulated proteins, growth factors, and proto-oncogenes in human breast cancer. *J. Pineal Res.* **18**, 93–103.
- Navajas C., Kokkola T., Poso A., Honka N., Gynther J. and Laitinen J. T. (1996) A rhodopsin-based model for melatonin recognition at its G protein-coupled receptor. *Eur. J. Pharmacol.* **304**, 173–183.
- Okada T., Fujiyoshi Y., Silow M., Navarro J., Landau E. M. and Shichida Y. (2002) Functional role of internal water molecules in rhodopsin revealed by X-ray crystallography. *Proc. Natl. Acad. Sci. USA* **99**, 5982–5987.
- Palczewski K., Kumasaka T., Hori T. *et al.* (2000) Crystal structure of rhodopsin: a G protein-coupled receptor. *Science* **289**, 739–745.
- Reiter R. J. (1996) Functional diversity of the pineal hormone melatonin: its role as an antioxidant. *Exp. Clin. Endocrinol. Diabetes* **104**, 10–16.
- Reppert S. M., Weaver D. R. and Ebisawa T. (1994) Cloning and characterization of a mammalian melatonin receptor that mediates reproductive and circadian responses. *Neuron* **13**, 1177–1185.
- Reppert S. M., Godson C., Mahle C. D., Weaver D. R., Slaugenhaupt S. A. and Gusella J. F. (1995a) Molecular characterization of a second melatonin receptor expressed in human retina and brain: the Mellb melatonin receptor. *Proc. Natl. Acad. Sci. USA* **92**, 8734–8738.
- Reppert S. M., Weaver D. R., Cassone V. M., Godson C. and Kola-kowski L. F. Jr (1995b) Melatonin receptors are for the birds: molecular analysis of two receptor subtypes differentially expressed in chick brain. *Neuron* **15**, 1003–1015.
- Sali A. and Overington J. P. (1994) Derivation of rules for comparative protein modeling from a database of protein structure alignments. *Protein Sci.* **3**, 582–596.
- Sugden D., Chong N. W. and Lewis D. F. (1995) Structural requirements at the melatonin receptor. *Br. J. Pharmacol.* **114**, 618–623.
- Thompson J. D., Gibson P. J., Plewniak F., Jeanmougin F. and Higgins D. G. (1997) The CLUSTAL\_X windows interface: flexible strategies for multiple sequence alignment aided by quality analysis tools. *Nucleic Acid Res.* **25**, 4876–4882.
- Vanecek J. (1998) Cellular mechanisms of melatonin action. *Physiol. Rev.* **78**, 687–721.



P2

## MOLECULAR DETERMINANTS OF THE AGONIST BINDING SITE OF HUMAN MT2 MELATONIN RECEPTOR

K. Berka<sup>1,2</sup>, P. Mazna<sup>2</sup>, I. Jelínková<sup>2</sup>, A. Balík<sup>2</sup>, P. Svoboda<sup>2</sup>, V. Obšilová<sup>2</sup>, T. Obšil<sup>1,2</sup>, and J. Teisinger<sup>2</sup>

<sup>1</sup>*Department of Physical and Macromolecular Chemistry, Faculty of Science, Charles University, 128 43 Prague,*

<sup>2</sup>*Institute of Physiology, Academy of Sciences of the Czech Republic, 142 20 Prague*

The hormone melatonin is known to play an important role in the regulation of physiological and neuroendocrine functions [1,2]. To better understand the mechanism of interactions between G protein-coupled melatonin receptors and their ligands we have generated a homology model of the helical part of the human MT2 melatonin (hMT2) receptor using the structure of bovine rhodopsin as a template [3]. Molecular modeling has been combined with site-directed mutagenesis to investigate the role of the specific amino acid residues within the transmembrane domains (TM) number 3, 5, 6 and 7 of hMT2 receptor in the interaction with 2-iodomelatonin. Selected residues were mutated and radioligand binding assay was used to test the binding affinities of hMT2 receptors transiently expressed in HEK293 cells. Our data demonstrates that residues N268 (N6.52) and A275 (A6.59) in TM6 as well as residues V291 (V7.36) and L295 (L7.40) in TM7 are essential for 2-iodomelatonin binding to the hMT2 receptor, while TM3 residues M120 (M3.32), G121 (G3.33), V124 (V3.36) and

I125 (I3.37) may participate in binding of other receptor agonists and/or antagonists.

*This work was supported by Grants 309/02/1479, 309/04/0496, and 204/03/0714 of the Grant Agency of the Czech Republic; by Grant B5011308 of the Grant Agency of the Czech Academy of Sciences; by Research Projects IK03020 and MSM 1131 00001 of the Ministry of Education, Youth and Sports of the Czech Republic, and by Research Project AVOZ 5011922.*

1. T.J. Bartness, J.B. Powers, M.H. Hastings, E.L. Bittman & B.D. Goldman, *J.Pineal Res.* 15 (1993) 161-190.
2. G.J. Maestroni, *J. Pineal Res.* 14 (1993) 1-10.
3. P. Mazna, V. Obsilova, I. Jelinkova, A. Balik, K. Berka, Z. Sovova, R. Etrich, P. Svoboda, T. Obsil & J. Teisinger, *J. Neurochem.* 91 (2004) 836-842.

P3

## INFLUENCE OF PYRENE ON THE STRUCTURE AND DYNAMICS OF DPPC BILAYER

J. Čurdová<sup>1</sup>, P. Čapková<sup>1</sup> and J. Plášek<sup>2</sup>

<sup>1</sup>*Department of Chemical Physics and Optics, Charles University, Ke Karlovu 3, 121 16 Prague 2, Czech Republic*

<sup>2</sup>*Institute of Physics, Faculty of Mathematics and Physics, Charles University, Ke Karlovu 5, 121 16 Prague 2, Czech Republic*

We have employed 20 ns molecular dynamics simulation to study the influence of pyrene probe on structure and dynamics of dipalmitoylphosphatidylcholine (DPPC) bilayer. Pyrene is an important fluorescent probe used for monitoring excimer fluorescence. Our simulated system contains 128 molecules of DPPC, 3655 water molecules and various concentrations of pyrene. The simulations were performed using the Gromacs package [1].

Concentrations of pyrene in lipid membrane were 0:128 and 3:128 at different temperatures. We have chosen two temperatures below the main phase transition of DPPC (314.15 K) and two above.

From our analysis of the trajectory we have obtained information about structural changes caused by presence of pyrene probe in the membrane. Molecular dynamic simulation has shown that the pyrene probe is located in the acyl

chains region of DPPC. The major influence of the probe on the lipid membrane is in the nearest surroundings of pyrene. On the other hand the influence of pyrene in the membrane-water interface is negligible.

We have found out decreases thickness of the DPPC membrane with increasing temperature. The membrane with pyrene probes is thicker than in the case without pyrene. The thickness of DPPC membrane without pyrene has decreased noticeably between the temperature of 310 K and 325 K which corresponds to main phase transition of DPPC. In the case of membrane with pyrene we have observed similar decrease of thickness already between 293 K and 310 K. These results probably indicate the decrease of temperature of the main phase transition due to the presence of pyrene in the membrane.



## Ligand binding to the human MT2 melatonin receptor: The role of residues in transmembrane domains 3, 6, and 7

Petr Mazna<sup>a</sup>, Karel Berka<sup>b</sup>, Irena Jelinkova<sup>a</sup>, Ales Balik<sup>a</sup>, Petr Svoboda<sup>a</sup>,  
Veronika Obsilova<sup>a</sup>, Tomas Obsil<sup>b</sup>, Jan Teisinger<sup>a,\*</sup>

<sup>a</sup> Institute of Physiology, Academy of Sciences of the Czech Republic, Videnska 1083, 142 20 Prague, Czech Republic

<sup>b</sup> Department of Physical and Macromolecular Chemistry, Faculty of Science, Charles University, Hlavova 203018, 128 43 Prague, Czech Republic

Received 28 April 2005

Available online 12 May 2005

### Abstract

To better understand the mechanism of interactions between G-protein-coupled melatonin receptors and their ligands, our previously reported homology model of human MT2 receptor with docked 2-iodomelatonin was further refined and used to select residues within TM3, TM6, and TM7 potentially important for receptor–ligand interactions. Selected residues were mutated and radioligand-binding assay was used to test the binding affinities of hMT2 receptors transiently expressed in HEK293 cells. Our data demonstrate that residues N268 and A275 in TM6 as well as residues V291 and L295 in TM7 are essential for 2-iodomelatonin binding to the hMT2 receptor, while TM3 residues M120, G121, V124, and I125 may participate in binding of other receptor agonists and/or antagonists. Presented data also hint at possible specific interaction between the side-chain of Y188 in second extracellular loop and *N*-acetyl group of 2-iodomelatonin.

© 2005 Elsevier Inc. All rights reserved.

**Keywords:** MT2 melatonin receptor; Site-directed mutagenesis; Homology modeling; G-protein-coupled receptor

Melatonin (*N*-acetyl-5-methoxytryptamine) is the main hormone synthesized by the vertebrate pineal gland. In mammals, the melatonin is known to play an important role in the regulation of physiological and neuroendocrine functions, such as synchronization of seasonal reproductive rhythms [1], and entrainment of circadian cycles (see [2] for review). In addition to its chronobiotic role, melatonin influences a number of other physiologically diverse processes including tumor suppression [3] and modulation of the free radical levels [4]. It has also been reported that melatonin reduces tissue destruction during inflammatory reactions [5] and shows immunotherapeutic potential (reviewed in [6]). To date, three mammalian melatonin receptors have

been described: MT1 [7], MT2 [8], and MT3 [9]. First two are G-protein-coupled receptors (GPCRs) and their activations modulate a wide range of intracellular messengers, e.g., cAMP, cGMP or  $[Ca^{2+}]_i$  (reviewed in [10,11]). The MT3-binding site has been identified as quinone reductase protein and its physiological significance remains to be clarified. In mammals, both MT1 and MT2 receptor subtypes are expressed in a wide variety of tissues including specific brain structures and peripheral organs [10].

All GPCRs are thought to share the basic structural organization characterized by a bundle of seven putative transmembrane domains (TMs), that form a ligand-binding site, connected by three extracellular (ECLs) and three intracellular loops [12]. Extracellular loops may participate in ligand recognition by the receptor whereas intracellular loops are believed to directly activate

\* Corresponding author. Fax: +420 2 4106 2488.

E-mail address: [teisingr@biomed.cas.cz](mailto:teisingr@biomed.cas.cz) (J. Teisinger).



G-proteins [13,14]. Despite growing collection of experimental data, in most cases the actual arrangement of TMs and their conformational changes induced by the ligand binding are not completely understood. Recently reported high-resolution crystal structure of bovine rhodopsin [15] allowed us to construct a homology model of the human MT2 (hMT2) receptor [16]. Interplay between homology modeling and site-directed mutagenesis led to the identification of several new amino acid residues critical for melatonin binding. Our findings suggested that V204 (V5.42) in TM5, G271 (G6.55), and L272 (L6.56) in TM6 participate in hydrophobic interactions with the indole moiety of the melatonin whereas Y298 in TM7 may specifically interact with its 5-methoxy group. The importance of H208 (H5.46) from TM5 in the ligand binding to the hMT2 receptor has been already established elsewhere [17]. It is entirely possible, however, that additional amino acid residues of the hMT2 receptor might be critical for the ligand binding.

To better understand the mechanism of interactions between melatonin receptors and their ligands, our previously reported model of hMT2 receptor with docked 2-[<sup>125</sup>I]iodomelatonin (2-iodomelatonin) was further refined and used to select residues within TM3, TM6, and TM7 potentially important for receptor–ligand interactions. Selected residues were mutated and radioligand-binding assay was used to test the binding affinities of hMT2 receptors transiently expressed in HEK293 cells. Our experiments indicate that residues N268 (6.52) and A275 (6.59) in TM6 as well as residues V291 (7.36) and L295 (7.40) in TM7 are essential for ligand binding to the hMT2 receptor. Presented data also suggest possible specific interaction between the side-chain of Y188 in ECL2 and *N*-acetyl group of 2-iodomelatonin.

## Methods

**Materials.** A cDNA containing the coding sequence of the hMT2 receptor cloned into pcDNA3 vector was kindly gifted by Dr. S.M. Reppert. HEK293 cells were provided by American Type Culture Collection. Cell culture media, supplements, and sera were purchased from Sigma Aldrich (St. Louis, MO, USA). 2-Iodomelatonin (2000 Ci/mmol) was obtained from Amersham Biosciences (Piscataway, NJ, USA). Molecular biology reagents and enzymes were purchased from New England Biolabs (Beverly, MA, USA) or Stratagene (La Jolla, CA, USA). Melatonin, *N*-acetylserotonin, 6-hydroxymelatonin, and general reagents were obtained from Sigma Aldrich. Luzindole (2-benzyl-*N*-acetyltryptamine), 4P-PDOT (4-phenyl-2-propionamidotetralin), *N*-acetyltryptamine, and 6-chloromelatonin were purchased from Tocris (Bristol, UK). The anti-FLAG M2 monoclonal antibody was obtained from Sigma Aldrich and the horse fluorescein-conjugated anti-mouse IgG antibody was purchased from Vector Laboratories (Burlingame, CA, USA).

**Construction of FLAG tagged hMT2 receptor and generation of receptor mutants.** Construction of the hMT2 receptor with N-terminally fused FLAG epitope (FLAG-hMT2) was described previously [16]. Set of point mutants (M120A, G121A, G121I, V124A, I125A,

Y188A, Y188F, N268A, N268D, N268L, N268Q, A275I, A275V, V291A, V291I, L295A, L295I, and L295V) was generated by standard PCR-based mutagenesis (QuikChange site-directed mutagenesis kit from Stratagene) using the FLAG-hMT2 cDNA as a template. Oligonucleotides introducing specific point mutations were synthesized by VBC-Genomics. The presence of the mutations and the integrity of the rest of the gene were confirmed by automated DNA sequencing (ABI Prism).

**Cell culture and transfection.** HEK293 cells were grown as monolayers in Dulbecco's modified Eagle's medium supplemented with 10% (v/v) fetal bovine serum, penicillin (50 U/ml), and streptomycin (50 µg/ml) in 95% O<sub>2</sub>/5% CO<sub>2</sub> at 37 °C. On the day before transfection, the cells were seeded (8–10 × 10<sup>6</sup>) into 100-mm Petri dishes. After 24 h, the cells were transiently transfected plasmid DNA encoding the wild-type or mutant receptors using Lipofectamine2000 transfection reagent (Invitrogen). Following additional 48 h incubation, the cells were washed with PBS solution (pH 7.4) containing 5 mM EDTA and harvested by gentle scraping. Cells were then pelleted by centrifugation (1600g, 6 min, 4 °C) and stored in aliquots at –70 °C. For immunological studies, the cells were trypsinized 24 h after transfection, reseeded onto poly-L-lysine treated coverslips (diameter 15 mm), and let grow for additional 24 h.

**Binding assays.** Cell pellets were resuspended in binding buffer (50 mM Tris–HCl, pH 7.4) and in case of saturation assays incubated for 1.5 h at 37 °C in a final volume of 150 µl with 2–1250 pM 2-iodomelatonin. Non-specific binding was assessed in the presence of 1 µM melatonin and typically 2–6 µg of cell protein per tube was used for experiment as determined by the method of Bradford [18]. For competitive experiments, the cell samples were incubated with receptor ligands of various concentration (0.1 pM–10 µM) and 2-iodomelatonin at a fixed concentration (~130 pM). Incubation was terminated by addition of 3 × 3 ml of ice-cold binding buffer, and bound and free ligands were separated by immediate vacuum filtration through Whatman GF/B filters. Radioactivity was measured by gamma counter with 55% efficiency (Packard Cobra).

**Immunocytochemistry and confocal microscopy.** Cells were rinsed three times in PBS (pH 7.4) and then fixed for 15 min in 2% paraformaldehyde in PBS. To block non-specific binding, fixed cells were washed three times for 5 min with PBS and then incubated for 15 min at room temperature (RT) in antibody diluent (3% horse serum in PBS with 0.05% Tween 20). Cells were then incubated with anti-FLAG M2 monoclonal antibody (1:200) for 1 h at 37 °C. After that, the cells were washed three times for 5 min with PBS and incubated with horse anti-mouse fluorescein-conjugated antibody for 1 h (1:200) at RT. Following three successive washes with PBS the cells were mounted in Vectashield medium (Vector Labs) onto glass slides. Slides were viewed using Leica TCS 1-B laser scanning confocal microscope.

**Molecular modeling.** Homology modeling of the hMT2 receptor structure has been published previously [16]. In order to obtain a model of receptor–ligand complex, the molecule of 2-iodomelatonin was first manually fitted into the binding site of the hMT2 receptor. The starting point for ligand docking was the orientation proposed previously by Grol and Jansen [19]. Ligand was positioned by avoiding steric overlaps with the receptor, trying to keep the hydrophobic parts close to the hydrophobic side-chains. Subsequently, the docking program GRAMM [20] was used to refine the position of 2-iodomelatonin molecule within the ligand-binding site of the hMT2 receptor.

**Residue numbering.** In addition to standard amino acid numbering based on their position in the receptor sequence, the residues in transmembrane domains are labeled using scheme proposed by Ballesteros and Weinstein [21]. This scheme designates the most highly conserved residue in each helix as X.50, where X represents the helix number.

**Data analysis.** Saturation-binding data were analyzed by non-linear regression analysis using the PRISM 4.0 program (GraphPad Software). *K<sub>i</sub>* values in competition experiments were calculated by using the equation of Cheng and Prusoff [22]. Statistical significances were

determined by Student's *t* test. Presented binding data represent results from at minimum triplicate experiments performed on at least two batches of transfected cells.

## Results

### Modeling of hMT2 receptor–ligand complexes

Molecular modeling of hMT2 receptor (this study and [16]) suggested that TM3 residues M120, G121, V124, and I125; TM6 residues N268, G271, L272, and A275; TM7 residues V291 and L295; and possibly residue Y188 from ECL2 might be important for ligand binding (Fig. 1). Residues M120, G121, V124, and I125 in TM3 probably participate in hydrophobic interactions with the ligand. TM6 residues L272 and A275 could interact with the indole group of the 2-iodomelatonin through hydrophobic interaction while N268 is found in the vicinity of its 5-methoxy group. TM7 residues V291 and L295 are located in close proximity of the *N*-acetyl chain of 2-iodomelatonin, suggesting a possible interaction with this part of the radioligand. Finally, the residue Y188 in putative ECL2, with its side-chain oriented towards the ligand-binding site might also contribute to the ligand binding.

### Expression of mutant receptors

In order to validate predictions discussed above experimentally, 18 receptor mutants were constructed, transiently expressed in HEK293 cells, and their binding properties were characterized using 2-iodomelatonin.

Table 1

2-Iodomelatonin binding to the wild-type hMT2 and mutant receptors

Saturation binding assays			
Receptor	General numbering	$K_d$ (pM)	$B_{max}$ (fmol/mg protein)
WT hMT2	—	145 ± 25	1182 ± 350
M120A (TM3)	(3.32)	165 ± 34	428 ± 135
G121A (TM3)	(3.33)	192 ± 18	854 ± 164
G121I (TM3)	(3.33)	180 ± 22	1367 ± 378
V124A (TM3)	(3.36)	169 ± 30	152 ± 43**
I125A (TM3)	(3.37)	165 ± 23	911 ± 286
Y188A (EL2)	—	NSB	—
Y188F (EL2)	—	NSB	—
N268A (TM6)	(6.52)	NSB	—
N268D (TM6)	(6.52)	NSB	—
N268L (TM6)	(6.52)	NSB	—
N268Q (TM6)	(6.52)	175 ± 37	1942 ± 384
A275I (TM6)	(6.59)	NSB	—
A275V (TM6)	(6.59)	194 ± 41	1711 ± 560
V291A (TM7)	(7.36)	NSB	—
V291I (TM7)	(7.36)	NSB	—
L295A (TM7)	(7.40)	NSB	—
L295I (TM7)	(7.40)	NSB	—
L295V (TM7)	(7.40)	NSB	—

Saturation and binding experiments were performed on whole cell lysates of HEK293 cells transiently expressing FLAG-tagged WT hMT2 and point-mutated receptors as described under Methods. Values represent means ± SEM of 3–5 experiments per construct performed on at least two batches of transfected cells. Each sample was determined in triplicate. NSB, no specific binding.

\*\* Significantly different ( $p < 0.01$ ) from FLAG-tagged hMT2 receptor.  $K_d$  represents the equilibrium dissociation constant,  $B_{max}$  represents the maximum binding capacity.

After 48 h incubation, receptors not displaying any detectable radioligand binding (see Table 1) were subjected to immunocytochemical analysis using specific anti-FLAG monoclonal antibody.

Examination under confocal microscope showed that all mutant receptors were inserted into the cell membrane and were expressed at levels comparable with those of the FLAG-hMT2 (wild-type) receptor and (Fig. 2).

### Analysis of residues in TM3

As shown in Table 1 and Fig. 3, saturation-binding experiments performed on mutants M120A, G121A, G121I, V124A, and I125A resulted in no significant change in receptor affinity for 2-iodomelatonin, but the replacement of valine at position 124 by alanine led to a decrease in receptor  $B_{max}$  (maximum binding capacity). On the other hand, experiments with competitors demonstrated distinct binding properties of several mutant receptors (see Table 2). The replacement of methionine at position 120 with alanine increased receptor-binding affinity for subtype-specific antagonist 4P-PDOT (Fig. 5) by about fivefold compared to the wild-type receptor. The mutation of neighboring glycine

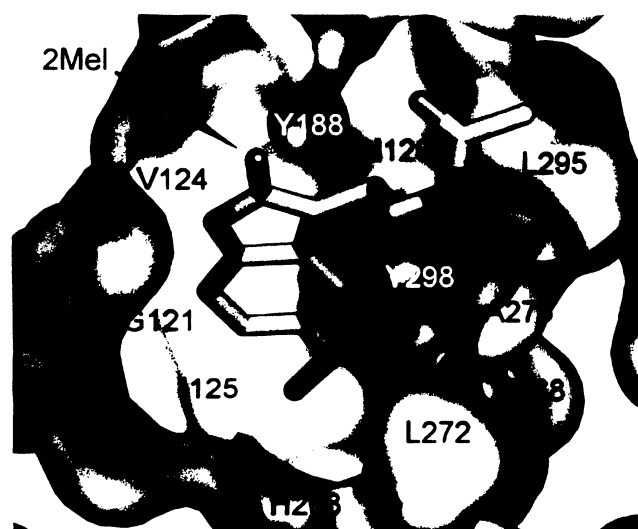


Fig. 1. Surface representation of the ligand binding pocket of the hMT2 receptor with docked 2-iodomelatonin (2Mel). Part of TM5 has been removed for better view into the binding pocket. This figure was generated using Pymol v0.93 (<http://www.pymol.org>).

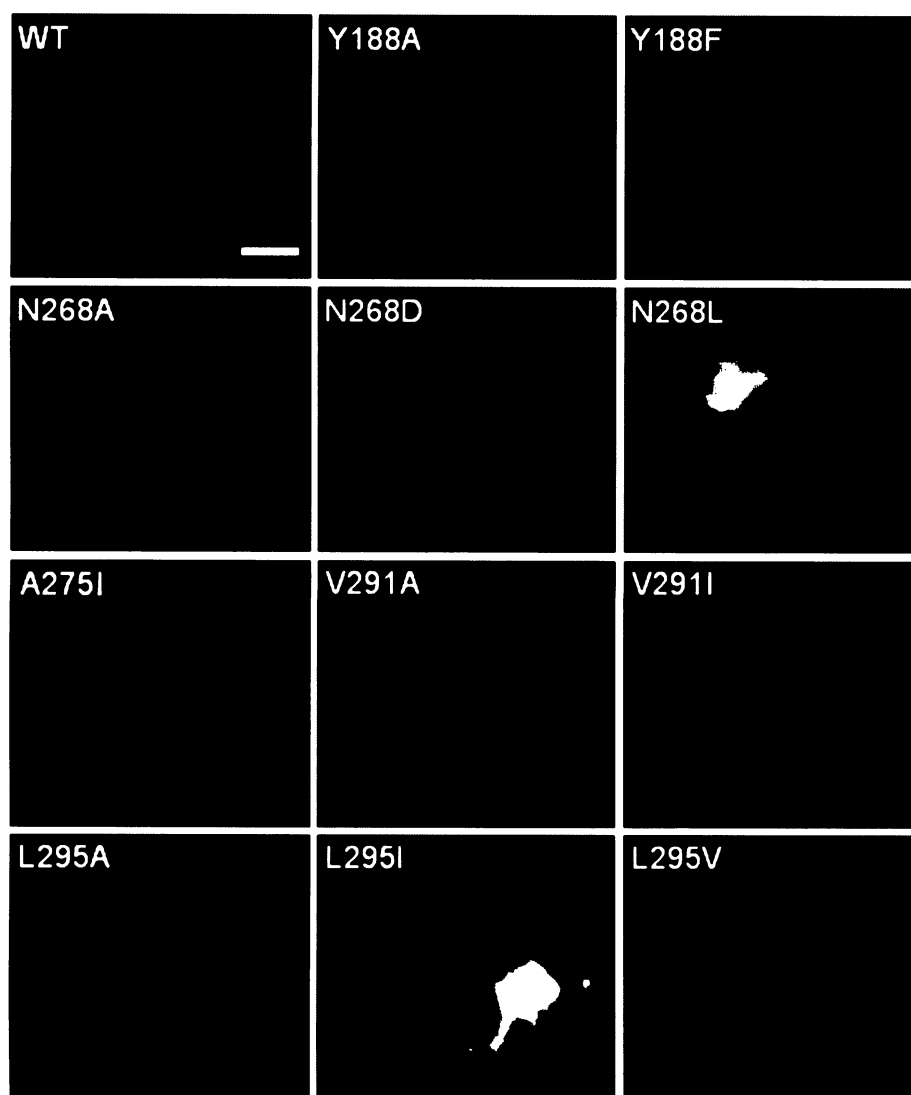


Fig. 2. Immunological localization of FLAG-tagged hMT2 receptor (WT) and selected mutants. Only the mutants where complete loss of specific ligand binding has been observed are shown. Non-permeabilized HEK293 cells were immunostained with an anti-FLAG M2 monoclonal antibody and a horse anti-mouse fluorescein-conjugated antibody. The scale bars indicate 5  $\mu$ m. No specific fluorescence signal was detected in untransfected HEK293 cells (data not shown).

121 to alanine led to more than a threefold decrease in receptor-binding affinity for its natural ligand melatonin, whereas introduction of leucine at the same position had no effect. The hMT2 receptor agonist 6-chloromelatonin displayed significantly lower affinity to mutant V124A (more than fivefold increase in  $K_i$ ), while the substitution of isoleucine at position 125 for alanine markedly reduced receptor-binding affinity for agonist *N*-acetylserotonin.

#### Analysis of residues in TM6

In TM6, residues N268 and A275 seem to be a part of the ligand-binding site. Mutation of polar and electrically neutral asparagine at position 268 to smaller and non-polar alanine or to non-polar but larger leucine led to a complete loss of radioligand binding to

the mutated receptors. The introduction of negatively charged side-chain by replacing asparagine with aspartate was not tolerated either (Table 1). However, we observed successful recovery of the 2-iodomelatonin binding for mutation N268Q. Mutant receptor with replaced alanine at position 275 by bulkier isoleucine failed to bind 2-iodomelatonin, whereas the substitution for valine rescued receptor-binding affinity for radioligand (Table 1). Further competition experiments with set of hMT2 receptor ligands did not reveal any significant modifications of the N268Q and A275V affinity (Table 2).

#### Analysis of residues in TM7

To validate our predictions concerning TM7 involvement in the ligand-binding hydrophobic residues

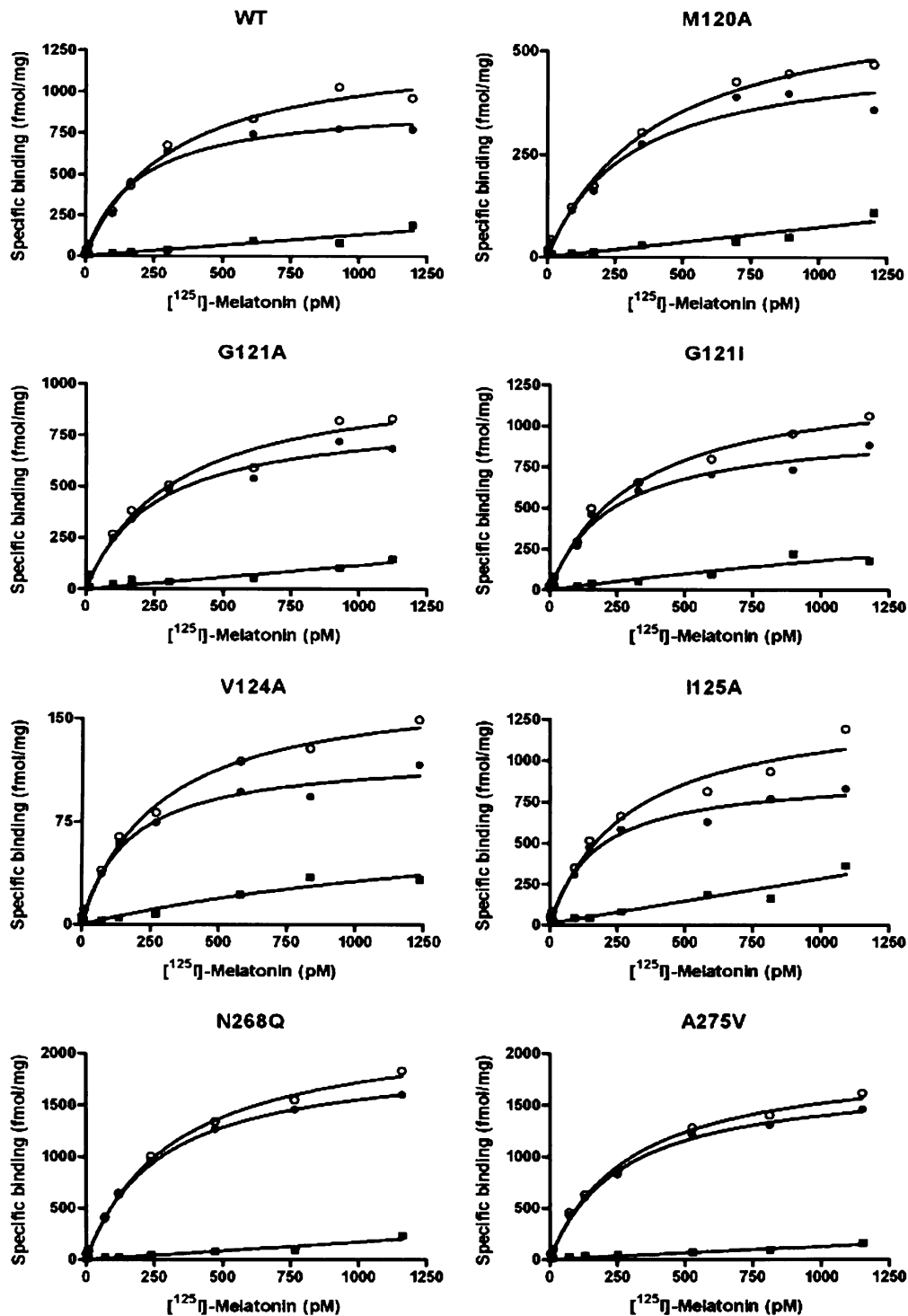


Fig. 3. Representative isotherms derived from saturation binding of 2-iodomelatonin to HEK293 cells expressing FLAG-tagged hMT2 receptor (WT) and mutant receptors M120A, G121A, G121I, V124A, I125A, N268Q, and A275V. Specific  $K_d$  and  $B_{max}$  values for WT and all mutants are given in Table 1. Empty circles, total binding; full circles, specific binding; full squares, nonspecific binding.

V291 and L295 were investigated. Valine at position 291 was replaced either by alanine or isoleucine. In both cases, no 2-iodomelatonin binding could be detected indicating strict structural requirements at this

position. Similarly, replacement of L295 by alanine caused complete loss of binding. Substitution of this residue by valine or isoleucine also did not rescue receptor binding (Table 1).

Table 2  
Binding of receptor ligands to the wild-type hMT2 and mutant receptors

Receptor	Competition binding assays ( $K_i \pm$ SEM)									
	Mel (nM)	6ClMel (nM)	6OHMel (nM)	NAT (nM)	NAS (nM)	Luz (nM)	4PP (nM)	$K_i/K_i$ WT	$K_i/K_i$ WT	$K_i/K_i$ WT
WT hMT2	0.49 ± 0.02	0.78 ± 0.2	10.1 ± 0.5	58.0 ± 1	420 ± 83	78 ± 6	2.65 ± 0.1	1.0	1.0	1.0
M120A (TM3)	0.99 ± 0.04	0.63 ± 0.1	6.7 ± 1.1	78 ± 5	604 ± 90	127 ± 19	<b>0.48 ± 0.1**</b>	1.4	1.6	0.2
G121A (TM3)	<b>1.55 ± 0.38*</b>	0.73 ± 0.09	12.8 ± 3.0	109 ± 13	804 ± 120	134 ± 23	1.25 ± 0.58	1.9	1.7	0.5
G121H (TM3)	1.19 ± 0.1	0.67 ± 0.05	13.1 ± 2.4	108 ± 17	1110 ± 197	128 ± 9	4.50 ± 0.4	2.6	1.7	1.7
V124A (TM3)	0.76 ± 0.44	<b>4.10 ± 1.3*</b>	9.1 ± 1.3	183 ± 83	320 ± 34	75 ± 11	1.46 ± 0.2	0.8	1.0	0.6
I125A (TM3)	0.47 ± 0.01	0.82 ± 0.1	10.2 ± 0.5	31 ± 6	<b>1560 ± 374*</b>	85 ± 6	2.81 ± 0.09	3.7	1.1	1.1
N268Q (TM6)	0.56 ± 0.03	1.39 ± 0.2	8.8 ± 1.2	61 ± 5	896 ± 170	66 ± 2	2.35 ± 0.06	2.1	2.5	0.9
A275V (TM6)	0.44 ± 0.1	1.12 ± 0.08	11.8 ± 0.7	85 ± 24	994 ± 162	134 ± 13	1.24 ± 0.34	2.4	1.7	0.5

Whole cell lysates of HEK293 cells transiently transfected with FLAG-tagged hMT2 (wild-type) or selected receptor mutants were incubated with 2-iodomelatonin in the presence of varying concentrations of receptor ligands as described under Methods. Values represent means  $\pm$  SEM of three experiments per receptor construct performed on at least two batches of transfected cells. Significantly different \* $p < 0.05$ , \*\* $p < 0.01$  from FLAG-tagged hMT2 receptor.  $K_i$  represents the equilibrium dissociation constant of the competitor. Mel, melatonin; 6ClMel, 6-chloromelatonin; 6OHMel, 6-hydroxymelatonin; NAT, *N*-acetyltryptamine; NAS, *N*-acetylserotonin; Luz, luzindole; 4PP, 4P-PDOT.

### Mutation of Y188 in ECL2

In second extracellular loop potentially important residue tyrosine 188 was subjected to the mutational analysis. Mutant receptor was not able to retain the 2-iodomelatonin binding when substituted for several times smaller alanine and similar results were obtained also after the introduction of aromatic phenylalanine (Table 1).

### Discussion

#### Residues in TM3

In this work, we have investigated the contribution of specific residues in TM3, TM6, TM7, and ECL2 to the ligand binding. Based on our homology model of hMT2 receptor residues M120 (M3.32), G121 (G3.33), V124 (V3.36), and I125 (3.37) in TM3 form significant part of the predicted ligand-binding site (Fig. 1). Despite the predicted localization of these residues within the ligand-binding site, their mutations did not affect the binding affinity for 2-iodomelatonin compared to the wild-type receptor (Table 1). On the other hand, we do observe significant differences in  $K_i$  values for other receptor ligands (Table 2). The mutation M120A probably increases the volume of the ligand-binding pocket, because this replacement had no effect on 2-iodomelato-

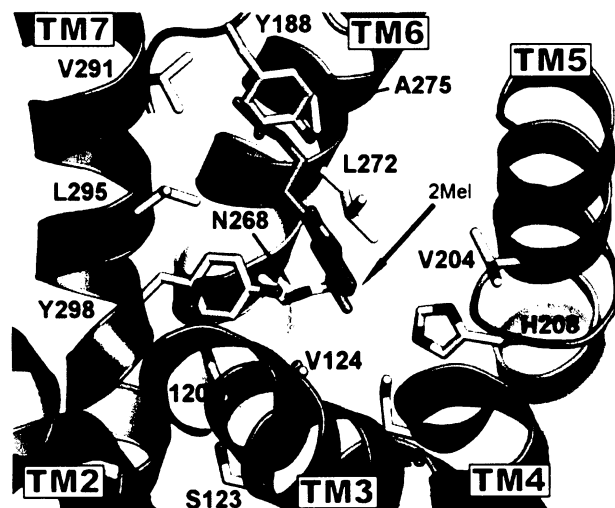


Fig. 4. Ribbon representation of the modeled hMT2 receptor with docked 2-iodomelatonin (2Mel). Only the amino acid residues mutated in this work (M120, V124, I125, Y188, N268, A275, V291, and L295) and selected residues that were tested previously (V204, S123, H208, L272, and Y298) are shown. Our model suggests that amino acid residues Y188, V204, H208, N268, L272, A275, V291, L295, and Y298 might be directly involved in the 2-iodomelatonin–receptor interaction. Parts of the TM3 and TM4 were removed for better view into the ligand binding site. This figure was generated using Pymol v0.93 (<http://www.pymol.org>).

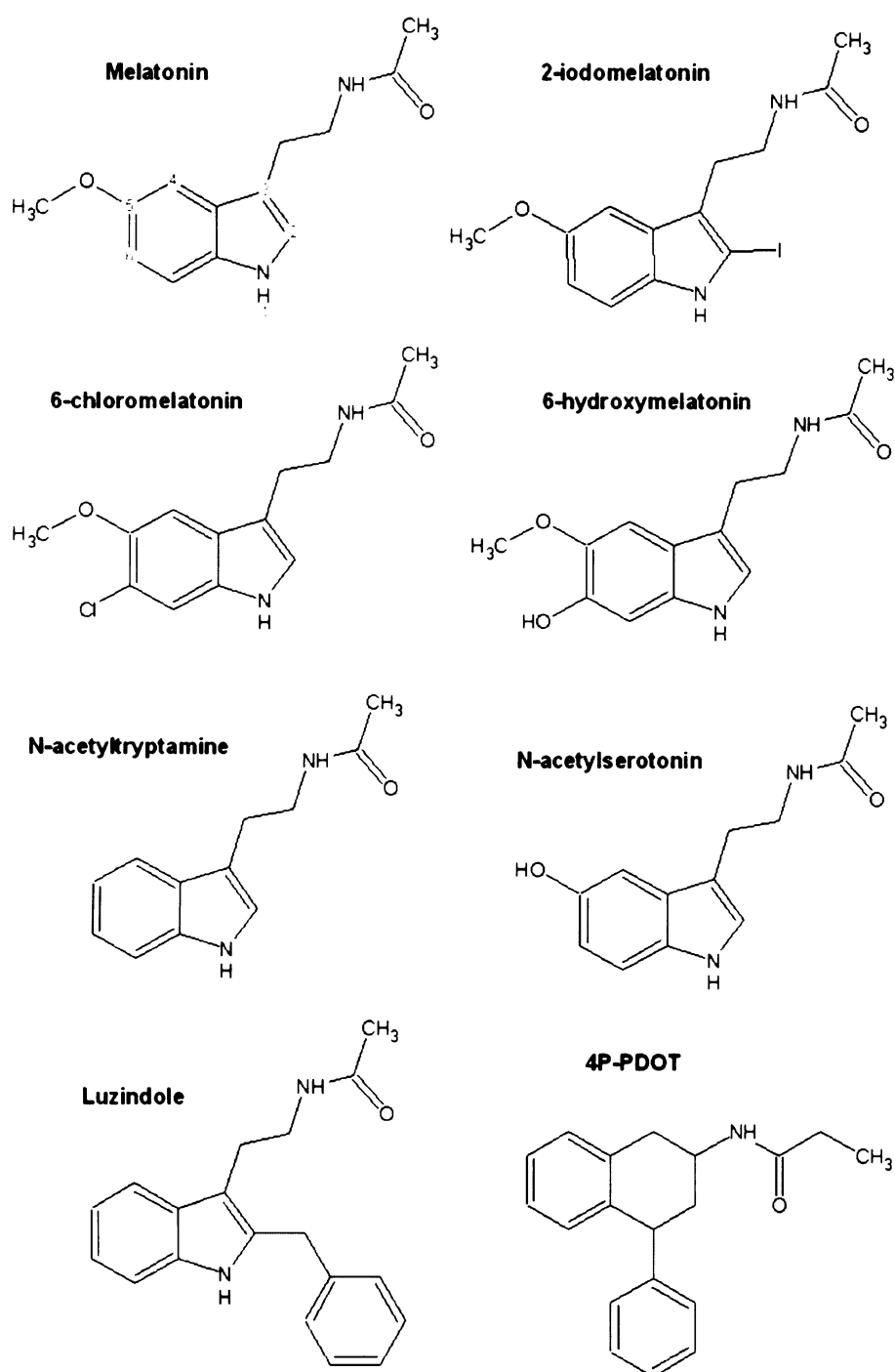


Fig. 5. Chemical structures of agonists and antagonists of the hMT2 receptor used in this study.

nin binding but increased the receptor affinity for more bulky 4P-PDOT (Fig. 5) by fivefold. Introduction of alanine at position 121 (G121A) decreased the receptor affinity for melatonin, mutation V124A reduced the binding affinity for 6-chloromelatonin, and mutation I125A decreased the receptor affinity for agonist *N*-acetylserotonin. These changes could be caused by minor alterations in the arrangement of hydrophobic residues forming the bottom part of putative hMT2 receptor-

binding site, which had no detectable effect on 2-iodomelatonin binding but significantly affected the binding of tested compounds. Reduced receptor expression demonstrated by significant decrease in  $B_{max}$  value of mutant V124A (Table 1) implicates possible impairment of receptor trafficking and/or cell membrane expression. In harmony with our results, it has been recently shown that residue M120 is not critical for 2-iodomelatonin binding to the hMT1 receptor subtype [23,24]. In the

hMT1 receptor, conserved serines at positions 123 and 127 in TM3 were suggested to be important for ligand binding [23]. However, their relevance was not confirmed in the case of the hMT2 receptor subtype [17] which is in good agreement with our model where S123 is facing away from the ligand-binding pocket (Fig. 4) and S127 is located relatively far (about 10 Å) from docked 2-iodomelatonin to be involved in any specific interaction (not shown).

#### Residues in TM6

In TM6, the dramatic change of binding affinity was observed for three of four studied receptor mutations involving asparagine 268 (N6.52). Replacement of N268 to alanine, leucine or aspartate led to a complete loss of radioligand binding to the mutant receptor (Table 1). Only the mutation of N268 to glutamine rescued 2-iodomelatonin binding to the receptor with the affinity of the wild-type. This indicates that hMT2 receptor requires at this position residue with polar and neutral side-chain. Moreover, the amide group of N268 is in hydrogen bond distance (3.3 Å) from the oxygen atom of hydroxyl group of Y298, which has been suggested to be hydrogen bonded with the 5-methoxy group of the 2-iodomelatonin [16]. Therefore, it is reasonable to speculate that amide group of N268 (or Q268) participates in polar contacts with Y298 and 5-methoxy group of the 2-iodomelatonin. As described previously, the mutation of asparagine at position 6.52 to alanine in TM6 of M1 muscarinic Ach receptor largely affected receptor affinity for antagonists [25], while in  $\beta$ 2 adrenergic receptor, Shi et al. [26] demonstrated that homologous F6.52 may participate in conformational changes in Pro-kink which are associated with receptor activation upon ligand binding.

Mutation of another TM6 residue A275 (A6.59) to isoleucine completely abolished 2-iodomelatonin binding whereas the mutation of A275 to valine had no effect (Table 1). We hypothesize that the isoleucine side-chain might create a sterical hindrance at the entrance into the ligand-binding pocket (Fig. 4) while less bulky valine does not block the ligand from accessing its binding site.

#### Residues in TM7

In the TM7 region, all receptors carrying mutations of residues V291 (V7.36) (mutations V291A and V291I) and L295 (L7.40) (mutations L295A, L295I, and L295V) were unable to bind 2-iodomelatonin (Table 1). The loss of receptor binding did not result from misexpression of mutant receptors due to trafficking problems, as indicated by immunological localization of all mutant receptors in the plasma membrane (Fig. 2). Therefore, we speculate that any change in the posi-

tions of residues 291 and 295 may disrupt the arrangement of tightly packed hydrophobic side-chains in this part of the ligand-binding pocket and thus affect the accommodation of the *N*-acetyl part of the radioligand. This is supported by our model where methyl groups of TM7 residues V291, L295 and residue A275 from TM6 are located relatively close (from 3 to 5 Å) from the *N*-acetyl chain of docked radioligand (see Figs. 1 and 4).

#### Residue Y188 in ECL2

According to our model, Y188 in ECL2 could specifically interact with *N*-acetyl moiety of 2-iodomelatonin, because the hydroxyl group of Y188 and the *N*-acetyl group of 2-iodomelatonin are in hydrogen bond distance (about 3 Å). In agreement with this prediction the mutation of Y188 to alanine, which lacks the aromatic ring, or more importantly the removal of the hydroxyl group by replacing Y188 with phenylalanine resulted in complete loss of receptor binding. Our data also indicate that the lack of specific binding in cells expressing mutant receptors was attributable to a loss of affinity and not to a lack of cell-surface expression (see Fig. 2). Nonetheless, we cannot exclude that the observed negative impacts on receptor binding might be indirect, e.g., because of improper folding of the ECLs which would still allow correct receptor expression and trafficking. In agreement with our data, it has been reported that tyrosine residues in ECL2 of the thyrotropin-releasing hormone receptor also specifically interact with the ligand [27,28].

In conclusion, we have used predictions derived from our homology model of the hMT2 melatonin receptor to analyze residues in TM3, TM5, TM7, and ECL2 that may participate in ligand binding. Our data demonstrate that residues N268 and A275 from TM6 as well as residues V291 and L295 are essential for 2-iodomelatonin binding to the hMT2 receptor, while TM3 residues M120, G121, V124, and I125 may participate in the binding of other receptor agonists and/or antagonists. Presented results also suggest that residue Y188 from ECL2 could directly interact with 2-iodomelatonin.

#### Acknowledgments

This research was supported by the Grant Agency of the Czech Republic (Grant Nos. 309/02/1479, 309/04/0496, and 204/03/0714), Internal Grant Agency of Academy of Sciences (Grant No. B5011308), by the Academy of Sciences of the Czech Republic (research project number AVOZ 501 1922), and the Ministry of Education of the Czech Republic (Grant Nos. MSM 113100001, MSM 113100003).

## References

- [1] R.J. Reiter, The pineal and its hormones in the control of reproduction in mammals, *Endocr. Rev.* 1 (1980) 109–131.
- [2] P. Pevet, B. Bothorel, H. Slotten, M. Saboureau, The chronobiotic properties of melatonin, *Cell Tissue Res.* 309 (2002) 183–191.
- [3] S.M. Hill, D.E. Blask, Effects of the pineal hormone melatonin on the proliferation and morphological characteristics of human breast cancer cells (MCF-7) in culture, *Cancer Res.* 48 (1988) 6121–6126.
- [4] R.J. Reiter, Functional diversity of the pineal hormone melatonin: its role as an antioxidant, *Exp. Clin. Endocrinol. Diab.* 104 (1996) 10–16.
- [5] R.J. Reiter, D.X. Tan, M. Allegra, Melatonin: reducing molecular pathology and dysfunction due to free radicals and associated reactants, *Neuro Endocrinol. Lett* 23 (Suppl. 1) (2002) 3–8.
- [6] G.J. Maestroni, The immunotherapeutic potential of melatonin, *Expert Opin. Investig. Drugs* 10 (2001) 467–476.
- [7] S.M. Reppert, D.R. Weaver, T. Ebisawa, Cloning and characterization of a mammalian melatonin receptor that mediates reproductive and circadian responses, *Neuron* 13 (1994) 1177–1185.
- [8] S.M. Reppert, C. Godson, C.D. Mahle, D.R. Weaver, S.A. Slaugenhaupt, J.F. Gusella, Molecular characterization of a second melatonin receptor expressed in human retina and brain: the Mel1b melatonin receptor, *Proc. Natl. Acad. Sci. USA* 92 (1995) 8734–8738.
- [9] O. Nosjean, M. Ferro, F. Coge, P. Beauverger, J.M. Henlin, F. Lefoulon, J.L. Fauchere, P. Delagrangé, E. Canet, J.A. Boutin, Identification of the melatonin-binding site MT3 as the quinone reductase 2, *J. Biol. Chem.* 275 (2000) 31311–31317.
- [10] J. Vanecek, Cellular mechanisms of melatonin action, *Physiol. Rev.* 78 (1998) 687–721.
- [11] M.I. Masana, M.L. Dubocovich, Melatonin receptor signaling: finding the path through the dark, *Sci. STKE* 2001 (2001) PE39.
- [12] J.M. Baldwin, Structure and function of receptors coupled to G proteins, *Curr. Opin. Cell Biol.* 6 (1994) 180–190.
- [13] J. Wess, G-protein-coupled receptors: molecular mechanisms involved in receptor activation and selectivity of G-protein recognition, *FASEB J.* 11 (1997) 346–354.
- [14] J.A. Ballesteros, L. Shi, J.A. Javitch, Structural mimicry in G protein-coupled receptors: implications of the high-resolution structure of rhodopsin for structure–function analysis of rhodopsin-like receptors, *Mol. Pharmacol.* 60 (2001) 1–19.
- [15] K. Palczewski, T. Kumasaka, T. Hori, C.A. Behnke, H. Motoshima, B.A. Fox, I. Le Trong, D.C. Teller, T. Okada, R.E. Stenkamp, M. Yamamoto, M. Miyano, Crystal structure of rhodopsin: a G protein-coupled receptor, *Science* 289 (2000) 739–745.
- [16] P. Mazna, V. Obsilova, I. Jelinkova, A. Balik, K. Berka, Z. Sovova, R. Ettrich, P. Svoboda, T. Obsil, J. Teisinger, Molecular modeling of human MT2 melatonin receptor: the role of Val204, Leu272 and Tyr298 in ligand binding, *J. Neurochem.* 91 (2004) 836–842.
- [17] M.J. Gerdin, F. Mseeh, M.L. Dubocovich, Mutagenesis studies of the human MT2 melatonin receptor, *Biochem. Pharmacol.* 66 (2003) 315–320.
- [18] M.M. Bradford, A rapid and sensitive method for the quantitation of microgram quantities of protein utilizing the principle of protein-dye binding, *Anal. Biochem.* 72 (1976) 248–254.
- [19] C.J. Grol, J.M. Jansen, The high affinity melatonin binding site probed with conformationally restricted ligands—II. Homology modeling of the receptor, *Bioorg. Med. Chem.* 4 (1996) 1333–1339.
- [20] E. Katchalski-Katzir, I. Shariv, M. Eisenstein, A.A. Friesem, C. Aflalo, I.A. Vakser, Molecular surface recognition: determination of geometric fit between proteins and their ligands by correlation techniques, *Proc. Natl. Acad. Sci. USA* 89 (1992) 2195–2199.
- [21] J.A. Ballesteros, H. Weinstein, in: *Integrated methods for the construction of three-dimensional models and computational probing of structure–function relations in G protein-coupled receptors*, *Methods in Neurosciences*, 1995, Academic Press, San Diego, CA, pp. 366–428.
- [22] Y. Cheng, W.H. Prusoff, Relationship between the inhibition constant ( $K_i$ ) and the concentration of inhibitor which causes 50 percent inhibition ( $IC_{50}$ ) of an enzymatic reaction, *Biochem. Pharmacol.* 22 (1973) 3099–3108.
- [23] S. Conway, E.S. Mowat, J.E. Drew, P. Barrett, P. Delagrangé, P.J. Morgan, Serine residues 110 and 114 are required for agonist binding but not antagonist binding to the melatonin MT(1) receptor, *Biochem. Biophys. Res. Commun.* 282 (2001) 1229–1236.
- [24] T. Kokkola, S.M. Foord, M.A. Watson, O. Vakkuri, J.T. Laitinen, Important amino acids for the function of the human MT1 melatonin receptor, *Biochem. Pharmacol.* 65 (2003) 1463–1471.
- [25] S.D. Ward, C.A. Curtis, E.C. Hulme, Alanine-scanning mutagenesis of transmembrane domain 6 of the M(1) muscarinic acetylcholine receptor suggests that Tyr381 plays key roles in receptor function, *Mol. Pharmacol.* 56 (1999) 1031–1041.
- [26] L. Shi, G. Liapakis, R. Xu, F. Guarneri, J.A. Ballesteros, J.A. Javitch, Beta2 adrenergic receptor activation. Modulation of the proline kink in transmembrane 6 by a rotamer toggle switch, *J. Biol. Chem.* 277 (2002) 40989–40996.
- [27] B. Han, A.H. Tashjian Jr., Importance of extracellular domains for ligand binding in the thyrotropin-releasing hormone receptor, *Mol. Endocrinol.* 9 (1995) 1708–1719.
- [28] J.H. Perlman, A.O. Colson, R. Jain, B. Czyzewski, L.A. Cohen, R. Osman, M.C. Gershengorn, Role of the extracellular loops of the thyrotropin-releasing hormone receptor: evidence for an initial interaction with thyrotropin-releasing hormone, *Biochemistry* 36 (1997) 15670–15676.